
On the Surprising Effectiveness of Large Learning Rates under Standard Width Scaling

Moritz Haas¹ Sebastian Bordt¹ Ulrike von Luxburg¹ Leena Chennuru Vankadara²

¹University of Tübingen, Tübingen AI Center
 {mo.haas,sebastian.bordt,ulrike.luxburg}@uni-tuebingen.de

²Gatsby Computational Neuroscience Unit, University College London
 l.vankadara@ucl.ac.uk

Abstract

The dominant paradigm for training large-scale vision and language models is He initialization and a single global learning rate (*standard parameterization*, SP). Despite its practical success, standard parametrization remains poorly understood from a theoretical perspective: Existing infinite-width theory would predict instability under large learning rates and vanishing feature learning under stable learning rates. However, empirically optimal learning rates consistently decay much slower than theoretically predicted. By carefully studying neural network training dynamics, we demonstrate that this discrepancy is not fully explained by finite-width phenomena such as catapult effects or a lack of alignment between weights and incoming activations. We instead show that the apparent contradiction can be fundamentally resolved by taking the loss function into account: In contrast to Mean Squared Error (MSE) loss, we prove that under cross-entropy (CE) loss, an intermediate *controlled divergence* regime emerges, where logits diverge but loss, gradients, and activations remain stable. Stable training under large learning rates enables persistent feature evolution at scale in all hidden layers, which is crucial for the practical success of SP. In experiments across optimizers (SGD, Adam), architectures (MLPs, GPT) and data modalities (vision, language), we validate that neural networks operate in this controlled divergence regime under CE loss but not under MSE loss. Our empirical evidence suggests that width-scaling considerations are surprisingly useful for predicting empirically optimal learning rate exponents. Finally, our analysis clarifies the effectiveness and limitations of recently proposed layerwise learning rate scalings for standard initialization.

1 Introduction

Scaling has become the dominant paradigm in building ever more capable vision and language models (Brown et al., 2020, Dosovitskiy et al., 2021, Kaplan et al., 2020, Hoffmann et al., 2022, Grattaflori et al., 2024). Training these models requires many choices, including initialization variances, learning rates, and other optimization hyperparameters. The dominant practice for training large models is *standard parameterization* (SP): networks are initialized using He initialization (He et al., 2015) and trained with a single global learning rate tuned at each scale (OLMo Team et al., 2024).

Infinite-width theory provides principled rules for scaling hyperparameters as network size increases. In particular, *Maximal Update Parameterization* (μP) prescribes how learning rates and initialization variances should scale layer-wise so that the training dynamics remain width-independent. This allows tuning small proxy models and transferring the optimal hyperparameters to large scales

(Yang and Hu, 2021, Yang et al., 2022). Crucially, infinite-width theory also predicts that under SP, network dynamics should become unstable with learning rates scaling larger than $\mathcal{O}(1/n)$ (where n is network width), and that feature learning vanishes with $\mathcal{O}(1/n)$ learning rates, causing the models to enter a kernel regime (Sohl-Dickstein et al., 2020, Yang and Hu, 2021). Empirically, however, networks trained in SP exhibit stable feature learning and excellent generalization performance, often with optimal learning rates decaying much slower than theoretically predicted (commonly around $\Omega(1/\sqrt{n})$). This is depicted in Figure 1, where we see that the optimal learning rates (solid lines) for different models trained in SP decay much slower than the theoretically predicted maximal stable scaling law (dashed gray lines). This discrepancy presents a fundamental puzzle:

*Why does SP remain stable and effective at large learning rates, despite the theoretical predictions?
And does there exist an infinite-width limit that corresponds more closely with the behaviour of practical finite-width networks?*

One possible resolution could be that assumptions underlying infinite-width theory fail at realistic finite widths. Recent studies have highlighted phenomena like the *catapult effect* (Lewkowycz et al., 2020) and the *edge of stability* (Cohen et al., 2021), suggesting classical stability bounds underestimate viable learning rates. However, our analysis of simplified linear models under SP indicates that these finite-width effects alone cannot explain why large learning rate scaling remains stable. In a similar spirit, Everett et al. (2024) hypothesized that certain infinite-width theory predictions of alignment between weight updates and activations may break down in practice - which could also have plausibly explained the discrepancy between theory and practice. Through careful empirical measurements, we also rule out this hypothesis.

Instead, we find a fundamental resolution in the previously overlooked role of the loss function. Specifically, unlike under MSE loss, where the effect of output logit divergence catastrophically cascades and destabilizes training, cross-entropy (CE) loss allows stable training under large learning rates even when output logits diverge. Consequently, the practical stability threshold in SP is determined solely by hidden or input layer stability constraints — not by output-layer divergence. Empirically, we find that while output-layer divergence under CE loss remains benign with respect to the stability threshold, it occasionally influences the optimal learning rate choice — particularly under SP with layerwise learning rates, as used by Everett et al. (2024). Moreover, we identify cases where output-layer divergence breaks the previously observed learning-rate transfer under layerwise learning rates.

Main Contributions. After reconciling the apparent contradictions between infinite-width theory and practice, we provide the first infinite-width proxy that has strong correspondence to practical finite-width networks, as they are initialized and trained in practice, in the following sense:

- Contrary to what was hypothesized in previous work (Everett et al., 2024), we show that the infinite-width alignment predictions between weights and incoming activations hold when measured with the right refined coordinate checks (RCC). Consequently, logits diverge at sufficient width in SP under empirically optimal learning rates.
- We show that the CE loss function enables a *controlled divergence* regime in which training remains stable despite logit divergence. This regime allows recovering feature learning at large widths under large learning rates $\eta_n = \Theta(n^{-1/2})$, which could explain the practical success of SP. To the best of our knowledge, this provides the first practical infinite-width limit in the feature-learning regime for SP.
- The controlled divergence regime also sheds light on the stability of other parameterizations, particularly SP with μ P learning rates (SP-full-align, Everett et al., 2024). However, we empirically show that SP-full-align does not provide learning rate transfer on vision datasets due to inherent width dependence.
- We show that our width-scaling considerations provide surprisingly good predictions of maximal stable learning rate exponents, which often dominate optimal learning rates, particularly in Transformers (Vaswani et al., 2017).

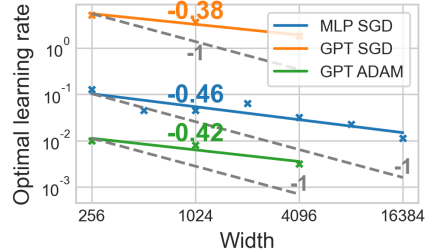


Figure 1: **Optimal learning rate exponents exceed the theoretically predicted stability threshold.** For MLPs on MNIST and GPT on language data, optimal learning rates in SP decay slower than the theoretically predicted maximal stable $\eta_n = \mathcal{O}(n^{-1})$ in gray.

Taken together, our results deepen the theoretical understanding of why SP remains effective at large scales, provide rigorous empirical validation for critical assumptions in infinite-width theory, and offer practical insights into stable hyperparameter transfer for scaling neural networks.

2 Background: Width-scaling arguments from Tensor Program theory

Before exploring plausible explanations for the empirical width-scaling properties of neural networks, we first define used notation and distill all necessary width-scaling arguments from Tensor Program (TP) theory (Yang and Hu, 2021, Yang and Littwin, 2023). We provide a more detailed introduction to TP scaling arguments in Appendix C.1, and a detailed account of related work in Appendix A.

Setting and Notation. We define an $(L + 1)$ -layer MLP of width n iteratively via

$$h^1(\xi) := W^1\xi, \quad x^l(\xi) := \phi(h^l(\xi)), \quad h^{l+1}(\xi) := W^{l+1}x^l(\xi), \quad f(\xi) := W^{L+1}x^L(\xi),$$

for inputs $\xi \in \mathbb{R}^{d_{in}}$ with trainable weight matrices $W^1 \in \mathbb{R}^{n \times d_{in}}$, $W^l \in \mathbb{R}^{n \times n}$ for $l \in [2, L]$, and $W^{L+1} \in \mathbb{R}^{d_{out} \times n}$. We call h^l preactivations, x^l activations, and $f(\xi)$ output logits. Training the MLP with Stochastic Gradient Descent (SGD) with global learning rate $\eta > 0$ under loss function $\mathcal{L} : \mathbb{R}^{d_{out}} \times \mathbb{R}^{d_{out}} \rightarrow \mathbb{R}$ with labelled training point $(\xi_t, y_t) \in \mathbb{R}^{d_{in}} \times \mathbb{R}^{d_{out}}$ is defined as $W_{t+1}^l = W_t^l - \eta \nabla_{W^l} \mathcal{L}(f_t(\xi_t), y_t)$. We denote updates accumulated over all time steps by $\Delta h_t^l = h_t^l - h_0^l$ and the change from a single update step by $\delta h_t^l = h_t^l - h_{t-1}^l$. The fan-notation has the purpose of unifying all weight matrices and simply means $W \in \mathbb{R}^{\text{fan}_{out} \times \text{fan}_{in}}$. In this paper, we define *standard parameterization (SP)* to mean He initialization $(W_0^l)_{ij} \sim N(0, c_\phi / \text{fan}_{in}(W_0^l))$ trained with SGD or Adam with a single possibly width-dependent learning rate $\eta_n = \eta \cdot n^\alpha$, $\alpha \in \mathbb{R}$, for all trainable weights $\{W_t^l\}_{l \in [L+1]}$. This models the typical practice, in which a global learning rate is tuned at each model scale. We denote the softmax function by $\sigma(f)_i = \exp(f_i) \cdot (\sum_{j \in [d_{out}]} \exp(f_j))^{-1}$. For naturally measuring the average scaling of entries in vectors $x \in \mathbb{R}^d$, we use the root-mean-squared norm $\|x\|_{RMS} := d^{-1/2} \cdot \|x\|_2$ as the standard vector norm. For matrices W , we write $\|W\|_F$ for the Frobenius norm and measure entry-wise scaling with the RMS norm $\|W\|_{RMS} := \left(\frac{1}{\text{fan}_{in} \cdot \text{fan}_{out}}\right)^{1/2} \|W\|_F$. The operator norm w.r.t. the RMS-norm is defined as $\|W\|_{op} := \|W\|_{RMS \rightarrow RMS} := \sup_{x \in \mathbb{R}^{\text{fan}_{in}(W)}} (\|Wx\|_{RMS} / \|x\|_{RMS})$. We use Bachmann-Landau notation $\mathcal{O}, \Theta, \Omega$ that purely tracks dependence on width n and omits all other dependencies.

Effective and Propagating Updates. When training neural networks, weights W_t^l of layer l evolve from their initialization W_0^l through updates ΔW_t^l , such that $W_t^l = W_0^l + \Delta W_t^l$. Although we directly control the scaling of these initial weights and updates, we are ultimately interested in their impact on subsequent activations in the network. For standard architectures, including convolutional networks and Transformers, weights typically act linearly on incoming activations. Thus, for weights W_t^l and incoming activations x_t^{l-1} , the change in the next layer’s pre-activations Δh_t^l can be decomposed into two distinct contributions: the *effective updates* arising directly from the change in weights ΔW_t^l of the current layer, and the *propagating updates*, arising indirectly from activation changes Δx_t^{l-1} in preceding layers:

$$\Delta h_t^l = \underbrace{(\Delta W_t^l) x_t^{l-1}}_{\text{Effective Updates}} + \underbrace{W_0^l (\Delta x_t^{l-1})}_{\text{Propagating Updates}}. \quad (\text{RCC})$$

We say the layer admits *maximal stable feature learning* if both the effective updates and propagating updates remain width-independent as network width $n \rightarrow \infty$, that is $\|(\Delta W_t^l) x_t^{l-1}\|_{RMS} = \Theta(1)$ and $\|W_0^l (\Delta x_t^{l-1})\|_{RMS} = \Theta(1)$.

Identifying the correct scaling exponents. In the spirit of Everett et al. (2024), we use p_l and q_l to denote the width-scaling exponents of the *alignment ratios* of the pairs $(\Delta W_t^l, x_t^{l-1})$ and $(W_0^l, \Delta x_t^{l-1})$ respectively, that is,

$$\frac{\|\Delta W_t^l x_t^{l-1}\|_{RMS}}{\|\Delta W_t^l\|_{RMS} \cdot \|x_t^{l-1}\|_{RMS}} = \Theta(n^{p_l}), \quad \frac{\|W_0^l \Delta x_t^{l-1}\|_{RMS}}{\|W_0^l\|_{RMS} \cdot \|\Delta x_t^{l-1}\|_{RMS}} = \Theta(n^{q_l}). \quad (\alpha\text{-rms})$$

A key insight from Yang and Hu (2021) and Yang and Littwin (2023) is that during training, correlations can emerge in certain layers between the two quantities in each pair in (RCC), causing

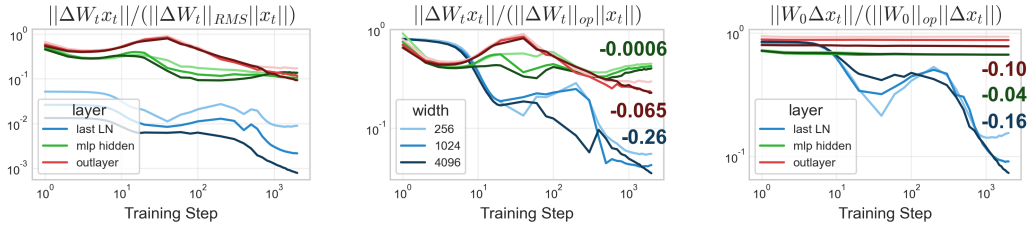


Figure 2: **Alignment has minimal width-dependence.** Alignment ratio between accumulated weight updates ΔW_t and incoming activations x_t in RMS norm (left) and operator norm (center) as well as between initial weights W_0 and activation updates Δx_t in operator norm (right) for the last layernorm layer, the first MLP layer in Transformer block 2 and the readout layer. RMS norm may be confounded by accumulated rank over the course of training (e.g. compare $(\Delta W_t, x_t)$ values for last LN). While operator norm alignment tends to decay over the course of training, it does not display strong width-dependence, even after 2000 batches (see annotated width-dependent exponents).

them to become *aligned* in the infinite-width limit and thereby inducing $p_l = 1$ and $q_l = 1$ due to a law of large numbers effect. If, instead, these quantities were uncorrelated, their product would exhibit smaller scaling exponents ($p_l = 1/2$ and $q_l = 1/2$) due to a central limit effect. In particular, infinite-width theory predicts the exponents $p_{1:L+1} = 1$, $q_{1:L} = 1/2$, and $q_{L+1} = 1$. The alignment exponents p_l, q_l are a consequence of the training dynamics and do not depend on the specific parameterization used (e.g., SP, NTP, or μP).

By adjusting the initialization variance, which controls the scale of initial weights W_0 , and the learning rate, which governs the magnitude of updates ΔW_t , we can ensure that both contributions in (RCC) remain width-independent as the network width n grows. The corresponding choice of hyperparameter scaling defines the *Maximal Update Parameterization* (μP). As we will discuss in Section 4, under the theoretically predicted alignment exponents, SP with $\mathcal{O}(1/n)$ learning rates leads to vanishing activation updates in all layers $\|\Delta x_t\|_{RMS} = o(1)$ and choosing the learning rate $\omega(1/n)$ leads to logit divergence in the infinite-width limit.

3 Finite-width distortions and long-training dynamics alone do not explain the stability of large learning rates in SP

Differing optimal learning rate exponents at finite width versus in the infinite-width limit may be caused by finite-width effects accumulating over many update steps and eventually inducing a phase transition, in particular when the number of update steps exceeds the width of the network. Here we investigate two such potential explanations.

3.1 Update alignment between weights and activations is barely width-dependent

Everett et al. (2024) highlight that at finite width and over extended training times, it is a priori unclear whether the pairs $(\Delta W_t^l, x_t^{l-1})$ and $(W_0^{L+1}, \Delta x_t^L)$ remain strongly correlated or whether their alignment exponents $(p_{1:L+1}, q_{L+1})$ should rather be thought of as dynamically changing over the course of training. If the alignment exponents instead transition towards the central-limit regime and in particular if $p_{1:L+1} = -1/2$, this could explain the observed \sqrt{n} gap between theoretically predicted and empirically observed optimal learning rate scalings.

Yang et al. (2023a) introduces an alignment metric that serves as a natural and unified metric to evaluate these infinite-width theory predictions,

$$\alpha_{A,x} = \frac{\|Ax\|_{RMS}}{\|A\|_{RMS \rightarrow RMS} \|x\|_{RMS}}. \quad (\alpha\text{-op})$$

Specifically, if the alignment exponents $p_{1:L+1} = 1$, $q_{1:L} = \frac{1}{2}$, $q_{L+1} = 1$ hold, both contributions in (RCC) must exhibit alignment metrics $\alpha_{\Delta W_t^l x_t^{l-1}}$ and $\alpha_{W_0^l \Delta x_t^{l-1}}$ of order $\Theta(1)$ in all layers.

In [Figure 2](#), we plot the alignment metrics at varying widths over the course of Transformer training with AdamW in SP. It shows that while alignment can decrease over the course of training, it exhibits minimal dependence on network width. Even after accumulating approximately 2000 batches of training, the width-scaling exponents are much closer to 0 than to -0.5 , indicating that infinite-width alignment predictions hold reasonably well. Hence a lack of alignment alone cannot explain the large optimal learning rate exponents observed in practice.

3.2 Does a catapult mechanism in the first update steps stabilize large learning rates in SP?

As another plausible explanation, initial divergence under large learning rates may be stabilized over the course of training at finite width. Unlike at infinite width, where there only exist a divergent regime and a lazy regime without feature learning, an intermediate catapult regime was identified by [Lewkowycz et al. \(2020\)](#) at finite width, for SGD training with MSE loss in Neural Tangent Parameterization (NTP). They provide theory for 2-layer linear networks. Under small learning rates $\eta \leq 2/\lambda_0$, where λ_0 denotes the largest eigenvalue of the Hessian at initialization, the network monotonically converges to a minimum. Under large learning rates $\eta > 4/\lambda_0$, training diverges. But in an *edge of stability* regime ([Cohen et al., 2021, 2022](#)) of intermediate learning rates, the loss increases in the first $\mathcal{O}(\log(n))$ update steps while the sharpness λ_t decreases. Once the sharpness lies below the edge of stability $2/\eta$, the loss decreases and the final learned function may generalize better as the solution lies in a basin with lower sharpness. But existing work does not study width-scaling with SP. May similar initial training dynamics be at play here?

In [Appendix C.4](#) we analyse the 2-layer linear network model from [Lewkowycz et al. \(2020\)](#) in NTP, SP and μ P trained with SGD under MSE loss, and provide loss and sharpness increase characterizations in [Proposition C.17](#). In μ P, the update equations of the learned function f_t and the sharpness λ_t are fully width-independent, which allows width-independent learning rates. In NTP, at least the conditions for loss and sharpness reduction are approximately width-independent. In SP, on the other hand, sharpness increases $\lambda_{t+1} \geq \lambda_t$ iff $\lambda_t \geq \frac{4}{n\eta_n}(1 + \frac{y}{f_t - y})$, requiring $\eta_n = \mathcal{O}(n^{-1})$ to avoid sharpness (as well as loss) divergence in the first update steps. The simulations shown in [Figure C.2](#) validate the maximal stable learning rate scaling $\eta = \mathcal{O}(n^{-1})$. Hence catapult dynamics alone do not suffice for explaining large learning rate stability in SP.

4 Cross-entropy loss enables stable feature learning under large learning rates in standard parameterization

First, let us briefly recall why infinite-width theory predicts divergence under SGD training in SP with learning rates $\eta_n = \eta \cdot n^{-\alpha}$ for $\alpha < 1$.

Recall that the alignment exponents in (α -rms) satisfy $p_{1:L+1} = 1$. In particular, for the output layer, we have $\|\Delta W_t^{L+1} x_t^L\|_{RMS} = \Theta(n \cdot \|\Delta W_t^{L+1}\|_{RMS} \cdot \|x_t^L\|_{RMS})$. For SGD, the weight update of the last layer after 1 update step is given by $\Delta W^{L+1} = -\eta \cdot n^{-\alpha} \cdot \chi_0 \cdot (x_0^L)^T$, where $\chi_0 := \partial_f \mathcal{L}(f_0(\xi_0), y_0)$. Under SP, at initialization, both $\|x_0^L\|_{RMS} = \Theta(1)$ and $\|\chi_0\|_{RMS} = \Theta(1)$. This implies logit divergence after 1 step of SGD with learning rates $\eta_n = \omega(1/n)$:

$$\|x^L\|_{RMS} = \Theta(1), \|\Delta W^{L+1}\|_{RMS} = \Theta(n^{-\alpha}), \implies \|\Delta W^{L+1} x^L\|_{RMS} = \Theta(n^{1-\alpha})$$

So, *why do larger learning rates remain stable and even effective, despite logit divergence?*

Here, we demonstrate that a simple yet fundamental aspect of training, the choice of loss function, resolves the large learning rate puzzle, and enables a well-defined and practical infinite-width limit that allows feature learning under SP. The key insight is that, under cross-entropy (CE) loss, the logits f never directly appear in the training dynamics; instead, the effective output function is $\sigma(f)$. Unlike the destabilizing logit blowup encountered under mean squared error (MSE) loss, under CE loss, logit growth has a harmless effect on training stability. In particular, the CE loss introduces an intermediate *controlled divergence* regime $\alpha \in [1/2, 1)$ that is absent for the MSE loss ([Figure 3](#)).

Proposition 1. (Asymptotic regimes in SP, informal) *For fixed $L \geq 2, t \geq 1, \eta > 0, \alpha \in \mathbb{R}$, consider training a $(L + 1)$ -layer MLP of width n in SP with SGD and global learning rate $\eta_n = \eta \cdot n^{-\alpha}$ for t steps. Then the logits f_t , training loss $\mathcal{L}(f_t(\xi_t), y_t)$, loss-logit derivatives $\chi_t := \partial_f \mathcal{L}(f_t(\xi_t), y_t)$, loss-weight gradients $\nabla_t^l := \nabla_{W^l} \mathcal{L}(f_t(\xi_t), y_t)$ and activations $x_t^l, l \in [L]$, after training scale as follows in the infinite-width limit $n \rightarrow \infty$.*

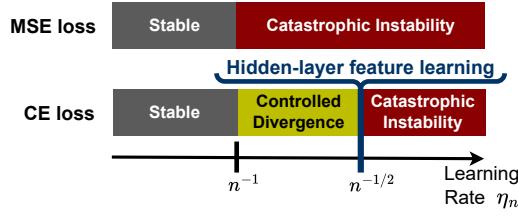


Figure 3: **Learning rate regimes for SGD in SP.** Under MSE loss, either training remains stable ($\alpha \geq 1$) or logits and activations diverge ($\alpha < 1$) in the infinite-width limit. Under CE loss, a ‘controlled divergence’ regime $\alpha \in [1/2, 1)$ emerges where logits diverge, but training does not diverge. At $\alpha = 1/2$, hidden layers learn features width-independently.

Under cross-entropy (CE) loss, three qualitatively distinct regimes arise:

- (a) **Stable regime** ($\alpha \geq 1$): Logits, loss, gradients and activations remain stable, that is $\|f_t\|_{RMS} = \mathcal{O}(1)$, $|\mathcal{L}(f_t(\xi_t), y_t)| = \mathcal{O}(1)$, $\|\chi_t\|_{RMS} = \mathcal{O}(1)$, $\|\nabla_t^l\|_{RMS} = \mathcal{O}(n^{-1/2})$ and $\|x_t^l\|_{RMS} = \mathcal{O}(1)$ for all $l \in [L]$.
- (b) **Controlled divergence** ($\frac{1}{2} \leq \alpha < 1$): Logits diverge $\|f_t\|_{RMS} = \Theta(n^{1-\alpha})$, but loss, gradients and activations remain stable, that is $\|x_t^l\|_{RMS} = \Theta(1)$, $|\mathcal{L}(f_t(\xi_t), y_t)| = \mathcal{O}(1)$, $\|\chi_t\|_{RMS} = \mathcal{O}(1)$ and $\|\nabla_t^l\|_{RMS} = \mathcal{O}(n^{-1/2})$ for all $l \in [L]$.
- (c) **Catastrophic instability** ($\alpha < \frac{1}{2}$): Logits, activations and weight gradients diverge, that is $\|f_t\|_{RMS} \rightarrow \infty$, $\|x_t^l\|_{RMS} \rightarrow \infty$ and $\|\nabla_t^l\|_{RMS} \rightarrow \infty$, $l \in [2, L]$.

Under mean-squared error (MSE) loss, a stable regime as in (a) above arises if $\alpha \geq 1$. If $\alpha < 1$, training is catastrophically unstable as in (c) above and, in addition, loss and loss-logit derivatives diverge, that is $|\mathcal{L}(f_t(\xi_t), y_t)| \rightarrow \infty$ and $\|\chi_t\|_{RMS} \rightarrow \infty$.

The formal statement together with a proof can be found in [Appendix C.3](#). For an intuitive understanding of this result, note that the only effect that the choice of loss function $\mathcal{L}(f, y)$ has on the final learned function is through the loss-logit gradients $\chi_t := \partial_f \mathcal{L}(f_t(\xi_t), y_t)$ over the course of training. Under MSE loss, the loss gradients are given by the residuals $\chi_t = f_t(\xi_t) - y_t$. But CE loss induces loss gradients $\chi_t = \sigma(f_t(\xi_t)) - y_t$. Crucially, it is the correct choice of loss function to effectively view $\sigma(f)$ as the output of the network instead of the unnormalized logits f . If one were to use $\text{MSE}(\sigma(f), y)$ as a loss function instead, additional derivative terms can induce vanishing gradients under exploding network output and not increase the optimal learning rate exponent ([Appendix F.3](#)). Under CE loss, the effective network output $\sigma(f)$ at most converges to one-hot predictions when the logits diverge, and with increasing width training points are sharply memorized after a single update step. At large learning rates $\eta_n = \Theta(n^{-1/2})$, training points are not just memorized in last-layer weights, but feature learning is recovered in the infinite-width limit:

Proposition 2 (Under CE loss, SP with large learning rates learns features at large width, informal). Consider the setting of [Proposition 1](#) of training a $(L+1)$ -layer MLP with SGD in SP with global learning rate $\eta_n = \eta \cdot n^{-\alpha}$, $\alpha \in \mathbb{R}$, in the infinite-width limit $n \rightarrow \infty$.

- (a) Under both MSE and CE loss in the stable regime ($\alpha \geq 1$), feature learning vanishes in all layers $l \in [L]$, that is $\|\Delta x_t^l\|_{RMS} = \mathcal{O}(n^{-1/2})$.
- (b) Under CE loss in the controlled divergence regime ($\frac{1}{2} \leq \alpha < 1$), input layer feature learning vanishes at rate $\|\Delta x_t^1\|_{RMS} = \Theta(n^{-1/2-\alpha})$, and hidden layers $l \in [2, L]$ learn features at rate $\|\Delta x_t^l\|_{RMS} = \Theta(n^{1/2-\alpha})$. In particular, when $\alpha = 1/2$, the weight updates of all hidden layers induce width-independent activation updates, that is $\|\Delta x_t^l\|_{RMS} = \Theta(1)$.

To the best of our knowledge, this provides the first infinite-width limit of SP in the practical feature learning regime. [Figure 4](#) empirically validates that the predicted width-scaling exponents that induce maximally stable feature learning despite logit blowup under $\eta_n = \eta \cdot n^{-1/2}$ are already accurate at moderate width 512. [Appendix E.4](#) shows that effective update predictions also hold accurately in Transformers trained with Adam. In the next section, we discuss the profound implications that training stability under logit blowup has on learning rate scaling exponents in practice.

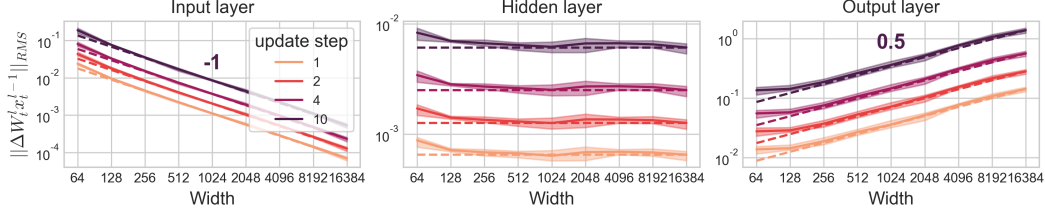


Figure 4: **Hidden-layer feature learning albeit logit divergence in SP under large learning rates.** Effective l -th layer update scalings $\|\Delta W_l^l x_t\|_{RMS}$ of MLPs trained with SGD in SP with $\eta_n = 0.0001 \cdot (n/256)^{-1/2}$ on CIFAR-10 under CE loss. Our TP scaling predictions are accurate: Hidden layers learn features width-independently, and input layers have vanishing feature learning. The update scaling exponents can already be accurately estimated at small width $n \leq 512$.

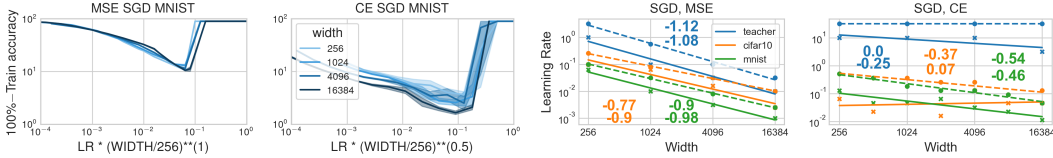


Figure 5: **Learning rates decay slower under CE loss than under MSE loss.** *Left versus center-left:* Width-scaled learning rate versus training error for MNIST showing approximate transfer with $\eta_n = \eta \cdot n^{-1}$ under MSE loss versus with $\eta_n = \eta \cdot n^{-1/2}$ under CE loss. *Center-right versus right:* Optimal learning rate (solid) and minimal unstable learning rate (dashed) for 2-layer MLPs on generated multi-index data and 8-layer MLPs on CIFAR-10 and MNIST. Optimal learning rates are often close to max-stable learning rates. Theoretical instability predictions $\mathcal{O}(n^{-1})$ for MSE loss, $\mathcal{O}(1)$ for 2-layer MLPs and $\mathcal{O}(n^{-1/2})$ for deep MLPs under CE loss are surprisingly accurate.

5 Consequences of training stability under logit divergence

In this section we perform extensive experiments to empirically evaluate the implications of the stability and feature learning predictions of our infinite-width theory from the previous section.

Experimental details. We train MLPs of varying depth up to width 16384 with plain SGD and Adam on CIFAR-10, MNIST and a generated multi-index model (reported in Appendix F). We also train Pythia-GPTs with warmup and cosine learning rate decay on the DCLM-Baseline dataset (Li et al., 2024) up to width 4096 or 1.4B parameters using both Adam with decoupled weight decay (Loshchilov and Hutter, 2019) and SGD (reported in Appendix F.2). If not stated otherwise, we consider SP with a global learning rate. All details can be found in Appendix D. Code will be made publicly available in a future version of this manuscript.

5.1 Infinite-width theory is a useful predictor of empirical optimal learning rate exponents

While our theory predicts maximal stable learning rates, in practice, we are interested in optimal learning rates. We hypothesize that maximal stable feature learning in all layers induces optimal performance at large width. However, since different layer types require different maximal stable learning rate exponents, the single global learning rate under SP is subject to opposing forces for recovering feature learning under the constraint of training stability. We now evaluate several instantiations of this hypothesis.

MLPs and Transformers with SGD. Figures 5 and 6 show that the empirical maximal learning rate exponents under CE loss closely follow $\alpha = 1/2$ for both MLPs on vision data and for GPTs on language data. The x-axis scales the learning rate with the closest clean exponent from $\{0, 0.5, 1\}$ to show that approximate empirical transfer is often enforced by the stability threshold $\mathcal{O}(n^{-1/2})$. While the theory only predicts the maximal stable exponent, Proposition 2 suggests that the optimal learning rate may follow the maximal stable exponent: $\alpha = 1/2$ since it is the only setting under which feature learning is preserved at large width in all hidden layers. The maximal stable learning rate under MSE loss also consistently scales as its infinite-width prediction $\mathcal{O}(n^{-1})$ and optimal learning rates closely follow this exponent, as under smaller exponents $\alpha > 1$, not even logits are updated

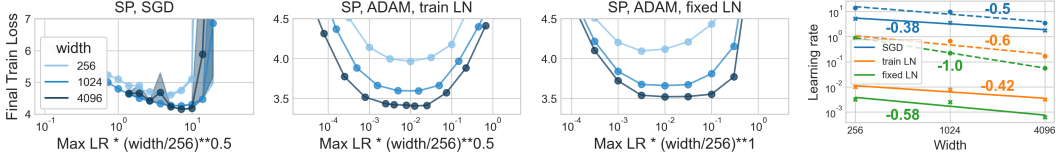


Figure 6: **Approximate learning rate transfer for GPT in SP.** *Left to center-right:* Width-scaled learning rate versus training loss for GPT trained with SGD, Adam with trainable LayerNorm parameters and Adam without trainable LayerNorm parameters. *Right:* Corresponding optimal (solid) and maximal stable (dashed) learning rate exponents. For SGD, hidden-layer stability $\eta_n = \mathcal{O}(n^{-1/2})$ clearly dominates the maximal stable as well as optimal learning rate scaling. For Adam without LayerNorm parameters, hidden-layer stability induces a stability threshold $\eta_n = \mathcal{O}(n^{-1})$. Trainable LayerNorm parameters further stabilize large learning rates and induce larger optimal learning rate scaling $\eta_n \approx \Theta(n^{-1/2})$ toward preserving input-layer feature learning at scale.

$\|\Delta f_t\|_{RMS} \rightarrow 0$. Overall, this shows that existing infinite-width theory was indeed predictive of the maximal stable learning rate exponents under MSE loss, but that CE loss induces qualitatively more favorable behaviour that is only captured by a sufficiently loss-specific analysis.

MLPs with Adam. Adam approximately normalizes the gradient and therefore further stabilizes training against misscaled gradients beyond the effect of CE loss, under sufficiently small $\varepsilon > 0$. W^l is effectively updated if the learning rate scaling counteracts the scaling accumulated in the inner product between normalized weight gradients and incoming activations. This leads to the ideal (μ P) learning rates $\eta(W^l) = \eta/\text{fan_in}(W^l)$. Thus Adam in SP with $\eta_n = \Theta(n^{-1})$ induces width-independent updates, except for vanishing input layer feature learning and logit divergence through $W_0^{L+1} \Delta x_t^L$. In deep MLPs, we typically observe optimal learning rates $\eta_n = \mathcal{O}(n^{-1})$, suggesting that hidden-layer stability dominates.

Transformer training with AdamW. In Transformers with trainable LayerNorm parameters, which scale input-like, training is stabilized, and the exponent is increased toward input layer feature learning. Without trainable LayerNorm parameters, in contrast, only the embedding layer scales input-like so that training becomes approximately width-independent under $\eta_n = \Theta(n^{-1})$. Figure 6 shows that the max-stable and optimal learning rate exponents shrink from $-1/2$ toward -1 if we remove the trainable layer-norm parameters. This suggests that trainable scale parameters in normalization layers play an essential role in maintaining learning rates in Transformers, which could explain why they are almost unanimously used in modern architectures (OLMo Team et al., 2024, Grattafiori et al., 2024, Gemma Team et al., 2024). Moreover, input layer learning vanishes at scale in SP, which may explain techniques like removing weight decay in the embedding layer (OLMo Team et al., 2024). Logit divergence under large learning rates may be a reason for regularizing techniques like the Z-loss (Chowdhery et al., 2023, Wortsman et al., 2024, OLMo Team et al., 2024).

Taken together, the empirical evidence suggests that infinite-width theory may serve as a helpful proxy for understanding practical neural networks at finite width. Since training divergence imposes a hard constraint on the optimal learning rate and activation divergence in multiple layers becomes harder to stabilize, width-scaling predictions seem to hold even more accurately on deep and sensitive architectures such as Transformers.

5.2 A novel understanding of standard initialization with layerwise learning rates

Everett et al. (2024) perform extensive Transformer experiments, and recommend training with Adam in SP with μ P learning rates (SP-full-align) as the overall best performing parameterization in terms of validation loss, learning rate transfer and learning rate sensitivity. This parameterization only differs from μ P through the larger last-layer He initialization $W_0^{L+1} \sim N(0, n^{-1})$. While the authors attribute the success of SP-full-align to a lack of alignment between W_0^{L+1} and Δx_t^L , they only measure the joint alignment between W_t and x_t for each layer, which confounds the individual alignment exponents of $(\Delta W_t, x_t)$ and $(W_0, \Delta x_t)$ from (RCC). We provide a detailed explanation in Appendix C.2. Our empirical alignment reevaluation in Figure 2 and Figure E.15 does not support the hypothesized lack of alignment. This implies that logits diverge through $W_0^{L+1} \Delta x_t^L$ as soon as feature learning does not vanish. Instead our theoretical results in Section 4 show that logit divergence

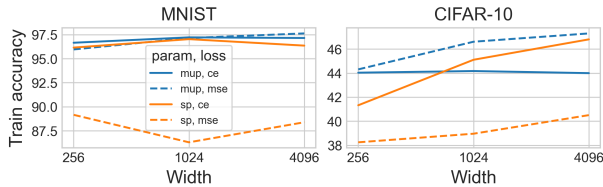


Figure 7: **Performance difference between losses is larger in SP than in μ P.** Optimal training accuracy of 8-layer MLPs trained with SGD on MNIST (left) and CIFAR-10 (right). The performance in μ P depends much less on the loss function since all layers learn width-independently.

is not necessarily harmful for training stability under CE loss. Just like SP with $\eta_n = \Theta(n^{-1/2})$, SP-full-align with $\eta_n = \Theta(1)$ lies at the feature learning edge of the controlled divergence regime.

Learning rate transfer of SP-full-align breaks on image datasets. Due to width-independent alignment between W_0^{L+1} and Δx_t^L , logits diverge with width in SP-full-align at sufficient width. We validate this claim for CIFAR-10 at moderate width in Figure F.34. This introduces width-dependent training dynamics. Consequently our single-pass experiments in Appendix F.8 consistently show decaying optimal learning rates in SP-full-align for both SGD and Adam on MNIST, CIFAR-10 and generated multi-index data. We also observe that the maximal stable learning rate remains width-independent as our theory would predict. This constitutes our only experiment in which the maximal stable learning rate scaling is suboptimal in deep nonlinear networks. We leave fully understanding the driving mechanism to future work.

5.3 A scaling-theoretic view on the practical success of CE loss in deep learning

Many success stories in deep learning, from computer vision to natural language processing, use the cross-entropy loss. We propose a scaling-theoretic explanation for this practical dominance. Our results show that networks trained under CE loss allow stable optimization at significantly larger learning rates in SP than under MSE loss, which recovers feature learning at large widths and consequently improves generalization. To empirically investigate this hypothesis, we compare the performance of CE and MSE losses under both SP and μ P. Since μ P admits asymptotically stable dynamics, both losses exhibit similar limiting behaviours. Thus we predict that CE loss only significantly outperforms MSE loss in SP, but not in μ P. Our empirical findings confirm this prediction (Figure 7), which suggests that MSE loss may deserve renewed consideration as a practical choice under stable parameterizations like μ P, especially given its theoretical simplicity and widespread use in theoretical analyses.

6 Discussion and future work

On the theoretical side, we have provided the first infinite-width proxy model for finite neural networks, as they are initialized and trained in practice. On the practical side, we have seen that infinite-width feature learning and instability predictions are surprisingly predictive indicators for empirical width-scaling exponents, in particular for deep Transformers.

Better understanding of the controlled divergence regime. Since practical neural networks operate at the edge of the controlled divergence regime, better understanding parameterizations beyond the stable regime from Yang and Hu (2021) is paramount. Since the NTK diverges in SP with $\eta_n = \Theta(n^{-1/2})$, studying this limit is subtle. However, investigating the rescaled NTK might still be a useful tool in better understanding this limit. While width dependence is undesirable from a transfer perspective, fast memorization under logit blowup may improve learning speed. How is generalization affected? Logit blowup may partially explain overconfidence in neural networks in SP, and suggests that wide networks in μ P may be more calibrated.

Numerical considerations. In this paper, we consider the regime of sufficient numerical precision. From a numerical perspective, signals that diverge fast can leave floating point range at moderate widths. Hence implementations that ensure minimal accumulation of width-dependent factors in SP akin to Blake et al. (2025) could stabilize large-scale model training in practice.

Understanding optimal learning rate exponents. The exact conditions that induce hyperparameter transfer are still poorly understood. Without full width-independence, the optimal learning rate scaling cannot be predicted with certainty. Both vanishing feature learning in input-like layers and

logit divergence can induce strong finite-width effects, so that we would still recommend μ P learning rates over SP from a width-scaling perspective. Similar to CE loss, normalization layers correct scaling in the forward pass. In combination with Adam which stabilizes the backward pass, such stabilizing components can correct most misscaled signals. Deeply understanding their interplay and effect on optimal learning rates remains an important direction for future work.

Acknowledgments and Disclosure of Funding

Funded by the Deutsche Forschungsgemeinschaft (DFG, German Research Foundation) under Germany’s Excellence Strategy – EXC number 2064/1 – Project number 390727645. The authors thank the International Max Planck Research School for Intelligent Systems (IMPRS-IS) for supporting Moritz Haas. Leena Chennuru Vankadara is supported by the Gatsby Charitable Foundation.

References

- Emmanuel Abbe, Enric Boix Adsera, and Theodor Misiakiewicz. Sgd learning on neural networks: leap complexity and saddle-to-saddle dynamics. In *The Thirty Sixth Annual Conference on Learning Theory (COLT)*, 2023. Cited on page 17.
- Jeremy Bernstein and Laker Newhouse. Modular duality in deep learning. *arXiv:2410.21265*, 2024. Cited on page 22.
- Stella Biderman, Hailey Schoelkopf, Quentin Gregory Anthony, Herbie Bradley, Kyle O’Brien, Eric Hallahan, Mohammad Aflah Khan, Shivanshu Purohit, USVSN Sai Prashanth, Edward Raff, et al. Pythia: A suite for analyzing large language models across training and scaling. In *International Conference on Machine Learning (ICML)*, 2023. Cited on page 30.
- Johan Bjorck, Alon Benhaim, Vishrav Chaudhary, Furu Wei, and Xia Song. Scaling optimal LR across token horizons. In *The Thirteenth International Conference on Learning Representations (ICLR)*, 2025. Cited on page 16.
- Charlie Blake, Constantin Eichenberg, Josef Dean, Lukas Balles, Luke Yuri Prince, Björn Deiseroth, Andres Felipe Cruz-Salinas, Carlo Luschi, Samuel Weinbach, and Douglas Orr. u - μ p: The unit-scaled maximal update parametrization. In *The Thirteenth International Conference on Learning Representations (ICLR)*, 2025. Cited on page 9, 17.
- Blake Bordelon and Cengiz Pehlevan. Self-consistent dynamical field theory of kernel evolution in wide neural networks. *Advances in Neural Information Processing Systems (NeurIPS)*, 35: 32240–32256, 2022. Cited on page 16.
- Blake Bordelon and Cengiz Pehlevan. Deep linear network training dynamics from random initialization: Data, width, depth, and hyperparameter transfer. *arXiv:2502.02531*, 2025. Cited on page 16.
- Blake Bordelon, Hamza Tahir Chaudhry, and Cengiz Pehlevan. Infinite limits of multi-head transformer dynamics. In *The Thirty-eighth Annual Conference on Neural Information Processing Systems (NeurIPS)*, 2024a. Cited on page 16.
- Blake Bordelon, Lorenzo Noci, Mufan Bill Li, Boris Hanin, and Cengiz Pehlevan. Depthwise hyperparameter transfer in residual networks: Dynamics and scaling limit. In *The Twelfth International Conference on Learning Representations (ICLR)*, 2024b. Cited on page 16.
- Tom Brown, Benjamin Mann, Nick Ryder, Melanie Subbiah, Jared D Kaplan, Prafulla Dhariwal, Arvind Neelakantan, Pranav Shyam, Girish Sastry, Amanda Askell, et al. Language models are few-shot learners. *Advances in Neural Information Processing Systems (NeurIPS)*, 33:1877–1901, 2020. Cited on page 1, 16, 48.
- Lenaic Chizat and Francis Bach. On the global convergence of gradient descent for over-parameterized models using optimal transport. *Advances in neural information processing systems*, 31, 2018. Cited on page 16.

- Lénaïc Chizat and Praneeth Netrapalli. The feature speed formula: a flexible approach to scale hyper-parameters of deep neural networks. In *The Thirty-eighth Annual Conference on Neural Information Processing Systems (NeurIPS)*, 2024. Cited on page 16.
- Lénaïc Chizat, Maria Colombo, Xavier Fernández-Real, and Alessio Figalli. Infinite-width limit of deep linear neural networks. *Communications on Pure and Applied Mathematics*, 77(10): 3958–4007, 2024. Cited on page 16.
- Aakanksha Chowdhery, Sharan Narang, Jacob Devlin, Maarten Bosma, Gaurav Mishra, Adam Roberts, Paul Barham, Hyung Won Chung, Charles Sutton, Sebastian Gehrmann, et al. Palm: Scaling language modeling with pathways. *Journal of Machine Learning Research*, 2023. Cited on page 8.
- Jeremy Cohen, Simran Kaur, Yuanzhi Li, J Zico Kolter, and Ameet Talwalkar. Gradient descent on neural networks typically occurs at the edge of stability. In *International Conference on Learning Representations (ICLR)*, 2021. Cited on page 2, 5, 17.
- Jeremy M Cohen, Behrooz Ghorbani, Shankar Krishnan, Naman Agarwal, Sourabh Medapati, Michal Badura, Daniel Suo, David Cardoze, Zachary Nado, George E Dahl, et al. Adaptive gradient methods at the edge of stability. *arXiv:2207.14484*, 2022. Cited on page 5, 17.
- Alex Damian, Eshaan Nichani, and Jason D. Lee. Self-stabilization: The implicit bias of gradient descent at the edge of stability. In *ICLR*, 2023. Cited on page 17.
- Francesco D’Angelo, Maksym Andriushchenko, Aditya Varre, and Nicolas Flammarion. Why do we need weight decay in modern deep learning? In *The Thirty-eighth Annual Conference on Neural Information Processing Systems (NeurIPS)*, 2024. Cited on page 17.
- Li Deng. The mnist database of handwritten digit images for machine learning research. *IEEE Signal Processing Magazine*, 29(6):141–142, 2012. Cited on page 30.
- Nolan Dey, Bin Claire Zhang, Lorenzo Noci, Mufan Li, Blake Bordelon, Shane Bergsma, Cengiz Pehlevan, Boris Hanin, and Joel Hestness. Don’t be lazy: Completex enables compute-efficient deep transformers. *arXiv:2505.01618*, 2025. Cited on page 16.
- Alexey Dosovitskiy, Lucas Beyer, Alexander Kolesnikov, Dirk Weissenborn, Xiaohua Zhai, Thomas Unterthiner, Mostafa Dehghani, Matthias Minderer, Georg Heigold, Sylvain Gelly, Jakob Uszkoreit, and Neil Houlsby. An image is worth 16x16 words: Transformers for image recognition at scale. In *International Conference on Learning Representations (ICLR)*, 2021. Cited on page 1.
- Katie Everett, Lechao Xiao, Mitchell Wortsman, Alexander A Alemi, Roman Novak, Peter J Liu, Izzeddin Gur, Jascha Sohl-Dickstein, Leslie Pack Kaelbling, Jaehoon Lee, et al. Scaling exponents across parameterizations and optimizers. *arXiv:2407.05872*, 2024. Cited on page 2, 3, 4, 8, 17, 18, 21, 45, 56, 57, 58, 59, 60, 61, 62.
- Gemma Team, Thomas Mesnard, Cassidy Hardin, Robert Dadashi, Surya Bhupatiraju, Shreya Pathak, Laurent Sifre, Morgane Rivière, Mihir Sanjay Kale, Juliette Love, et al. Gemma: Open models based on gemini research and technology. *arXiv:2403.08295*, 2024. Cited on page 8.
- Justin Gilmer, Behrooz Ghorbani, Ankush Garg, Sneha Kudugunta, Behnam Neyshabur, David Cardoze, George Edward Dahl, Zachary Nado, and Orhan Firat. A loss curvature perspective on training instabilities of deep learning models. In *International Conference on Learning Representations (ICLR)*, 2022. Cited on page 17.
- Eugene A. Golikov. Dynamically stable infinite-width limits of neural classifiers. *arXiv:2006.06574*, 2020. Cited on page 16.
- Aaron Grattafiori, Abhimanyu Dubey, Abhinav Jauhri, Abhinav Pandey, Abhishek Kadian, Ahmad Al-Dahle, Aiesha Letman, Akhil Mathur, Alan Schelten, Alex Vaughan, et al. The llama 3 herd of models. *arXiv:2407.21783*, 2024. Cited on page 1, 8.
- Moritz Haas, Jin Xu, Volkan Cevher, and Leena Chennuru Vankadara. μP^2 : Effective sharpness aware minimization requires layerwise perturbation scaling. In *The Thirty-eighth Annual Conference on Neural Information Processing Systems (NeurIPS)*, 2024. Cited on page 16.

- Soufiane Hayou and Greg Yang. Width and depth limits commute in residual networks. In *International Conference on Machine Learning (ICML)*, 2023. Cited on page 16.
- Bobby He, Lorenzo Noci, Daniele Paliotta, Imanol Schlag, and Thomas Hofmann. Understanding and minimising outlier features in transformer training. In *The Thirty-eighth Annual Conference on Neural Information Processing Systems (NeurIPS)*, 2024. Cited on page 17.
- Kaiming He, Xiangyu Zhang, Shaoqing Ren, and Jian Sun. Delving deep into rectifiers: Surpassing human-level performance on imagenet classification. In *IEEE international conference on computer vision (ICCV)*, 2015. Cited on page 1, 30.
- Jordan Hoffmann, Sebastian Borgeaud, Arthur Mensch, Elena Buchatskaya, Trevor Cai, Eliza Rutherford, Diego de Las Casas, Lisa Anne Hendricks, Johannes Welbl, Aidan Clark, et al. An empirical analysis of compute-optimal large language model training. *Advances in Neural Information Processing Systems (NeurIPS)*, 35:30016–30030, 2022. Cited on page 1, 16.
- Arthur Jacot, Franck Gabriel, and Clément Hongler. Neural Tangent Kernel: Convergence and generalization in neural networks. In *Advances in Neural Information Processing Systems (NeurIPS)*, 2018. Cited on page 16.
- Dayal Singh Kalra, Tianyu He, and Maissam Barkeshli. Universal sharpness dynamics in neural network training: Fixed point analysis, edge of stability, and route to chaos. In *The Thirteenth International Conference on Learning Representations (ICLR)*, 2025. Cited on page 26.
- Jared Kaplan, Sam McCandlish, Tom Henighan, Tom B Brown, Benjamin Chess, Rewon Child, Scott Gray, Alec Radford, Jeffrey Wu, and Dario Amodei. Scaling laws for neural language models. *arXiv:2001.08361*, 2020. Cited on page 1, 16.
- Atli Kosson, Bettina Messmer, and Martin Jaggi. Rotational equilibrium: How weight decay balances learning across neural networks. In *Forty-first International Conference on Machine Learning (ICML)*, 2024. Cited on page 17.
- Alex Krizhevsky, Geoffrey Hinton, et al. Learning multiple layers of features from tiny images. 2009. Cited on page 30.
- Daniel Kunin, Allan Raventos, Clémentine Carla Juliette Dominé, Feng Chen, David Klindt, Andrew M Saxe, and Surya Ganguli. Get rich quick: exact solutions reveal how unbalanced initializations promote rapid feature learning. In *The Thirty-eighth Annual Conference on Neural Information Processing Systems*, 2024. Cited on page 17, 30.
- Aitor Lewkowycz, Yasaman Bahri, Ethan Dyer, Jascha Sohl-Dickstein, and Guy Gur-Ari. The large learning rate phase of deep learning: the catapult mechanism. *arXiv:2003.02218*, 2020. Cited on page 2, 5, 17, 25, 26.
- Jeffrey Li, Alex Fang, Georgios Smyrnis, Maor Ivgi, Matt Jordan, Samir Yitzhak Gadre, Hritik Bansal, Etash Guha, Sedrick Scott Keh, Kushal Arora, et al. Datacomp-lm: In search of the next generation of training sets for language models. *Advances in Neural Information Processing Systems (NeurIPS)*, 37:14200–14282, 2024. Cited on page 7, 31.
- Lightning AI. Litgpt. <https://github.com/Lightning-AI/litgpt>, 2023. Cited on page 30.
- Liyuan Liu, Haoming Jiang, Pengcheng He, Weizhu Chen, Xiaodong Liu, Jianfeng Gao, and Jiawei Han. On the variance of the adaptive learning rate and beyond. In *International Conference on Learning Representations (ICLR)*, 2020. Cited on page 17.
- Peter J. Liu, Roman Novak, Jaehoon Lee, Mitchell Wortsman, Lechao Xiao, Katie Everett, Alexander A. Alemi, Mark Kurzeja, Pierre Marcenac, Izzeddin Gur, Simon Kornblith, Kelvin Xu, Gamaleldin Elsayed, Ian Fischer, Jeffrey Pennington, Ben Adlam, and Jascha Sohl-Dickstein. Nanodo: A minimal transformer decoder-only language model implementation in JAX. *GitHub repository*, 0.1.0, 2024. <http://github.com/google-deepmind/nanodo>. Cited on page 18.
- Ilya Loshchilov and Frank Hutter. Decoupled weight decay regularization. In *International Conference on Learning Representations (ICLR)*, 2019. Cited on page 7.

- Sam McCandlish, Jared Kaplan, Dario Amodei, and OpenAI Dota Team. An empirical model of large-batch training. *arXiv:1812.06162*, 2018. Cited on page 17.
- Song Mei, Andrea Montanari, and Phan-Minh Nguyen. A mean field view of the landscape of two-layer neural networks. *Proceedings of the National Academy of Sciences*, 115(33):E7665–E7671, 2018. Cited on page 16.
- Lorenzo Noci, Sotiris Anagnostidis, Luca Biggio, Antonio Orvieto, Sidak Pal Singh, and Aurelien Lucchi. Signal propagation in transformers: Theoretical perspectives and the role of rank collapse. *Advances in Neural Information Processing Systems (NeurIPS)*, 35:27198–27211, 2022. Cited on page 17.
- Lorenzo Noci, Chuning Li, Mufan Li, Bobby He, Thomas Hofmann, Chris J Maddison, and Dan Roy. The shaped transformer: Attention models in the infinite depth-and-width limit. *Advances in Neural Information Processing Systems (NeurIPS)*, 36, 2024a. Cited on page 16.
- Lorenzo Noci, Alexandru Meterez, Thomas Hofmann, and Antonio Orvieto. Super consistency of neural network landscapes and learning rate transfer. In *The Thirty-eighth Annual Conference on Neural Information Processing Systems (NeurIPS)*, 2024b. Cited on page 16.
- OLMo Team, Pete Walsh, Luca Soldaini, Dirk Groeneveld, Kyle Lo, Shane Arora, Akshita Bhagia, Yuling Gu, Shengyi Huang, Matt Jordan, et al. 2 olmo 2 furious. *arXiv:2501.00656*, 2024. Cited on page 1, 8.
- Elliot Paquette, Courtney Paquette, Lechao Xiao, and Jeffrey Pennington. 4+3 phases of compute-optimal neural scaling laws. In *The Thirty-eighth Annual Conference on Neural Information Processing Systems (NeurIPS)*, 2024. Cited on page 16.
- Adam Paszke, Sam Gross, Francisco Massa, Adam Lerer, James Bradbury, Gregory Chanan, Trevor Killeen, Zeming Lin, Natalia Gimelshein, Luca Antiga, Alban Desmaison, Andreas Kopf, Edward Yang, Zachary DeVito, Martin Raison, Alykhan Tejani, Sasank Chilamkurthy, Benoit Steiner, Lu Fang, Junjie Bai, and Soumith Chintala. Pytorch: An imperative style, high-performance deep learning library. In *Advances in Neural Information Processing Systems (NeurIPS)*, 2019. Cited on page 30.
- Dan Qiao, Kaiqi Zhang, Esha Singh, Daniel Soudry, and Yu-Xiang Wang. Stable minima cannot overfit in univariate relu networks: Generalization by large step sizes. In *The Thirty-eighth Annual Conference on Neural Information Processing Systems (NeurIPS)*, 2024. Cited on page 17.
- Yunwei Ren, Eshaan Nichani, Denny Wu, and Jason D Lee. Emergence and scaling laws in sgD learning of shallow neural networks. *arXiv:2504.19983*, 2025. Cited on page 17.
- Christopher J Shallue, Jaehoon Lee, Joseph Antognini, Jascha Sohl-Dickstein, Roy Frostig, and George E Dahl. Measuring the effects of data parallelism on neural network training. *arXiv:1811.03600*, 2018. Cited on page 17.
- Jascha Sohl-Dickstein, Roman Novak, Samuel S Schoenholz, and Jaehoon Lee. On the infinite width limit of neural networks with a standard parameterization. *arXiv:2001.07301*, 2020. Cited on page 2, 16.
- Alexander Tsigler, Luiz FO Chamon, Spencer Frei, and Peter L Bartlett. Benign overfitting and the geometry of the ridge regression solution in binary classification. *arXiv:2503.07966*, 2025. Cited on page 17.
- Leena Chennuru Vankadara, Jin Xu, Moritz Haas, and Volkan Cevher. On feature learning in structured state space models. In *The Thirty-eighth Annual Conference on Neural Information Processing Systems (NeurIPS)*, 2024. Cited on page 16, 31.
- Ashish Vaswani, Noam Shazeer, Niki Parmar, Jakob Uszkoreit, Llion Jones, Aidan N Gomez, Łukasz Kaiser, and Illia Polosukhin. Attention is all you need. *Advances in Neural Information Processing Systems (NeurIPS)*, 2017. Cited on page 2, 30.
- Roman Vershynin. Introduction to the non-asymptotic analysis of random matrices. *arXiv:1011.3027*, 2010. Cited on page 42.

- Nikhil Vyas, Alexander Atanasov, Blake Bordelon, Depen Morwani, Sabarish Sainathan, and Cengiz Pehlevan. Feature-learning networks are consistent across widths at realistic scales. *Advances in Neural Information Processing Systems (NeurIPS)*, 36, 2024. Cited on page 16, 17.
- Jonathan Wenger, Felix Dangel, and Agustinus Kristiadi. On the disconnect between theory and practice of overparametrized neural networks. *arXiv:2310.00137*, 2023. Cited on page 16.
- Mitchell Wortsman, Peter J Liu, Lechao Xiao, Katie E Everett, Alexander A Alemi, Ben Adlam, John D Co-Reyes, Izzeddin Gur, Abhishek Kumar, Roman Novak, Jeffrey Pennington, Jascha Sohl-Dickstein, Kelvin Xu, Jaehoon Lee, Justin Gilmer, and Simon Kornblith. Small-scale proxies for large-scale transformer training instabilities. In *The Twelfth International Conference on Learning Representations (ICLR)*, 2024. Cited on page 8, 17, 30, 46.
- Ruibin Xiong, Yunchang Yang, Di He, Kai Zheng, Shuxin Zheng, Chen Xing, Huishuai Zhang, Yanyan Lan, Liwei Wang, and Tieyan Liu. On layer normalization in the transformer architecture. In *International Conference on Machine Learning (ICML)*, 2020. Cited on page 17.
- Greg Yang. Wide feedforward or recurrent neural networks of any architecture are gaussian processes. *Advances in Neural Information Processing Systems (NeurIPS)*, 32, 2019. Cited on page 16.
- Greg Yang and Edward J. Hu. Tensor programs iv: Feature learning in infinite-width neural networks. In *International Conference on Machine Learning (ICML)*, 2021. Cited on page 2, 3, 9, 16, 19, 20, 21, 22, 24, 27, 57.
- Greg Yang and Etai Littwin. Tensor programs ivb: Adaptive optimization in the infinite-width limit. *arXiv:2308.01814*, 2023. Cited on page 3, 16, 23, 24.
- Greg Yang, Edward J Hu, Igor Babuschkin, Szymon Sidor, Xiaodong Liu, David Farhi, Nick Ryder, Jakub Pachocki, Weizhu Chen, and Jianfeng Gao. Tensor programs v: Tuning large neural networks via zero-shot hyperparameter transfer. *arXiv:2203.03466*, 2022. Cited on page 2, 16, 17, 18, 31.
- Greg Yang, James B. Simon, and Jeremy Bernstein. A spectral condition for feature learning. *arXiv:2310.17813*, 2023a. Cited on page 4, 16, 18, 31.
- Greg Yang, Dingli Yu, Chen Zhu, and Soufiane Hayou. Tensor programs vi: Feature learning in infinite-depth neural networks. *arXiv:2310.02244*, 2023b. Cited on page 16.
- Yang You, Jing Li, Sashank Reddi, Jonathan Hseu, Sanjiv Kumar, Srinadh Bhojanapalli, Xiaodan Song, James Demmel, Kurt Keutzer, and Cho-Jui Hsieh. Large batch optimization for deep learning: Training bert in 76 minutes. In *International Conference on Learning Representations (ICLR)*, 2020. Cited on page 17.
- Zixiong Yu, Songtao Tian, and Guhan Chen. Divergence of empirical neural tangent kernel in classification problems. *International Conference on Learning Representations (ICLR)*, 2025. Cited on page 16.
- Ruiqi Zhang, Jingfeng Wu, Licong Lin, and Peter L Bartlett. Minimax optimal convergence of gradient descent in logistic regression via large and adaptive stepsizes. *arXiv:2504.04105*, 2025. Cited on page 17.

Appendices

Appendix Contents.

A Detailed Related Work	16
B Take-aways for practitioners	18
C Theoretical considerations	19
C.1 Distilled TP scaling arguments	19
C.2 Measuring Alignment	21
C.3 Formal statements and proofs of Propositions 1 and 2	22
C.4 Scaling dynamics in 2-layer linear networks	25
D Experimental details	30
D.1 MLPs	30
D.2 Multi-index data	30
D.3 Language modeling	30
D.4 Figure Details	31
E Refined coordinate checks	31
E.1 SGD	32
E.2 Adam	38
E.3 Normalization layers and Adam provide robustness to miss-initialization	41
E.4 Alignment and update scaling in Transformers	42
F Empirical learning rate exponents	44
F.1 Summary of the MLP experiments in this section	44
F.2 Transformer experiments	45
F.3 Cross-entropy loss enables large-learning rate training	48
F.4 MLPs with SGD on MNIST	49
F.5 MLPs with ADAM on MNIST	51
F.6 MLPs with SGD on CIFAR-10	52
F.7 MLPs with ADAM on CIFAR-10	54
F.8 Effective update parameterizations beyond μP	56

A Detailed Related Work

Here we provide a more detailed account of related work than what is possible in the main body of the paper.

Neural networks in the infinite-width limit. Past work has extensively analysed the *Neural Tangent Parameterization (NTP)* (Jacot et al., 2018) due to its tractability. But due to lacking feature learning in the infinite-width limit, finite networks in NTP behave qualitatively differently and hence NTP is not the ideal model for understanding finite neural networks. Finite-width deviations already accumulate after a few steps of training (Wenger et al., 2023), in particular under CE loss (Yu et al., 2025). Considerable effort has been invested in finding a descriptive infinite-width model for SP. Sohl-Dickstein et al. (2020) note that the NTK diverges under large learning rates $\eta_n = \omega(n^{-1})$ in SP, which motivates them to consider a different parameterization which preserves a finite NTK in the infinite-width limit, but consequently does not correspond to SP anymore. Golikov (2020) studies a class of ‘dynamically stable’ parameterizations, allowing large learning rates under a variant of SP, they call ‘sym-default’ parameterization, which again is not equivalent SP. Another popular width-dependent parameterization is the Maximal Update Parameterization (μ P). It achieves a width-independent effect of updates in all trainable weights on the output function. Its infinite-width limit has been observed to closely track finite networks in μ P well over long periods of training in, for example, feature learning strength, the learned function, or gradient and Hessian statistics (Vyas et al., 2024, Noci et al., 2024b). As an important practical consequence, it allows to tune small proxy models and train the large model only once with the optimal HPs (Yang et al., 2022). μ P was derived using *Tensor Programs (TP)* framework (Yang, 2019, Yang and Hu, 2021, Yang and Littwin, 2023) that, in theory, allows to exactly track the learning dynamics of many popular architectures like MLPs, ResNets and Transformers trained with SGD or Adam in arbitrary parameterizations in the infinite-width limit. Haas et al. (2024) derive a μ P-like parameterization for sharpness aware minimization algorithms achieving transfer of the optimal learning rate and perturbation radius jointly by showing that perturbations should be scaled like updates in μ P. Vankadara et al. (2024) derive an initialization and learning rate scaling rule that achieves width-independent training dynamics for the state-space model Mamba, which shows that the spectral condition on the weights and weight updates in every layer for achieving μ P provided by Yang et al. (2023a) does not apply to arbitrary architectures. At sufficient numerical precision, the mean-field parameterization (Mei et al., 2018, Chizat and Bach, 2018) is equivalent to μ P. While it was initially restricted to shallow neural networks, the dynamical mean-field theory (DMFT) by Bordelon and Pehlevan (2022) generalizes it to more complex architectures, including Transformers (Bordelon et al., 2024a). Although still expensive, the approximate solvers from DMFT are more computationally feasible than iteratively solving the exact TP limit equations. Chizat et al. (2024) studies deep linear networks in μ P and shows convergence of gradient flow to a minimum l_2 -norm solution.

Other neural network scaling limits. Beyond width scaling, depth scaling $L \rightarrow \infty$ has been studied in detail. For ResNets, Yang et al. (2023b), Hayou and Yang (2023), Bordelon et al. (2024b) show that $L^{-1/2}$ -scaling of shallow residual blocks induces depth-independence and this limit commutes with width scaling, implying that depth can be scaled independent of width. Using approximative DMFT theory, Bordelon et al. (2024a) suggest that L^{-1} -depth scaling may be necessary to preserve feature learning in attention blocks although they consider a pure depth limit. Dey et al. (2025) confirm L^{-1} -block scaling to be the ‘correct’ scaling by providing additional desiderata and empirical evidence on Transformers. Bordelon et al. (2024a) also show that the infinite within-head dimension limit effectively leads to a single-head Transformer, as the infinite number of heads limit concentrates by aggregating over the coordinate distribution at fixed within-head size, closer to how scaling is typically performed in practice (Brown et al., 2020). Noci et al. (2024a) study a joint width and depth limit close to initialization for Transformers with the goal of preventing rank collapse. Long training time is much less understood. Bordelon and Pehlevan (2025) study the training dynamics of deep and wide linear networks trained on structureless Gaussian data. Chizat and Netrapalli (2024) considers the angle between activations and gradients to give scaling rules for hyperparameters toward automatic HP scaling. They correct output layer scaling of MLPs in μ P depth-dependently, only for SGD.

Scaling laws. Robust compute-optimal scaling laws in LLMs were reported by Kaplan et al. (2020), Hoffmann et al. (2022). Paquette et al. (2024) provide theory on random feature models trained with one-pass SGD and identify 4 phases and 3 subphases depending on properties of the data and the target. Bjorck et al. (2025) observe no transfer across token horizons but a predictable scaling

law with exponent -0.32 on LLama. [McCandlish et al. \(2018\)](#) suggests that the optimal learning rate scales as $a/(1 + b/batchsize)$ with setting-dependent constants a, b . Hence for sufficiently large batch size the optimal learning rate is roughly constant, which is in line with the empirical observations by [Shallue et al. \(2018\)](#), [Yang et al. \(2022\)](#). [Ren et al. \(2025\)](#) study SGD training of 2-layer MLPs on isotropic Gaussian data under MSELoss and find that different teacher neurons are abruptly learned at different timescales leading to a smooth scaling law in the cumulative objective. Further work toward assessing the compute-optimal and data-optimal Pareto frontiers under realistic assumptions remains an important and challenging task for future work.

Finite width training dynamics. Understanding finite-width training dynamics complements infinite-width theory very well, as the former line of work operates at fixed width, while the latter ask what changes with increasing width. From a practical perspective, scaling networks with μP appears to preserve the properties from base width ([Vyas et al., 2024](#), [Noci et al., 2022](#)). Deep understanding of neural network training dynamics is still limited to 2-layer nonlinear MLP ([Ren et al., 2025](#), [Zhang et al., 2025](#)) or (deep) linear MLP ([Kunin et al., 2024](#), [Tsigler et al., 2025](#)) toy models under strong distributional assumptions.

[Kunin et al. \(2024\)](#) explain for 2-layer networks that varying layerwise initialization variance and learning rate scaling induces differing learning regimes: fast feature learning in balanced parameterizations (desirable for linear nets), faster learning of earlier layers in upstream parameterizations with small parameter movement (desirable in nonlinear networks, as it reduces time to grokking and sample complexity of hierarchical data structures), faster learning of later layers in downstream initializations (that is initial lazy fitting followed by slow feature learning). [Abbe et al. \(2023\)](#) show that, opposed to lazy networks, feature learning networks can learn low rank spikes in hidden layer weights/kernels to help with sparse tasks. [Qiao et al. \(2024\)](#) show that large learning rates induce sparse linear spline fits in univariate gradient descent training by showing that all stable minima are flat, non-interpolating and produce small first order total variation, hence avoid overfitting and learn functions with bounded first order total variation

Edge of stability. Large learning rates have broadly been observed to induce optimal generalization. [Lewkowycz et al. \(2020\)](#) observe that under large learning rates at the edge of stability, $2/\lambda_0 < \eta < c_{arc}/\lambda_0$ (where $c_{arc} = 12$ for ReLU nets) an initial blowup at training time at least $\log(n)$ induces a bias towards flatter minima. ([Cohen et al., 2021](#)) find loss spikes during training, but that training self-stabilizes through sharpness reduction. [Damian et al. \(2023\)](#) develops some understanding of the mechanisms behind EOS dynamics. For Adam, the preconditioner matrix provides an additional mechanism by which stabilization can occur ([Cohen et al., 2022](#), [Gilmer et al., 2022](#)).

Warmup. Warmup allows stability under larger learning rates via slow sharpness reduction (?). ? also shows that warmup allows using larger learning rates than otherwise stable by constantly operating at the edge of stability. Warmup does not improve performance but stabilizes training; by allowing training with larger learning rates, these often induce improved performance. Large catapults harm Adam by persisting in its memory. Hence Adam’s optimal learning rate is further away from the failure boundary than for SGD, and Adam benefits more from longer warmup. Above the optimal learning rate, Adam has a regime of training failure, where early catapults persist in the second moment and prevent learning. Warmup also widens the regime of near-optimal learning rate choices. [Liu et al. \(2020\)](#) find that particularly Adam needs warmup due to large initial variance.

Effective learning rates. [Kosson et al. \(2024\)](#) study the effect of weight decay on rotation in weight vectors, which influences the effective learning rate. Also see references therein for literature on effective learning rates, which is related to the alignment discussion in this paper.

Stability of Transformer training. More empirically, a plethora of works study the training stability of large-scale Transformers with respect to warmup, weight decay ([D’Angelo et al., 2024](#)), batch size ([You et al., 2020](#)), the optimizer ([Kosson et al., 2024](#)), the position of normalization layers ([Xiong et al., 2020](#)) and their interplay with the parameterization and numerical considerations ([Wortsman et al., 2024](#), [Blake et al., 2025](#), [Everett et al., 2024](#)). [Wortsman et al. \(2024\)](#) find that qk-Layernorm stabilizes Transformer training beyond the stabilizing effect from using μP . [Xiong et al. \(2020\)](#) propose pre-LN for enhanced training stability requiring less warmup. [He et al. \(2024\)](#) observe that outlier features (=extremely activated coordinates in activations) emerge quickly in Transformer training with AdamW and that rank-collapse under strong correlations between inputs is correlated with more outlier features. Non-diagonal preconditioning like SOAP and Shampoo resolves the issue.

Most relevant to our work, [Everett et al. \(2024\)](#) perform extensive and insightful experiments for NanoDO decoder-only Transformers ([Liu et al., 2024](#)) in SP, μ P, NTP and mean field parameterizations with corrected layerwise learning rate scalings, questioning the infinite-width alignment predictions between weights and incoming activations at finite width over the course of long training. They recommend SP with ADAM in conjunction with μ P-learning rate scaling (they call SP-full-align) as the best-performing empirical parameterization in terms of generalization, learning rate transfer and learning rate sensitivity.

B Take-aways for practitioners

In this paper, the term *parameterization* refers to width-dependent scaling of initialization and learning rate of each trainable weight tensor separately. Studying parameterizations then means applying a scaling rule for layerwise initialization variances and learning rates and understanding how relevant quantities such as update scaling in activations and logits evolves, and where instabilities may arise at large widths. At some fixed base width, all parameterizations can be considered equivalent, if we allow tuning constant multipliers.

For properly comparing the performance of parameterizations, constant weight and initialization multipliers should be tuned at some fixed base width for each parameterization at base width separately ([Yang et al., 2022](#)). This adjusts the layerwise activation and gradient size at finite width. The parameterization then prescribes the rule, by which the layerwise initialization and updates are rescaled when changing the width in relation to that base width $\text{width}/\text{base_width}$. Alternatively, parameterizations may be equivalent at base width such that only one set of weight multipliers has to be tuned. The extensive LLM experiments in [Everett et al. \(2024\)](#) suggest that the advantage of large last-layer initialization may just be an artifact of the community extensively tuning performance in SP, and after also tuning all layerwise multipliers for μ P, the performance difference vanishes.

While SP performs better than naive theory would predict, and can learn hidden-layer features width-independently under CE loss, feature learning still vanishes in input-like layers like embedding or Layernorm layers under both SGD and Adam. Still only μ P learning rate scaling effectively updates all layers. Small last-layer initialization then recovers full width-independent and hence predictable scaling dynamics under sufficient precision in the regime $n \gg d_{\text{out}}$, whereas standard last-layer initialization induces logit blowup at sufficient width, which is not necessarily harmful for generalization but reduces predictability as scaling is not fully width-independent. Standard initialization with μ P learning rates (SP-full-align) can induce ‘practical transfer’ and empirically update all weights effectively without logit blowup at moderate scales $n \ll d_{\text{out}}$ in the regime where the width is much smaller than the output dimension, as is relevant for NLP settings, but likely exhibits unexpected changed behaviour at sufficient scale, when logits start to diverge due to the last-layer term $W_0^{L+1} \Delta x_t^L$. This can be read off from differing dominating terms in $\|W_0^{L+1}\|_{RMS \rightarrow RMS}$, assuming width-independent alignment $\alpha_{W_0^{L+1} \Delta x_t^L} = \Theta(1)$ as we measure. For uniform non-asymptotic transfer for both $n \gg d_{\text{out}}$ and $n \ll d_{\text{out}}$, by the same argument we suggest a last-layer initialization $\sigma_{L+1} = (\frac{\text{fan_in}}{\sqrt{\text{fan_out}}} + \sqrt{\text{fan_in}})^{-1}$, that transitions from SP initialization in the regime $n \ll d_{\text{out}}$ to μ P initialization in the regime $n \gg d_{\text{out}}$, as proposed in [Yang et al. \(2023a\)](#).

For AdamW without using width-dependent weight multipliers, layer-balancing μ P learning rates are simply given by the learning rate scaling $\eta(W) = \eta/\text{fan_in}(W)$. Here, all biases as well as normalization layer weights should be understood as weights to the one-dimensional input 1, hence $\text{fan_in} = 1$. For recovering width-independent weight decay, weight decay requires the inverse scaling $\text{wd} \cdot \text{fan_in}(W)$.

TP-like width scaling arguments are very useful for identifying sources of divergence or shrinkage with scale, and architecture components such as normalization layers and training algorithms such as Adam correct most *but not all* divergent or vanishing scalings in the forward and backward pass, respectively. Of particular importance for evaluating the width-dependent signal propagation is the refined coordinate check (RCC) for disentangling effective updates in the current layer from updates propagating forward through the network. Ideally, all $W_0 \Delta x_t^L$ and $\Delta W_t x_t$ should remain width-independent, which is only guaranteed in μ P at sufficient width.

C Theoretical considerations

C.1 Distilled TP scaling arguments

Here we aim to provide a more detailed, comprehensive introduction to the essential width-scaling arguments inspired by Tensor Program (TP) theory.

Effective Updates. When training neural networks, we have control over the initial scaling W_0 and update scaling ΔW_t of trainable weights $W_t = W_0 + \Delta W_t$, but we are ultimately interested in their effect on the activations in the following layers. In standard architectures (including convolutional networks and Transformers), weights typically act linearly on the incoming activations. For such weights W_t and incoming activations x_t , we can decompose the next layer’s (pre-)activation updates Δh_t into effective updates of W_t and activation updates Δx_t propagating forward from previous layers. Evaluating the contributions of both terms separately yields a *refined coordinate check*,

$$\Delta h_t = (\Delta W_t)x_t + W_0(\Delta x_t). \quad (\text{RCC})$$

Note that updates of previous layers can propagate forward through the term $W_0\Delta x_t$ even when the current layer’s effect on the output vanishes $\Delta W_t x_t \rightarrow 0$ as width $n \rightarrow \infty$. Hence, we say that the weight W_t is *effectively updated* only if $\Delta W_t x_t$ contributes non-vanishingly. Plotting the width-dependent scaling of $\|(\Delta W_t)x_t\|_{RMS}$ and $\|W_0(\Delta x_t)\|_{RMS}$ as a *refined coordinate check*, has been very useful for us to gain insights into the network internal signal propagation. The usefulness of (RCC) for effective update scalings is illustrated in Figure C.1. While the activations and activation updates in a Layernorm layer evolve width-independently when training GPT with Adam in SP and global learning rate scaled as $\eta_n = \eta \cdot n^{-1}$, the refined coordinate check reveals that the effective updates in the current (input-like) layer and the activation update scaling instead stems from effective updates propagating forward from previous (hidden-like) layers.

By choosing layerwise initialization variances and learning rates according to the Maximal Update Parameterization (μP), both terms in (RCC) become width-independent in all layers in each update step. Consequently, width-scaling becomes predictable, stable and feature learning is preserved even at large width. Starting from SP, μP can be realized with smaller last-layer initialization $\|W_0^{L+1}\|_{RMS} = O(n^{-1})$, larger input layer learning rate $\eta_{W^1} = \eta \cdot n$ and smaller last-layer learning rate $\eta_{W^{L+1}} = \eta \cdot n^{-1}$ for SGD.

Predicting scaling exponents. While the TP framework formally requires writing out all forward and backward pass computations performed during training and provides the exact infinite-width limit objects of output logits and activation coordinate distributions, we simplify its implications on width-scaling exponents for practical purposes as follows. A linear transformation either maps fixed to width-scaling dimension (*input-like*), width-scaling to width-scaling (*hidden-like*) or width-scaling to fixed dimension (*output-like*). Here, all bias vectors and normalization layer weights can be understood as input-like weights to the one-dimensional input 1. Any sum of length $n \rightarrow \infty$ that occurs in individual terms in (RCC) either accumulates a factor $n^{1/2}$ under sufficient independence of 0-mean summands (CLT-like behaviour) or a factor n when the summands are correlated or have non-zero mean (LLN-like behaviour). Crucially, not any sum may be evaluated with this heuristic but only weight and activation (update) pairs as in (RCC) (see Yang and Hu (2021, Appendix H)). If, for example, we considered the confounded term $(W_0 + \Delta W_t)x_0$, the initial part W_0x_0 clearly scales CLT-like but $\Delta W_t x_0$ scales LLN-like; evaluating the scaling of their sum might result in wrong scaling predictions.

At sufficient width, all width-scaling inner products $(\Delta W_t, x_t)$ from (RCC), however, are expected to behave LLN-like, that is $\|\Delta W_t x_t\|_{RMS} = \Theta(n \cdot \|\Delta W_t\|_{RMS} \cdot \|x_t\|_{RMS})$.

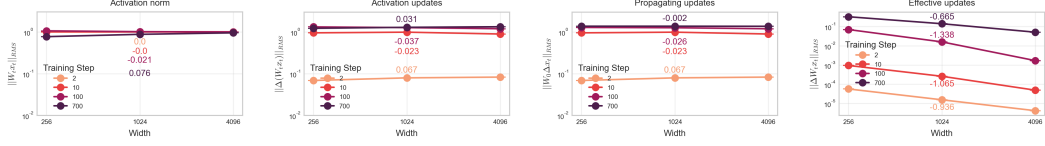


Figure C.1: **(Tracking effective updates requires refined coordinate check)** Activation norm $\|W_t x_t\|_{RMS}$, activation update norm $\|\Delta(W_t x_t)\|_{RMS}$, propagating update norm $\|W_0 \Delta x_t\|_{RMS}$ and effective update norm $\|\Delta W_t x_t\|_{RMS}$ for the last normalization layer in GPT trained with Adam and learning rate scaling $\eta_n = 0.01 \cdot n^{-1}$ for width-independent hidden layer feature learning. While activations and activation updates appear width-independent due to propagating updates, our refined coordinate check (RCC) reveals that Layernorm weight updates have vanishing effect in SP. Over time, effective updates accumulate effective rank, but do not lose alignment with width (Figure 2).

Concrete examples. Complementing the more generic introduction to TP scaling arguments above, we now provide more concrete examples for illustrating how weight updates affect activations in subsequent forward passes. Consider the Tensor Program for training MLPs with SGD from Yang and Hu (2021, Appendix H). We restate the relevant update scalings when using large learning rates in SP that induce output blowup. Since divergence is not allowed in the TP framework, it does not formally cover the unstable case, but we can still heuristically write down the scaling predictions, assuming that correlations still induce LLN-like exponents and independence still induces CLT-like exponents, as we have measured to hold empirically. The crucial insight is that training with cross-entropy loss effectively means that we are considering $f_t(\xi) = \sigma(W_t^{L+1} x_t^L(\xi))$ as the output function and the loss derivative also becomes $\chi_t := \frac{\partial \mathcal{L}_t}{\partial f} = \sigma(W_t^{L+1} x_t^L) - y_t$. Hence, from a stability point of view, we can allow $\tilde{f}_t := W^{L+1} x^L \rightarrow \infty$, which results in a saturated softmax. Under one-hot labels $y \in \{0, 1\}^C$ with $\sum_c y_c = 1$, this means fast memorization of training points (x_i, y_i) . For width-independent hidden-layer feature learning, we may still require activations to have width-independent coordinate-scaling, but let the output function be arbitrary, since the softmax renormalizes.

Definition C.1 (Activation stability). A parameterization is *activation stable* iff $\|x_t^l\|_{RMS} = \Theta(1)$ for all times $t \geq 0$ and all layers $l \in [L]$. ◀

We now show heuristically that MLPs trained with SGD in SP are activation stable and feature learning under global learning rate scaling $\eta = \Theta(n^{-1/2})$.

Backward pass. Here we denote the entry-wise scaling in width-scaling vectors as $v = \Theta(n^c)$, meaning $\|v\|_{RMS} = \Theta(n^c)$. Assuming $\|\phi'(h_t^l)\|_{RMS} = \Theta(1)$ as for ReLU (otherwise we would get vanishing gradients), the entries of the following width-scaling vectors scale as

$$\begin{aligned} \frac{\partial f}{\partial x_t^L} &= W_t^{L+1} = W_0^{L+1} - \Delta W_t^{L+1} = O(n^{-1/2}), & \frac{\partial f}{\partial h_t^L} &= \frac{\partial f}{\partial x_t^L} \odot \phi'(h_t^L) = \Theta\left(\frac{\partial f}{\partial x_t^L}\right), \\ \frac{\partial f}{\partial x_t^{l-1}} &= (W_0^l)^\top \frac{\partial f}{\partial h_t^l} - \eta \theta_{W^l} \sum_{s=0}^{t-1} \chi_s \frac{(\frac{\partial f}{\partial h_s^l})^\top \frac{\partial f}{\partial h_s^l}}{n} x_s^{l-1} = \Theta(\max(\frac{\partial f}{\partial h_t^l}, \eta (\frac{\partial f}{\partial h_s^l})^2 x_s^{l-1})) = \Theta(n^{-1/2}). \end{aligned}$$

Note that any larger learning rate scaling would induce exploding gradients. For example, $\eta = \Theta(1)$ induces $\delta W_1^{L+1} = \Theta(1)$, so $\frac{\partial f}{\partial x_1^L} = \Theta(1)$ and $\frac{\partial f}{\partial x_1^{L-k}} = \Theta(n \frac{\partial f}{\partial x_1^{L-k+1}}) = \Theta(n^{2k-1})$ for $k \geq 1$. This results in exploding activations in the next forward pass, and even larger gradients in the following backward pass.

We therefore continue with $\eta = \Theta(n^{-1/2})$, and get the activation updates

$$\begin{aligned} \delta h_t^1 &= -\eta \chi_{t-1} \frac{\partial f}{\partial h_{t-1}^1} (\xi_{t-1})^\top \xi = \Theta(n^{-1/2} \cdot 1 \cdot n^{-1/2} \cdot 1) = \Theta(n^{-1}), \\ \delta h_t^l &= W_{t-1}^l \delta x_t^{l-1} + \delta W_t^l x_t^{l-1} \end{aligned}$$

$$\begin{aligned}
&= \theta_x \left(W_0^l \delta x_t^{l-1} - \eta \theta_{W^l} \sum_s \chi_{s-1} \underbrace{\frac{\partial f}{\partial h_{s-1}^l}}_{\Theta(n)^{-1/2}} \underbrace{(x_{t-1}^{l-1})^\top \delta x_t^{l-1}}_{O(n)} \right) \\
&\quad - \eta \chi_{t-1} \theta_W \underbrace{\frac{\partial f}{\partial h_{t-1}^l}}_{\Theta(n)^{-1/2}} \underbrace{(x_{t-1}^{l-1})^\top x_t^{l-1}}_{\Theta(n)} = \Theta(1),
\end{aligned}$$

The output updates are

$$\begin{aligned}
\delta \tilde{f}_t(\xi) &= \delta W_t^{L+1} x_t^L(\xi) + (W_0^{L+1} + \Delta W_{t-1}^{L+1}) \delta x_t^L(\xi) \\
&= -\eta \chi_{t-1} \underbrace{x_{t-1}^L x_t^L(\xi)}_{\Theta(n)} + \underbrace{W_0^{L+1} \delta x_t^L(\xi)}_{\Theta(1)} + \underbrace{\Delta W_{t-1}^{L+1} \delta x_t^L(\xi)}_{\Theta(n^{1/2})} = \Theta(n^{1/2}), \\
\delta f_t(\xi) &= \sigma(\tilde{f}_{t-1} + \delta \tilde{f}_t) - \sigma(\tilde{f}_{t-1}) = \Theta(1).
\end{aligned}$$

2 layer networks. Observe that in 2 layer nets, there are no hidden layers, so that a larger learning rate can be chosen. Let $\eta = \Theta(n^c)$. Then in the first step, $\delta h_1^1 = \Theta(\eta \frac{\partial f}{\partial h_0^1}) = \Theta(n^c n^{-1/2})$.

But note that the gradient scaling may grow after the first step, $\frac{\partial f}{\partial x_t^1} = W_1^{L+1} = \Theta(n^c)$, so that $\delta h_2^1 = \Theta(n^c n^c)$. Hence activation stability requires $\eta = O(1)$, which results in feature learning after 2 steps $\delta x_2^1 = \Theta(1)$. Then $\tilde{f}_t = \Theta(\eta (x_{t-1}^L)^\top x_t^L(\xi)) = \Theta(n)$.

Random feature models. In random feature models, we only train the last layer and keep all other weights fixed $W_t^l = W_0^l$ for all $l \leq L$. There, by definition, we do not get feature learning and the backward pass does not matter. The only gradient that matters is the last-layer gradient which has fixed scaling $\Theta(\chi_{t-1} x_{t-1}^L) = \Theta(1)$ at all times $t \geq 0$. The function update becomes $\delta W_t^{L+1} x^L(\xi) = -\eta \chi_{t-1} (x^L(\xi_{t-1}))^\top x^L(\xi) = \Theta(n^c n)$, where the inner product between activations converges to the NNGP kernel in the infinite-width limit. Hence large learning rates $\eta = \omega(n^{-1})$ result in immediate extreme memorization of the training points $f_t(\xi_{t-1}) \rightarrow \text{one-hot}(y_{t-1})$ as $n \rightarrow \infty$, and $\eta_n = \Theta(n^{-1})$ results in fully width-independent dynamics.

Adam. Adam with small enough ε normalizes the gradients in each layer before updating the weights. Since the gradients $\nabla_{W^l} \mathcal{L} = \chi \frac{\partial f}{\partial h^l} (x^{l-1})^\top$ are generally correlated with the incoming activations x^{l-1} , their inner product accumulates $\Theta(\text{fan_in})$. Non-vanishing correlation persists when only recovering the signs of the gradient. Hence for a width-independent effect on the output of the current layer, the learning rate should always be chosen as $\eta(W) = \frac{\eta}{\text{fan_in}(W)}$. Since both hidden and output layers have $\text{fan_in} = n$, activation stability requires a global learning rate $\eta = O(n^{-1})$, which results in effective hidden and output layer learning, but vanishing input layer updates. Networks recover input layer feature learning under $\eta = \Theta(1)$, where $\tilde{f}_t = \Theta(n)$. In random feature models, η just determines the extremeness of memorization of the training labels, where $\eta = \Theta(n^{-1})$ induces width-independence and $\eta = \omega(n^{-1})$ increasing memorization.

C.2 Measuring Alignment

Everett et al. (2024, Fig. 2) provides RMS-alignment exponents between weights W_t and incoming activations x_t . But only measuring the alignment between ΔW_t and x_t as well as W_0 and Δx_t from (RCC) separately allows to evaluate the width-scaling predictions from Yang and Hu (2021). For example hidden layers in μP scale as $(W_0^l)_{ij} = \Theta(n^{-1/2})$ at initialization, as 0-mean independence induces CLT-like scaling $W_0^l x_0^{l-1} = \Theta(n^{1/2} \cdot \|W_0^l\|_{RMS} \cdot \|x_0^{l-1}\|_{RMS})$. But updates are correlated with incoming activations, so that $\Delta W_t x_t = \Theta(n \cdot \|\Delta W_t\|_{RMS} \cdot \|x_t\|_{RMS})$ which necessitates $\|\Delta W_t\|_{RMS} = \Theta(n^{-1})$. This implies that the entry size of $W_t = W_0 + \Delta W_t$ is dominated by the initialization and confounds $\|W_t\|_{RMS}$ for accurately measuring the alignment exponent of the layer's updates ΔW_t . For correct width-scaling of the layer's learning rate, the influence of W_0 is irrelevant so that the joint alignment between W_t and x_t does not reveal the alignment exponent

that is relevant for correct learning rate scaling. Additionally, replacing the RMS-norm $\|A\|_{RMS}$ by the operator norm $\|\Delta W_t\|_{RMS \rightarrow RMS}$ provides a more natural measure of alignment (Bernstein and Newhouse, 2024), since the RMS-norm is confounded by accumulated rank whereas under maximal alignment for the operator norm it holds that $\|\Delta W_t x_t\|_{RMS} = \|\Delta W_t\|_{RMS \rightarrow RMS} \|x_t\|_{RMS}$, and the left-hand side is smaller under less alignment. Under perfect alignment we expect the ratio $\frac{\|\Delta W_t x_t\|_{RMS}}{\|\Delta W_t\|_{RMS \rightarrow RMS} \|x_t\|_{RMS}}$ to remain width-independent. We are not interested in constant prefactors, but only width-dependent scaling.

C.3 Formal statements and proofs of Propositions 1 and 2

Before providing the full formal statements of Proposition 1 and Proposition 2, we formally introduce all definitions and assumptions.

C.3.1 Definitions

In this section, we collect all definitions that do not appear in the main text. We adopt all definitions from Yang and Hu (2021), up to minor modifications. If not stated otherwise, limits are taken with respect to width $n \rightarrow \infty$.

Definition C.2 (Big-O Notation). Given a sequence of scalar random variables $c = \{c_n \in \mathbb{R}\}_{n=1}^\infty$, we write $c = \Theta(n^{-a})$ if there exist constants $A, B \geq 0$ such that for almost every instantiation of $c = \{c_n \in \mathbb{R}\}_{n=1}^\infty$, for n large enough, $An^{-a} \leq |c_n| \leq Bn^{-a}$. Given a sequence of random vectors $x = \{x_n \in \mathbb{R}^n\}_{n=1}^\infty$, we say x has coordinates of size $\Theta(n^{-a})$ and write $x = \Theta(n^{-a})$ to mean the scalar random variable sequence $\left\{ \sqrt{\|x_n\|^2/n} \right\}_n$ is $\Theta(n^{-a})$. For the definition of $c = O(n^{-a})$ and $c = \Omega(n^{-a})$, adapt the above definition of $c = \Theta(n^{-a})$ by replacing $An^{-a} \leq |c_n| \leq Bn^{-a}$ with $|c_n| \leq Bn^{-a}$ and $An^{-a} \leq |c_n|$, respectively. We write $x_n = o(n^{-a})$ if $n^a \cdot \sqrt{\|x_n\|^2/n} \rightarrow 0$ almost surely. ◀

Definition C.3 (SGD update rule). Given a $(L+1)$ -layer MLP with layerwise initialization variances $\{\sigma_l\}_{l \in [L+1]}$ and (potentially) layerwise learning rates $\{\eta_{W^l}\}_{l \in [L+1]}$, we define the *SGD update rule* as follows:

- (a) Initialize weights iid as $(W_0^l)_{ij} \sim \mathcal{N}(0, \sigma_l^2)$.
- (b) Update the weights via

$$W_{t+1}^l = W_t^l - \eta_{W^l} \cdot \nabla_{W^l} \mathcal{L}(f_t(\xi_t), y_t).$$

Definition C.4 (Parameterization). We define a *width-scaling parameterization* as a collection of exponents $\{b_l\}_{l \in [L+1]} \cup \{c_l\}_{l \in [L+1]}$ that determine layerwise initialization variances $\sigma_l^2 = c_l \cdot n^{-b_l}$ and layerwise learning rates $\eta_l = \eta \cdot n^{-c_l}$, with width-independent constants $c_l, \eta > 0$ for all $l \in [L+1]$. ◀

Definition C.5 (Training routine). A *training routine* is a combination of base learning rate $\eta \geq 0$, training sequence $\{(\xi_t, y_t)\}_{t \in \mathbb{N}}$ and a continuously differentiable loss function $\mathcal{L}(f(\xi), y)$ using the SGD update rule. ◀

Definition C.6 (Stability). We say a parametrization of a $(L+1)$ -layer MLP is *stable* if

1. For every nonzero input $\xi \in \mathbb{R}^{d_{in}} \setminus \{0\}$,

$$h_0^l, x_0^l = \Theta_\xi(1), \quad \forall l \in [L], \quad \text{and} \quad \mathbb{E} f_0(\xi)^2 = O_\xi(1),$$

where the expectation is taken over the random initialization.

2. For any training routine, any time $t \in \mathbb{N}$, $l \in [L]$, $\xi \in \mathbb{R}^{d_{in}}$, we have

$$h_t^l(\xi) - h_0^l(\xi), x_t^l(\xi) - x_0^l(\xi) = O_*(1), \quad \text{and} \quad f_t(\xi) = O_*(1),$$

where the hidden constant in O_* can depend on the training routine, t, ξ, l and the initial function f_0 . ◀

Definition C.7 (Nontriviality). We say a parametrization is *trivial* if for every training routine, $f_t(\xi) - f_0(\xi) \rightarrow 0$ almost surely for $n \rightarrow \infty$, for every time $t > 0$ and input $\xi \in \mathbb{R}^{d_{in}}$. Otherwise the parametrization is *nontrivial*. ◀

Definition C.8 (Feature learning). We say a parametrization *admits feature learning in the l -th layer* if there exists a training routine, a time $t > 0$ and input ξ such that $x_t^l(\xi) - x_0^l(\xi) = \Omega_*(1)$, where the constant may depend on the training routine, the time t , the input ξ and the initial function f_0 but not on the width n . ◀

Definition C.9 (σ -gelu). Define σ -gelu to be the function $x \mapsto \frac{x}{2} (1 + \operatorname{erf}(\sigma^{-1}x)) + \sigma \frac{e^{-\sigma^{-2}x^2}}{2\sqrt{\pi}}$. ◀

In order to apply the Tensor Program Master Theorem, all Nonlin and Moment operations in the NE \otimes OR \top program (Yang and Littwin, 2023), which do not only contain parameters as inputs, are required to be pseudo-Lipschitz in all of their arguments. For training with SGD, this is fulfilled as soon as ϕ' is pseudo-Lipschitz. σ -gelu fulfills this assumption.

Definition C.10 (Pseudo-Lipschitz). A function $f : \mathbb{R}^k \rightarrow \mathbb{R}$ is called *pseudo-Lipschitz of degree d* if there exists a $C > 0$ such that $|f(x) - f(y)| \leq C\|x - y\|(1 + \sum_{i=1}^k |x_i|^d + |y_i|^d)$. We say f is *pseudo-Lipschitz* if it is so for any degree d . ◀

C.3.2 Full formal statements of Propositions 1 and 2

Assumptions. For all of the results in this section, we assume that the used activation function is σ -gelu for $\sigma > 0$ sufficiently small. For small enough $\sigma > 0$, σ -gelu (Definition C.9) approximates ReLU arbitrarily well. We assume constant training time $t \geq 1$ as width $n \rightarrow \infty$. We assume batch size 1 for clarity, but our results can be extended without further complications to arbitrary fixed batch size.

Proposition C.11. (Asymptotic regimes in SP) For fixed $L \geq 2$, $t \geq 1$, $\eta > 0$, $\alpha \in \mathbb{R}$, consider training a $(L + 1)$ -layer MLP of width n in SP with SGD and global learning rate $\eta_n = \eta \cdot n^{-\alpha}$ for t steps. Then the logits f_t , training loss $\mathcal{L}(f_t(\xi_t), y_t)$, loss-logit derivatives $\chi_t := \partial_f \mathcal{L}(f_t(\xi_t), y_t)$, loss-weight gradients $\nabla_t^l := \nabla_{W^l} \mathcal{L}(f_t(\xi_t), y_t)$ and activations x_t^l , $l \in [L]$, after training scale as follows in the infinite-width limit $n \rightarrow \infty$. The hidden constants in O_* , Ω_* and ω_* below can depend on the training routine, t , ξ , l and the initial function f_0 .

Under cross-entropy (CE) loss, three qualitatively distinct regimes arise:

- (a) **Stable regime** ($\alpha \geq 1$): For any training routine, all $l \in [L]$ and any $\xi \in \mathbb{R}^{d_{in}}$, it holds that $\|f_t(\xi)\|_{RMS} = O_*(1)$, $|\mathcal{L}(f_t(\xi_t), y_t)| = O_*(1)$, $\|\chi_t\|_{RMS} = O_*(1)$, $\|\nabla_t^l\|_{RMS} = O_*(n^{-1/2})$ and $\|x_t^l(\xi)\|_{RMS} = O_*(1)$.
- (b) **Controlled divergence** ($\frac{1}{2} \leq \alpha < 1$): For any training routine, all $l \in [L]$ and any $\xi \in \mathbb{R}^{d_{in}}$, it holds that $\|n^{\alpha-1} \cdot f_t(\xi)\|_{RMS} = O_*(1)$, $\|x_t^l(\xi) - x_0^l(\xi)\|_{RMS} = O_*(1)$, $|\mathcal{L}(f_t(\xi_t), y_t)| = O_*(1)$, $\|\chi_t\|_{RMS} = O_*(1)$ and $\|\nabla_t^l\|_{RMS} = O_*(n^{-1/2})$. In addition, there exists a training routine and input ξ such that $\|n^{\alpha-1} \cdot f_t(\xi)\|_{RMS} = \Omega_*(1)$.
- (c) **Catastrophic instability** ($\alpha < \frac{1}{2}$): For any $l \in [L]$, there exists a training routine and a $\xi \in \mathbb{R}^{d_{in}}$, such that $\|f_t(\xi)\|_{RMS} = \omega_*(1)$, $\|x_t^l(\xi)\|_{RMS} = \omega_*(1)$ and $\|\nabla_t^l\|_{RMS} = \omega_*(1)$.

Under mean-squared error (MSE) loss, a stable regime as in (a) above arises if $\alpha \geq 1$. If $\alpha < 1$, training is catastrophically unstable as in (c) above and, in addition, there exists a training routine such that $|\mathcal{L}(f_t(\xi_t), y_t)| = \omega_*(1)$ and $\|\chi_t\|_{RMS} = \omega_*(1)$.

Proposition C.12 (Under CE loss, SP with large learning rates learns features at large width). Consider the setting of Proposition 1 of training a $(L+1)$ -layer MLP with SGD in SP with global learning rate $\eta_n = \eta \cdot n^{-\alpha}$, $\alpha \in \mathbb{R}$, in the infinite-width limit $n \rightarrow \infty$. The hidden constants in O_* , Ω_* and ω_* below can depend on the training routine, t , ξ , l and the initial function f_0 .

- (a) Under both MSE and CE loss in the stable regime ($\alpha \geq 1$), for any training routine, $l \in [L]$ and $\xi \in \mathbb{R}^{d_{in}}$ it holds that $\|\Delta x_t^l(\xi)\|_{RMS} = O_*(n^{-1/2})$.
- (b) Under CE loss in the controlled divergence regime ($\frac{1}{2} \leq \alpha < 1$), for any training routine, $l \in [L]$ and $\xi \in \mathbb{R}^{d_{in}}$ it holds that $\|\Delta x_t^l(\xi)\|_{RMS} = O_*(n^{-1/2-\alpha})$, and $\|\Delta x_t^l(\xi)\|_{RMS} = O_*(n^{1/2-\alpha})$. For any $l \in [L]$, there exists a training routine and $\xi \in \mathbb{R}^{d_{in}}$ such that $\|\Delta x_t^l(\xi)\|_{RMS} = \Omega_*(n^{-1/2-\alpha})$, and $\|\Delta x_t^l(\xi)\|_{RMS} = \Omega_*(n^{1/2-\alpha})$.

Remark C.13 (2-layer networks recover stable training dynamics and width-independent feature learning at $\alpha = 0$). Similarly, it can be shown that 2-layer MLPs remain activation stable under width-independent learning rate scaling $\eta_n = \Theta(1)$. The controlled divergence regime is given by $0 \leq \alpha < 1/2$, with width-independent input layer feature learning at $\alpha = 0$. ◀

Remark C.14 (Adam recovers stable training dynamics and width-independent hidden-layer feature learning at $\alpha = 1$). For Adam and $L \geq 2$, an analogous NE \otimes ORT-based proof (Yang and Littwin, 2023) would show that $\eta_n = \Theta(n^{-1})$ recovers feature learning in all hidden layers $l \in [2, L]$, stable activations and loss-logit gradients, while logits blow up only through $W_0^{L+1} \Delta x_t^L = \Theta(n^{1/2})$. To avoid logit blowup, $\eta_n = \Theta(n^{-3/2})$ would be necessary. In that case, only the term $W_0^{L+1} \Delta x_t^L$ would contribute non-vanishingly to the logit updates. Hence, for Adam under CE loss, the controlled divergence regime is given by $1 \leq \alpha < 3/2$, with hidden-layer feature learning at $\alpha = 1$. ◀

C.3.3 Proof of Propositions 1 and 2

The proof in Yang and Hu (2021) for general stable abc -parameterizations directly covers the stable regimes of both losses, showing a kernel regime and vanishing feature learning for $\alpha \geq 1$.

For the controlled divergence regime under CE loss, however, note that the TP framework does not allow diverging computations. Here, we need to replace the logit updates by rescaled logit updates, before computing the softmax limit outside of the TP framework.

Formally, under standard initialization, $W_0^{L+1} \sim N(0, 1/n)$ is replaced in the TP by $\hat{W}_\varepsilon^{L+1}$ constructed via Nonlin, conditioning on $f_0(\xi)$ (see Yang and Hu (2021, Appendix H) for all details). For stable parameterizations, the function updates are defined in the TP as

$$\delta \hat{f}_t = \theta'_{L+1} \frac{\delta W_t^{L+1} x_t^L}{n} + \theta'_{L_f} \frac{\hat{W}_{t-1}^{L+1} \delta x_t^L}{n},$$

where $\theta'_{L+1} = n^{1-\alpha}$ and $\theta'_{L_f} = n^{1-r-b_{L+1}}$. In the controlled divergence regime $\alpha < 1$, we now define rescaled logit updates in the TP as

$$\delta \hat{f}_t = \hat{\theta}_{L+1} \frac{\delta W_t^{L+1} x_t^L}{n} + \hat{\theta}_{L_f} \frac{\hat{W}_{t-1}^{L+1} \delta x_t^L}{n},$$

by replacing θ'_{L+1} by $\hat{\theta}_{L+1} := \theta_\alpha \theta'_{L+1}$ and replacing θ'_{L_f} by $\hat{\theta}_{L_f} := \theta_\alpha \theta'_{L_f}$, where $\theta_\alpha := n^{\alpha-1}$. The adapted pre-factors ensure that $\delta \hat{f}$ remains $O_*(1)$ for a well-defined TP. The TP master theorem now implies almost sure convergence of the rescaled logit updates $\delta \hat{f}_t \rightarrow \delta \hat{f}_t \in \mathbb{R}^{d_{\text{out}}}$ a.s.

Now we compute the softmax limit outside of the TP framework, as we want to recover the softmax values of the original diverging logits. Thus, given the convergent sequence $\delta \hat{f}_t \rightarrow \delta \hat{f}_t \in \mathbb{R}^{d_{\text{out}}}$ a.s., due to the smoothness and saturation properties of the softmax it follows that there exists a $\hat{\chi}_t \in \mathbb{R}^{d_{\text{out}}}$ such that $\sigma(\theta_\alpha^{-1} \cdot \delta \hat{f}_t) - y_t \rightarrow \hat{\chi}_t$ a.s. Since $|\sigma(\theta_\alpha^{-1} \cdot \delta \hat{f}_t) - y_t| \leq 1 + |y_t|$ and $|\hat{\chi}_t| \leq 1 + |y_t|$, this sequence can again be used as a TP scalar. Now the last-layer weights are TP vectors updated with $\delta W_t^{L+1} = -\eta_n \chi_t x_t^L$ which do not change the scaling of $\hat{W}_t^{L+1} = \hat{W}_{t-1}^{L+1} + \theta_{L+1/f} \cdot \delta W_1^{L+1}$ with $\theta_{L+1/f} \leq 1$ as long as $\alpha \geq 1/2$. Thus the backward pass scalings are not affected and the rest of the TP can remain unchanged.

For larger learning rates $\alpha < 1/2$ under CE loss, we provide heuristic scaling arguments. Observe that preactivations diverge after the first update step $\delta h_1^2 = -\eta_n \frac{\partial f_0}{\partial h^2}(x_0^1)^\top x_1^1 = \Theta(n^{1/2-\alpha})$. The updates of the next hidden layer's preactivations scale even larger, that is $\delta h_1^3 = -\eta_n \frac{\partial f_0}{\partial h^3}(x_0^2)^\top x_1^2 = \Theta(n^{2(1/2-\alpha)})$. In this way, the exponent growth continues throughout the forward pass. But even if there is only a single hidden layer, the scaling of the backpropagated gradient is increased after the second step, $\frac{\partial f_2}{\partial x^L} = W_0 - \eta_n \chi_0 x_0^L - \eta_n \chi_1 x_1^L = \Omega(\eta_n \chi_1 \delta x_1^L) = \Omega(n^{1/2-2\alpha}) = \omega(n^{-1/2})$. This, in turn, increases the preactivation update scaling $\delta h_3^2 = -\eta_n \frac{\partial f_2}{\partial h^2}(x_2^1)^\top x_3^1 = \Omega(n^{-\alpha} \frac{\partial f_2}{\partial x^L} n) = \Omega(n^{3(1/2-\alpha)})$, which in turn increases the gradient scaling in the next step, inducing a feedback loop of cascading exponents between diverging activations and gradients, inducing fast training divergence.

Under MSELoss, observe how, already for $\alpha < 1$, diverging logits $\delta f_1 = W_0^{L+1} \delta x_1^L - \eta_n \chi_0 (x_0^L)^\top x_0^L = \Theta(n^{1-\alpha})$ increase the gradient scaling through $\chi_1 = f_1 - y_1 = \Theta(n^{1-\alpha})$ which in

turn increases the activation as well as logit scaling in the next step, and induces a divergent feedback loop even worse than above.

C.4 Scaling dynamics in 2-layer linear networks

Here, we rederive the training dynamics of the minimal model from Lewkowycz et al. (2020) that shows an initial catapult mechanism in NTP. They observe that the training dynamics of repeatedly updating a 2-layer linear network in NTP on the same training point is fully captured by update equations of the current function output f_t and the current sharpness λ_t .

C.4.1 Deriving the update equations for SP, NTP and μP

NTP. The original model by Lewkowycz et al. (2020) is given by

$$f = n^{-1/2}vux,$$

where $u \in \mathbb{R}^{n \times d}$, $v \in \mathbb{R}^n$ are initialized as $u_{ij}, v_i \sim N(0, 1)$ and trained with MSE loss $L(f, x, y) = \frac{1}{2}(f(x) - y)^2$, loss derivative $\chi_t = f(x) - y$ and a global learning rate η .

Repeated gradient descent updates using (x, y) , then results in the update equations,

$$\begin{aligned} f_{t+1} &= f_t(1 + n^{-1}\eta^2\chi^2\|x\|^2) - \eta\chi_t\lambda_t, \\ \lambda_{t+1} &= \lambda_t + n^{-1}\eta\chi_t\|x\|^2(\eta\chi_t\|x\|^2\lambda_t - 4f_t), \end{aligned}$$

where the *update kernel* is defined as

$$\tilde{\Theta}(x, x') = n^{-1}(\|u\|^2 + \|v\|^2).$$

Note that the width-dependence in f_t and λ_t results in qualitatively different behaviour in the infinite-width limit. In particular, in the limit, the sharpness cannot evolve over the course of training, $\lambda_t = \lambda_0$.

Maximal Update Parameterization. We define a 2-layer linear network in μP with arbitrary weight multipliers as

$$f = \bar{v}\bar{u}x,$$

with *reparameterization-invariant weights* $\bar{u}_{ij} \sim N(0, 1/d_{in})$ and $\bar{v}_i \sim N(0, 1/n^2)$, $\bar{u} = n^{-a_u}u$, $\bar{v} = n^{-a_v}v$, and the *original weights* u, v are trained with MSE loss and layerwise learning rates $\eta_u = \eta n^{1+2a_u}$ and $\eta_v = \eta n^{-1+2a_v}$, which results in reparameterization-invariant layerwise learning rates $\bar{\eta}_u = \eta n$ and $\bar{\eta}_v = \eta n^{-1}$.

Formally, we now perform updates on u and v , but we can work with \bar{u} and \bar{v} instead. For gradients it holds that $\frac{\partial f}{\partial u} = \frac{\partial f}{\partial \bar{u}} \frac{\partial \bar{u}}{\partial u} = \frac{\partial f}{\partial \bar{u}} n^{-a_u}$; this width scaling has to be accounted for when transitioning between representatives of the μP equivalence class. For updates $\bar{\eta}_u, \bar{\eta}_v$ should be used instead of η_u, η_v , as the layerwise learning rate rescaling was exactly chosen to cancel out the effect of the weight rescaling,

$$\bar{u}_{t+1} - \bar{u}_t = -n^{-a_u}\eta_u \frac{\partial f}{\partial \bar{u}} \frac{\partial \bar{u}}{\partial u} = -n^{-2a_u}\eta_u \frac{\partial f}{\partial \bar{u}} = -\bar{\eta}_u \frac{\partial f}{\partial \bar{u}}.$$

The derivatives for backpropagation are given by,

$$\chi_t := \frac{\partial L}{\partial f} = f(x_t) - y_t, \quad \frac{\partial f}{\partial \bar{v}} = x^\top \bar{u}^\top, \quad \frac{\partial f}{\partial \bar{u}} = \bar{v}^\top x^\top.$$

The updated weights are then given by

$$\bar{v}_{t+1} = \bar{v}_t - \eta n^{-1}\chi_t x^\top \bar{u}^\top, \quad \bar{u}_{t+1} = \bar{u}_t - \eta n \chi_t \bar{v}^\top x^\top.$$

In the case $d_{in} = 1$, the updated function is then given by

$$\begin{aligned} f_{t+1} &= \bar{v}_{t+1}\bar{u}_{t+1}x = f_t + \eta^2\chi_t^2x^\top \bar{u}^\top \bar{v}^\top x^\top x - \bar{\eta}_u\chi_t\bar{v}\bar{v}^\top x^\top x - \bar{\eta}_v\chi_t x^\top \bar{u}^\top \bar{u}x \\ &= f_t(1 + \eta^2\chi_t^2\|x\|^2) - \eta\chi_t(n\|\bar{v}\|^2 + n^{-1}\|\bar{u}\|^2)\|x\|^2 \end{aligned}$$

$$= f_t(1 + \eta^2 \chi_t^2 \|x\|^2) - \eta \chi_t \tilde{\Theta}(x, x),$$

where we call $\tilde{\Theta}$ the reparameterization-invariant *update kernel* defined as

$$\tilde{\Theta}(x, x') = \sum_l \frac{\eta_l}{\eta} \frac{\partial f(x)}{\partial W^l} \frac{\partial f(x')}{\partial W^l} = x^\top (n^{-1} \|\bar{u}\|^2 + n \|\bar{v}\|^2) x'.$$

The update kernel evolves via the reparameterization-invariant update equation

$$\begin{aligned} \lambda_{t+1} &= \tilde{\Theta}_{t+1}(x, x) = \|x\|^2 (n \|\bar{v}_{t+1}\|^2 + n^{-1} \|\bar{u}_{t+1}\|^2) \\ &= \|x\|^2 \left(n \|\bar{v}_t\|^2 + n^{-1} \|\bar{u}_t\|^2 + n^{-1} \bar{\eta}_u^2 \chi_t^2 \bar{v} \bar{v}^\top x^\top x \right. \\ &\quad \left. - 2n \bar{\eta}_v \chi_t \bar{v} \bar{u} x + n \bar{\eta}_v^2 \chi_t^2 x^\top \bar{u}^\top \bar{u} x - 2n^{-1} \bar{\eta}_u \chi_t \bar{v} \bar{u} x \right) \\ &= \lambda_t + \|x\|^2 (\eta^2 \chi_t^2 \|x\|^2 (n^{-1} \|\bar{u}\|^2 + n \|\bar{v}\|^2) - 4\eta \chi_t f_t) \\ &= \lambda_t + \|x\|^2 (\eta^2 \chi_t^2 \lambda_t - 4\eta \chi_t f_t) \\ &= \lambda_t + \|x\|^2 \eta \chi_t (\eta \chi_t \lambda_t - 4f_t). \end{aligned}$$

Now note that, even under $f_0 = 0$, we get non-trivial, width-independent dynamics. Due to the LLN, at initialization, we have $n^{-1} \|\bar{u}_0\|^2 \approx 1$ and $n \|\bar{v}_0\|^2 \approx 1$ ($=n^{-1}$ times sum over n iid χ^2 variables), hence $\lambda_0 \approx 2$.

To conclude, the training dynamics for repeatedly updating with the same training point (x, y) are fully described by the update equations,

$$f_{t+1} = f_t(1 + \eta^2 \chi_t^2 \|x\|^2) - \eta \chi_t \lambda_t, \quad (\text{C.1})$$

$$\lambda_{t+1} = \lambda_t + \|x\|^2 \eta \chi_t (\eta \chi_t \lambda_t - 4f_t). \quad (\text{C.2})$$

This can be rewritten in terms of the error (or function-loss derivative under MSE loss) $\chi_t = f_t - y$, akin to [Kalra et al. \(2025\)](#), as

$$\chi_{t+1} = \chi_t (1 - \eta \lambda_t + \eta^2 \|x\|^2 \chi_t (\chi_t + y)), \quad (\text{C.3})$$

$$\lambda_{t+1} = \lambda_t + \|x\|^2 \eta \chi_t (\eta \chi_t \lambda_t - 4(\chi_t + y)). \quad (\text{C.4})$$

First observe that all terms in the update equations become width-independent in μP . Only the initial conditions are width-dependent with vanishing variance, $f_0 = \Theta(n^{-1/2})$. As opposed to NTP, the sharpness update term $\eta^2 \chi_t^2 \|x\|^2$ is not vanishing anymore. While [Lewkowycz et al. \(2020\)](#) simply use labels $y = 0$, non-trivial dynamics in μP require $y \neq f_0 \rightarrow 0$.

Importantly, $\eta \chi_t$ always appear jointly, so that interpolation effectively reduces the learning rate.

Remark C.15 (Characterizing sharpness increase: Critical threshold depends on the labels.). When both sharpness and the loss increase, then training diverges as the learning rate lies even further from its edge of stability. In μP , since $f_0 \rightarrow 0$, λ_t will grow in the first step. For subsequent steps, the sharpness update equation (C.4) implies that sharpness increases ($\lambda_{t+1} \geq \lambda_t$) if and only if $\lambda_t \geq \frac{4}{\eta} (1 + \frac{y}{\chi}) = \frac{4}{\eta} \frac{f_t}{\chi_t}$. [Kalra et al. \(2025\)](#) provides a more extensive analysis of the dynamics and fixed points of this model in μP . \blacktriangleleft

Remark C.16 (Weight multipliers). A natural choice of weight multipliers for μP can be considered to be $a_l = 1/2 \cdot \mathbb{I}(l = L + 1) - 1/2 \cdot \mathbb{I}(l = 1)$, as this choice allows using a width-independent global learning rate $\eta_n = \eta \cdot n^0$, and the update kernel does not require width-dependent scaling factors, $\tilde{\Theta}(x, x') = x^\top (\|u\|^2 + \|v\|^2) x'$. In other words, under these weight multipliers, width-independence in parameter space translates into width-independence in function space. \blacktriangleleft

Standard Parameterization. We define training a 2-layer linear network in SP with global learning rate scaling n^{-c} as

$$f = \bar{v} \bar{u} x,$$

with initialization $\bar{u} \sim N(0, 1/d_{in}), \bar{v} \sim N(0, 1/n)$ and global learning rate $\bar{\eta}_u = \bar{\eta}_v = \eta n^{-c}$. Parameter multipliers affect all scalings in the same way as for μ P. Only the learning rate has a different prefactor, and the last layer has larger initialization. The adapted update equations become

$$\begin{aligned} f_{t+1} &= f_t(1 + n^{-2c}\eta^2\chi^2\|x\|^2) - n^{1-c}\eta\chi_t\lambda_t, \\ \lambda_{t+1} &= \lambda_t + \|x\|^2 n^{-c}\eta\chi_t(n^{-c}\eta\chi_t\lambda_t - 4n^{-1}f_t), \end{aligned}$$

where we define, as for NTP,

$$\tilde{\Theta}(x, x') = n^{-1}(\|\bar{u}\|^2 + \|\bar{v}\|^2),$$

where $n^{-1}\|\bar{v}\|^2 \approx n^{-1}$ at initialization (n^{-2} times sum over n iid χ^2 -variables with positive mean).

Choosing $c < 1$ results in output blowup of the term $n^{1-c}\eta\chi_t\lambda_t$. While this can in principle be counteracted by shrinking λ_t at finite width, a well-defined stable and non-trivial infinite-width limit is only attained at $c = 1$, where $f_{t+1} = f_t - \eta\chi_t\lambda_t$ and $\lambda_{t+1} = \lambda_t$. We now show that also at finite width, stable training with a constant learning rate in SP requires $\eta = O(n^{-1})$.

C.4.2 Finding the maximal stable learning rate scaling by characterizing the conditions for loss and sharpness decrease

The following proposition characterizes the choices of η that result in a decrease in loss at any present state.

Writing $n_{sp} = \begin{cases} n, & \text{in SP,} \\ 1, & \text{else,} \end{cases} n_{ntp} = \begin{cases} n, & \text{in NTP,} \\ 1, & \text{else,} \end{cases}$, we can write the update equations of parameterizations jointly as

$$\begin{aligned} \chi_{t+1} &= \chi_t(1 - n_{sp}\eta\lambda_t + n_{ntp}^{-1}\eta^2\chi\|x\|^2(\chi_t + y)), \\ \lambda_{t+1} &= \lambda_t + \eta\chi_t\|x\|^2 n_{ntp}^{-1}(\eta\chi_t\lambda_t - 4n_{sp}^{-1}(\chi_t + y)). \end{aligned}$$

Proposition C.17 (Characterizing loss decrease in SP and NTP). *Let $\eta \geq 0$. For n_{sp} or n_{ntp} large enough, we write the update equations of repeatedly updating the wv -model with SGD on the training point (x, y) with $\|x\| = 1$ in SP or NTP jointly as provided above. The loss decreases at any step, omitting time t ,*

1. *in the case $f(f - y) \geq 0$, if and only if $\eta \leq \frac{2}{n_{sp}\lambda} + O(n_{sp}^{-3}n_{ntp}^{-1})$ or $\eta \in [\frac{n_{sp}n_{ntp}\lambda}{\|x\|^2\chi f} - \frac{2}{n_{sp}\lambda} - O(n_{sp}^{-3}n_{ntp}^{-1}), \frac{n_{sp}n_{ntp}\lambda}{\|x\|^2\chi f}]$,*
2. *in the case, $f(f - y) < 0$, if and only if $\eta \leq \frac{2}{n_{sp}\lambda} - O(n_{sp}^{-3}n_{ntp}^{-1})$.*

It holds that $\lambda_{t+1} \geq \lambda_t$ if and only if $\lambda_t \geq \frac{4}{n_{sp}\eta_t}(1 + \frac{y}{\chi_t})$.

Remark C.18 (Instability in SP). The crucial insight from [Proposition C.17](#) for SP is that both loss and sharpness increase early in training as soon as $\eta = \omega(n^{-1})$, unless an extensively large learning rate that depends on the current sharpness, training point and output function, is accurately chosen at each time step in a slim interval of benign large learning rates, which is unlikely to hold in practice. [Figure C.2](#) shows that in simulated training with constant learning rates, the maximal stable learning rate indeed scales as $\Theta(n^{-1})$. This instability prediction is in line with the infinite-width prediction from [Yang and Hu \(2021\)](#), and hence does not explain large learning rate stability in SP in practice. \blacktriangleleft

Proof. From the update equations, it holds that $\lambda_{t+1} \geq \lambda_t$ if and only if $\eta_t n_{ntp} \chi_t (\eta_t \chi_t \lambda_t - \frac{4}{n_{sp}} f_t) \geq 0$ if and only if $\lambda_t \geq \frac{4}{n_{sp}\eta_t}(1 + \frac{y}{\chi_t})$.

Observe that the loss decreases if and only if $|\chi_{t+1}| \leq |\chi_t|$, which holds if and only if $|1 - n_{sp}\eta\lambda_t + \eta^2 n_{ntp}^{-1} \chi\|x\|^2(\chi_t + y)| \leq 1$, which can be written as, omitting all subscripts \cdot_t ,

$$\eta^2 n_{ntp}^{-1} \|x\|^2 \chi f - \eta n_{sp} \lambda \in [-2, 0].$$

Assuming $\eta \geq 0$, the above holds if and only if $(\eta\chi f \leq \frac{n_{sp}n_{ntp}\lambda}{\|x\|^2}$ and $n_{ntp}^{-1}\eta^2\|x\|^2\chi f - \eta n_{sp}\lambda \geq -2)$. The first constraint is a mild one that states $\eta = O(n)$. We will now focus on the second one.

Solving for the roots of this polynomial in η , we get

$$\eta_{1,2} = \frac{1}{2\|x\|^2\chi f} \left(n_{ntp}n_{sp}\lambda \pm \sqrt{n_{ntp}^2n_{sp}^2\lambda^2 - 8\|x\|^2n_{ntp}\chi f} \right).$$

Assuming $n_{sp}^2n_{ntp}\lambda^2 \gg 8\|x\|^2\chi f =: C$, we get $n_{sp}n_{ntp}\lambda\sqrt{1 - \frac{C}{n_{sp}^2n_{ntp}\lambda^2}} \approx n_{sp}n_{ntp}\lambda(1 - \frac{C}{2n_{sp}^2n_{ntp}\lambda^2} - \frac{1}{4}(\frac{C}{n_{sp}^2n_{ntp}\lambda^2})^2)$. In that case $\eta_1 \approx \frac{2}{n_{sp}\lambda}$ and $\eta_2 \approx \frac{n_{sp}n_{ntp}\lambda}{\|x\|^2\chi f} - \frac{2}{n_{sp}\lambda}$.

Hence, if $\chi f \geq 0$, we get loss decrease if $\eta \leq \frac{2}{n_{sp}\lambda} + O(n_{sp}^{-3}n_{ntp}^{-1})$ or $\eta \in [\frac{n_{sp}n_{ntp}\lambda}{\|x\|^2\chi f} - \frac{2}{n_{sp}\lambda} - O(n_{sp}^{-3}n_{ntp}^{-1}), \frac{n_{sp}n_{ntp}\lambda}{\|x\|^2\chi f}]$.

If $\chi f < 0$, we get loss decrease if $\eta \in [\frac{n_{sp}n_{ntp}\lambda}{\|x\|^2\chi f} - \frac{2}{n_{sp}\lambda} + O(n_{sp}^{-3}n_{ntp}^{-1}), \frac{2}{n_{sp}\lambda} - O(n_{sp}^{-3}n_{ntp}^{-1})]$, where the left end of the interval is negative. The upper end resembles the edge of stability that vanishes as n_{sp}^{-1} for SP but not for NTP.

□

Note the interesting slim regime of benign large learning rates $\eta \approx \frac{n\lambda}{\|x\|^2\chi f} - \frac{1}{n_{sp}\lambda} = \Theta(n)$ when $f(f - y) > 0$. As all of the involved quantities are known at training time, an adaptive learning rate schedule may significantly speed up training by stable learning with excessive learning rates. However it remains unclear whether a similar regime exists in practical architectures under CE loss. In that case, the sharpness computation would also be much more computationally expensive.

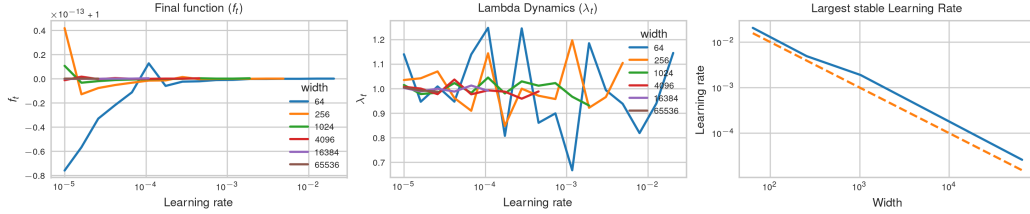


Figure C.2: **Stable SP.** f_t (left) and λ_t (center) after training to convergence for several widths. The largest stable learning rate for SP indeed scales as n^{-1} (right). When lines end, training diverged for larger learning rates. The first subplot shows that training has succeeded in memorizing the training label $y = 1$ at the optimal learning rate at all widths. The second subplot shows that the randomness in λ_t due to random initial conditions vanishes with increasing width, as SP is approaching its kernel regime.

C.4.3 μ P converges faster to its limit than SP and NTP

Here we study the convergence speed of the uv -model from Appendix C.4 to the infinite-width limit in SP, NTP and μ P through simulations in the gradient flow regime $\eta \in \{0.001, 0.01\}$. We draw new data points without signal $x, y \sim N(0, I_2)$ for every update. Convergence of the function to $y = 1$ would confound the findings. If we draw the initial \hat{f}_0 from $N(0, 1)$ for SP and NTP versus $N(0, n^{-1})$ for μ P independent of f_0 at finite width, we only see convergence $f_t \rightarrow \hat{f}_t$ for μ P due to non-vanishing variance in the initial output function in SP and NTP (Figure C.6). Therefore, in all following experiments in this section, we start the update equations of the limit from the same f_0 to just measure the deviations over training. We let λ_0 differ from $\hat{\lambda}_0$, as otherwise μ P at finite width would exactly coincide with its limit, as it follows width-independent update equations. Observe that μ P still converges faster to its limit than NTP, which converges faster than SP (Figure C.5). The convergence exponent of μ P seems to lie around -0.45 . Observe large variance of the difference to the limit between random initial seeds (Figures C.3 and C.4). This requires many runs for an accurate estimation of the exponent. Note that the slow convergence of SP here may be due to the kernel regime enforced by MSE loss, and convergence to our feature learning limit under $\eta_n = \Theta(n^{-1/2})$ may be much faster.

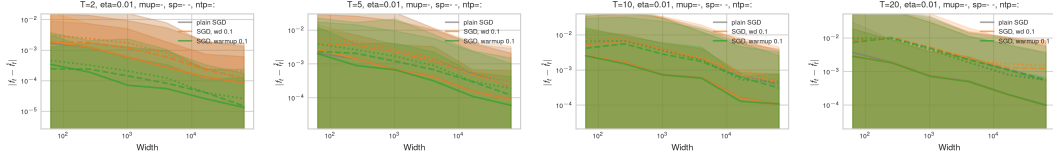


Figure C.3: (**$\mu\mathbf{P}$ remains closest to its limit across training**) Difference between finite networks and their infinite-width limit from the same initial condition across 100 random seeds for $\mu\mathbf{P}$ (line), \mathbf{SP} (dotted line) and \mathbf{NTP} (dashed line) after $T = 2, 5$ or 10 steps (left to right), running plain SGD in gray, 0.1 warmup in green and 0.1 weight decay in orange. Initially, warmup retains the most closeness to the limit, as the learning rate is very small. In later steps, $\mu\mathbf{P}$ clearly remains closer to its limit. All parameterizations converge to their limit, but with large variance.

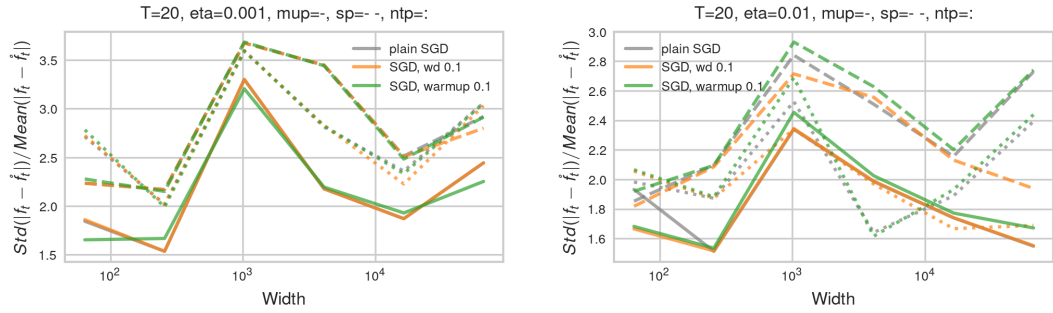


Figure C.4: (**Large variance in convergence to limit**) Standard deviation divided by mean of $|f_t - \hat{f}_t|$ across random initialization. Note that in all parameterizations the variance of the difference to the limit is very large.

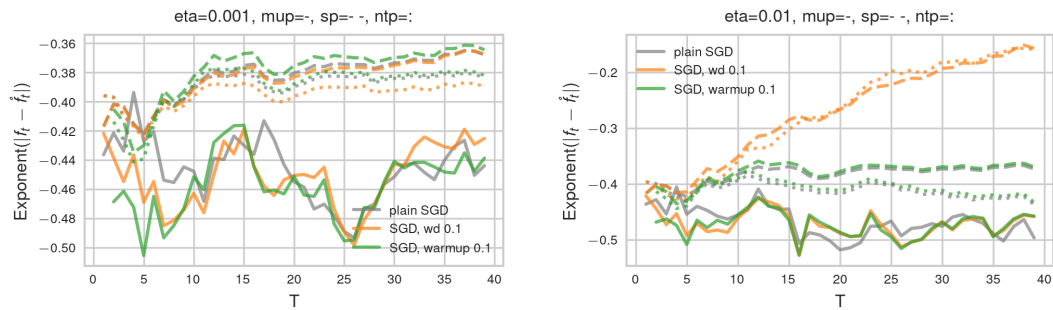


Figure C.5: (**$\mu\mathbf{P}$ converges faster to its limit**) Width convergence exponent of the decay of the difference of learned finite neural networks to their limit derived between smallest and largest width 64 and 65536 for learning rate 0.001 (left) and 0.01 (right) across 100 random seeds for $\mu\mathbf{P}$ (line), \mathbf{SP} (dotted line) and \mathbf{NTP} (dashed line) against number of training iterations T , running plain SGD in gray, 0.1 warmup in green and 0.1 weight decay in orange. While the exponents are still noisy even from means of 100 random seeds, $\mu\mathbf{P}$ clearly converges faster to its limit than \mathbf{NTP} which converges faster than \mathbf{SP} , even when starting from the same initial conditions. \mathbf{SP} and \mathbf{NTP} with weight decay seem to systematically deviate from their limit only at large learning rate and late in training as their exponent decreases with the amount of training.

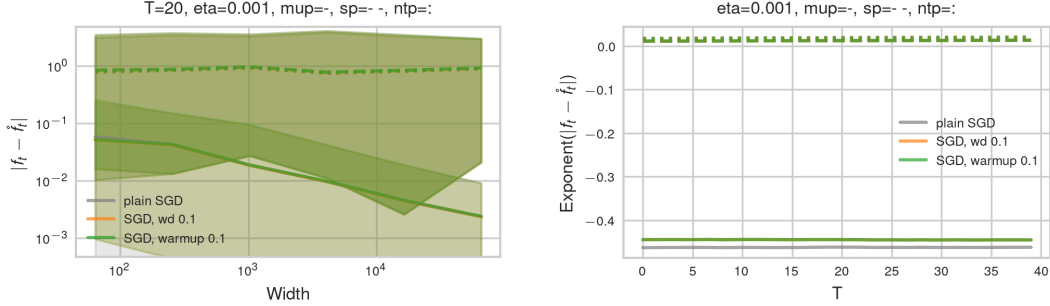


Figure C.6: **(Non-vanishing initial variance in SP and NTP prevent convergence)** Difference to limit after 20 steps (left) and corresponding exponents (right) for differing initial \hat{f}_0 drawn independently from f_0 . Only μP converges to its limit at exponent around -0.45 .

D Experimental details

If not otherwise specified, we train a single epoch to prevent confounding from multi-epoch overfitting effects.

D.1 MLPs

We implement our MLP experiments on MNIST (Deng, 2012) and CIFAR-10 (Krizhevsky et al., 2009) in PyTorch (Paszke et al., 2019). We train ReLU MLPs with the same width n in all hidden dimensions with plain SGD/Adam with a single learning rate for all trainable parameters, batch size 64 without learning rate schedules, weight decay or momentum to prevent confounding. We use Adam with the PyTorch standard hyperparameters. By standard initialization we mean He initialization variance $c_\phi/\text{fan_in}$ with $c_\phi = 2$ for the ReLU activation function (He et al., 2015).

D.2 Multi-index data

We generate multi-index teacher data, inspired by Kunin et al. (2024), but setting a deterministic teacher for ensuring a balanced classification task.

We draw the covariates $\xi \sim \mathcal{U}(\mathbb{S}^{d_{in}-1})$ i.i.d. from the uniform distribution on the unit sphere in $\mathbb{R}^{d_{in}}$ with input dimension $d_{in} = 100$. The training set consists of 10^3 training points. We also draw a test set consisting of 10^4 test points.

For the target function f^* , drawing 3 random directions as in Kunin et al. (2024) results in heavily unbalanced classes and $f^* = 0$ on large part of the support with high probability. Instead, we set 4 teacher neurons deterministically for less noisy results. The teacher net is a shallow ReLU network given by $f^*(\xi) = \text{sign}(\sum_{i=1}^4 s_i \phi(w_i^\top \xi))$ with unit vectors $w_1 = e_1, w_2 = e_2, w_3 = -e_1, w_4 = -e_2$ and signs $s_1 = s_3 = +1$ and $s_2 = s_4 = -1$. This results in the nonlinear target function $f^*(\xi) = \text{sign}(\xi_1 - \xi_2)$ for all $\xi \in \mathbb{R}^{d_{in}}$ with $\xi_1 > 0$ or $\xi_2 > 0$, but $f^*(\xi) = \text{sign}(\xi_2 - \xi_1)$ for all $\xi \in (-\infty, 0) \times (-\infty, 0)$. We do not use label noise.

This dataset requires learning to attend to the first 2 covariate dimensions (ξ_1, ξ_2) , where all of the signal for the labels $f^*(\xi)$ lies. If the input layer does not learn to align with these dimensions, the sparse signal is obscured in the activations (random features) after the first layer due to the large variance in the remaining covariate dimensions.

D.3 Language modeling

We train small Transformer models (Vaswani et al., 2017) using LitGPT (Lightning AI, 2023). We adapt the Pythia (Biderman et al., 2023) architecture with 6 Transformer blocks, standard $d_{\text{head}}^{-1/2}$ attention scaling, pre-attention and qk-Layernorm (Wortsman et al., 2024). We purely scale width, proportionally scaling the number of attention heads and the MLP hidden size while keeping the number of layers and head dimension $d_{\text{head}} = 32$ fixed. For widths 256, 1024 and 4096, this results in 8, 32 and 128 heads per Transformer block and a total of $30M$, $167M$ and $1.4B$ parameters.

Standard training means AdamW with a single, tuned maximal learning rate, $(\beta_1, \beta_2) = (0.9, 0.95)$, $\varepsilon = 10^{-12}$, sequence length 512, batch size 256, 700 steps of warmup followed by cosine learning rate decay to 10% of the maximal learning rate, weight decay 0.1, gradient clipping. We train for 10681 steps in mixed precision on the DCLM-Baseline dataset (Li et al., 2024). We train all models on the same number of tokens to prevent confounding effects from increased training time.

D.4 Figure Details

Figure 1: The training accuracy of 8-layer MLPs is averaged over 4 runs to reduce noise from random initialization. The training loss of GPT trained with SGD is averaged over 3 runs. GPT with Adam was only run once.

Figure 2: The readout layer and last Layernorm layer are chosen due to their particular importance for logit blowup. The MLP layer was chosen to add a layer that scales hidden-like. This layer was not cherry picked. We observe other MLP layers to have similar scaling properties.

Figure 4: 3-layer MLP trained with SGD on CIFAR-10 with width-dependent learning rate $\eta_n = 0.0001 \cdot n^{-0.5}$. Averages over 4 random seeds.

Figure 5: Minimal unstable learning rates are defined as the smallest learning rates to produce NaN entries when using MSE loss, or, under CE loss, accuracy $< 20\%$ on MNIST and CIFAR-10, and $< 54\%$ on binary multi-index data. For 2-layer MLPs, our theory predicts $\eta_n = O(1)$ as the instability threshold, since there are no hidden layers, and input layers are updated width-independently at $\eta_n = \Theta(1)$. The x-axes showing learning rates are scaled as $(n/256)^\alpha$. In this way, the learning rate at base width 256 remains the same for comparability of the constants. If the optimal or maximal stable learning rate indeed scales as $\eta_n = \eta \cdot n^{-\alpha}$, then the width-dependent scaling of the x-axis $\eta_n \cdot n^\alpha$ shows learning rate transfer.

Figure 6: SGD runs are averaged over 3 random seeds, due to noisy individual outcomes. The results for Adam stem from a single random seed due to limited computational resources. Minimal unstable learning rates are defined as the smallest learning rates to produce loss worse than (optimal CE loss +1) at each width. The x-axes showing learning rates are scaled as $(n/256)^\alpha$. In this way, the learning rate at base width 256 remains the same for comparability of the constants. If the optimal or maximal stable learning rate indeed scales as $\eta_n = \eta \cdot n^{-\alpha}$, then the width-dependent scaling of the x-axis $\eta_n \cdot n^\alpha$ shows learning rate transfer.

Figure 7: Shown is the training accuracy at the end of training for one epoch for the optimal learning rate at each width.

E Refined coordinate checks

The standard coordinate check as provided in the readme of the mup-package Yang et al. (2022) may be considered the plot of activation norms $\|x_t^l\|_{RMS}$ after t steps of training for all layers l and the network output norm $\|f\|_{RMS}$ with $f := W_t^{L+1}x_t^L$ as a function of width. Completely width-independent dynamics under μP then result in an approximately width-independent coordinate check of all layers. However, width-dependence in the activations of previous layers would confound the l -th layer activation scaling, so that measuring the effective l -th layer updates requires measuring $\|\Delta W_t^l x_t^l\|_{RMS}$ in each layer, where one may be interested in the weight updates accumulated over the entire course of training $\Delta W_t^l = W_t^l - W_0^l$ or the update in a single step $\delta W_t^l = W_t^l - W_{t-1}^l$. In standard architectures, one can equivalently measure the operator norm of the weight updates $\|\Delta W_t^l\|_{2 \rightarrow 2} \cdot \sqrt{\text{fan_in}(W_t^l) / \text{fan_out}(W_t^l)} \stackrel{!}{=} \Theta(1)$ (Yang et al., 2023a); however in non-standard architectures such as Mamba this spectral condition has been shown to fail, so that, in the general case, care should be taken in how exactly weight updates affect the output function (Vankadara et al., 2024). The difference between $\|\Delta W_t x_t\|$ and the preactivation updates $\|\Delta(W_t x_t)\|$ is precisely $\|W_0 \Delta x\|_{RMS}$ which measures the effect of updates propagating from previous layers.

All coordinate checks are run over 4 random seeds either at small learning rate or the optimal learning rate η_{256} at base width 256 (after 1 epoch of training) on CIFAR-10. The learning rate is then scaled in relation to that base width $\eta_n = \eta \cdot (n/256)^\alpha$ with $\alpha \in \{-1, -0.5, 0\}$.

E.1 SGD

Figure E.1 shows the refined coordinate check for a 3-layer MLP in SP with global learning rate scaling $\eta_n = \eta \cdot n^{-1/2}$. As predicted by Proposition 2, the input layer updates decay as n^{-1} , the hidden layer learns features width-independently, and the output scales as $n^{1/2}$ which results in one-hot predictions after the softmax in wide models, but not necessarily unstable training dynamics.

Both $\|\Delta W_t^l x_t^l\|_{RMS}$ and $\|\Delta W_t^l\|_{RMS \rightarrow RMS}$ measure the effective update effect in the l -th layer equivalently and accurately even in narrow MLPs of width 64. Naively tracking the activation updates $\Delta x_t^l = x_t^l - x_0^l$ however is confounded by non-vanishing feature learning in narrow models, and only shows the correct hidden- and last-layer scaling exponents for $n \geq 4000$, even after only a single update step.

Figure E.2 shows a refined coordinate check for a 3-layer MLP in SP with width-independent global learning rate scaling $\eta_n = 0.0001 \cdot n^0$. While infinite-width theory predicts the input layer to learn width-independently and the hidden layer to explode as $\Theta(n)$, both empirical exponents are $n^{-1/2}$ smaller, so that the input layer has vanishing feature learning and the hidden layer is still exploding. This ostensible contradiction is resolved when repeating the coordinate check but initializing the last layer to 0 (Figure E.3). Now the predicted scaling exponents are recovered, already at small width. The reason for this subtle but important difference is that the gradient that is back-propagated is given by the last-layer weights, $\partial f / \partial x^L = W_t^{L+1} = W_0^{L+1} + \Delta W_t^{L+1}$. Under standard initialization at the optimal learning rate, the initialization $W_0^{L+1} = \Theta(n^{-1/2})$ still dominates the updates $\Delta W_t^{L+1} = \Theta(\eta_n)$ in absolute terms after a few update steps at widths up to 16384. Comparing the absolute scales of $\|\Delta W_t^l x_t^l\|_{RMS}$ or $\|W_t^l\|_*$ in both figures confirms this hypothesis. The pure update effects in Figure E.3 have lower order of magnitude in the constant before the scaling law, but follow clear scaling exponents. Therefore the faster scaling law under last-layer zero initialization can be extrapolated with certainty to induce a phase transition under standard initialization around width $4 \cdot 10^7$. We do not have sufficient computation resources to validate this but arrive at this order of magnitude irrespective of whether we extrapolate the scaling laws of $\|\Delta W_t^l x_t^l\|_{RMS}$ or $\|W_t^l\|_*$ as well as of the input or hidden layer laws. For base width n_0 and width-dependent statistics Δ_n^1 and Δ_n^2 with differing scaling exponents c_1 and c_2 , Δ_n^1 and Δ_n^2 intersect at width $n_0 \cdot (\Delta_{n_0}^2 / \Delta_{n_0}^1)^{1/(c_1 - c_2)}$.

This consequential difference in empirical scaling exponents at realistic widths due to a subtle difference in last-layer initialization highlights the attention to detail that is required to make accurate scaling predictions from infinite-width limit theory, but, as we show in this paper, apparent contradictions can often be reconciled with enough attention to detail, and the clean scaling laws we arrive at as a result already hold at moderate scales and prove the usefulness of investing this extra effort.

Hence, one reason why scaling exponents in SGD can be larger than predicted up to very large widths, is due to differing orders of magnitude in the constant pre factors in the initialization versus update terms in the backward pass. Without our refined coordinate check, the phase transition around width 10^7 is hard to predict.

As predicted, the width-exponents of 2-layer nets behave like the input and output layer in 3-layer nets (Figure E.4).

When choosing the optimal learning rate $\eta_{256} = 0.03$ at width 256, stronger finite-width effects due to non-vanishing input layer feature learning already occur after a few steps and make the update scaling exponents after 10 steps only visible at larger width $n \geq 2048$ (Figure E.5). As long as divergence is prevented in the first few steps, self-stabilization mechanisms such as activation sparsification can quickly contain the initial catapult (Figure E.6). In deeper networks, explosion of several hidden layers is increasingly difficult to stabilize, and finite width effects are reduced.

Figure E.5 shows the effective update rank and the alignment between activations at initialization versus at time t for the same input training points under unstable width-independent learning rate scaling. The updates in each layer are remarkably strongly dominated by a single direction. As hidden-layer activations are slowly diverging, their alignment is only beginning to decrease at large widths $n \geq 4096$. The beginning instability of $\|\Delta x^2\|_{RMS}$ will eventually induce training instability and suboptimal accuracy at large width, which is hard to predict without tracking the layerwise effective update scaling across widths.

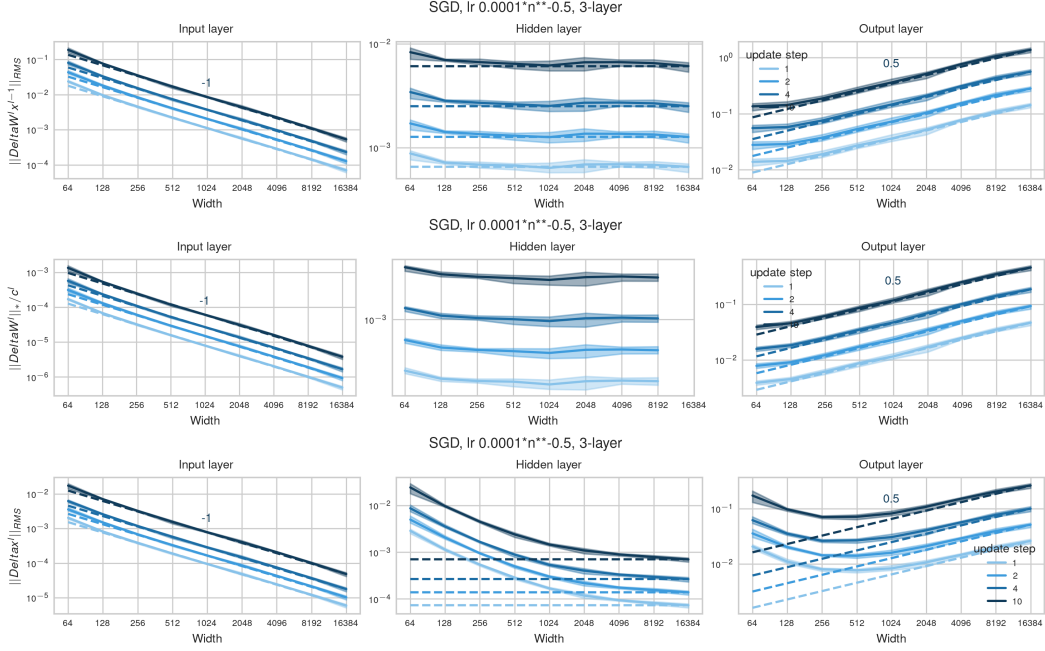


Figure E.1: (Hidden layer feature learning in SP under intermediate learning rate scaling) Effective l -th layer update scalings $\|\Delta W_t^l x_t^{l-1}\|_{RMS}$ (top), weight update spectral norm $\|\Delta W_t^l\|_*$ (2nd row) and activation updates δx^l (bottom) of MLPs trained in SP with small learning rate $\eta_n = 0.0001 \cdot (n/256)^{-1/2}$ scaled to preserve hidden-layer feature learning. The TP scaling predictions are accurate. Hidden layers learn features width-independently, and input layers have vanishing feature learning. At moderate widths, activation updates are confounded by previous layer updates, and thus do not provide an accurate metric for effective update scaling.

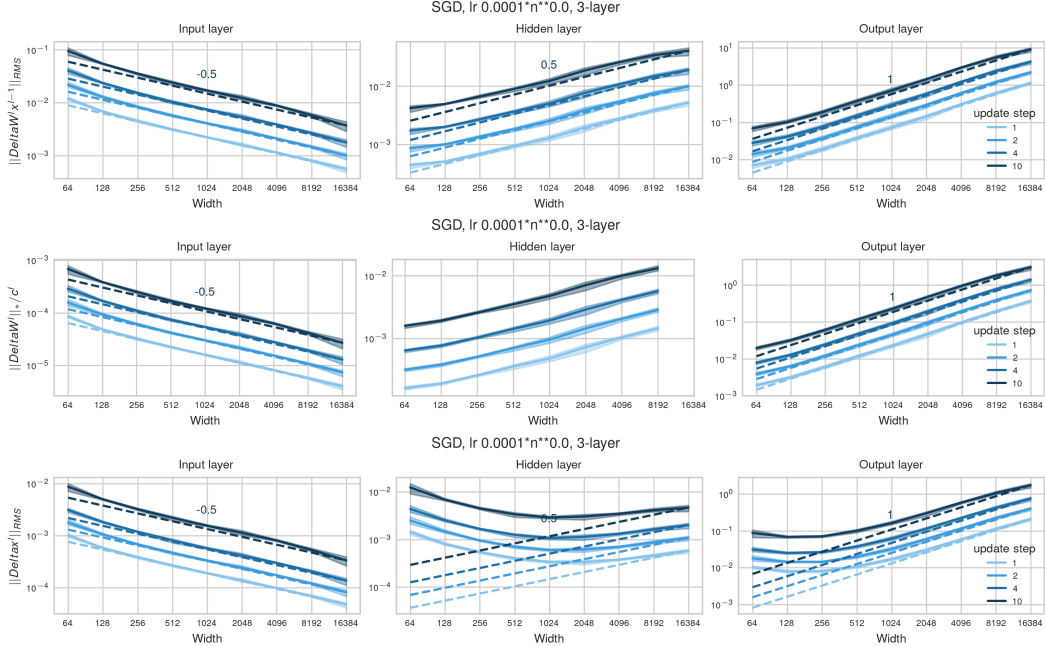


Figure E.2: **(Inaccurate exponent predictions under standard initialization with large learning rate scaling)** Effective l -th layer update scalings $\|\Delta W_t^l x_t^{l-1}\|_{RMS}$ (top), weight update spectral norm $\|\Delta W_t^l\|_*$ (2nd row) and activation updates δx^l (bottom) of 3-layer MLPs trained in SP with width-independent $\eta_n = 0.0001$. Hidden layer activation updates explode, and input layers have vanishing feature learning. By TP scaling predictions, however, the input layer should learn features width-independently. Instead, the TP scaling exponents are **only accurate under last-layer zero initialization, not under standard initialization** (see Figure E.3 for last-layer zero initialization) as the initialization scaling $W_0^{L+1} = \Theta(n^{-1/2})$ still dominates the update scaling $\Delta W_t^{L+1} = \Theta(\eta_n)$ at realistic widths after a few updates under the optimal learning rate. Hence, the backpropagated gradient $\partial f / \partial x^L = W_t^{L+1}$, relevant for the hidden and input layer updates, behaves for several steps like it should only behave in the first step. By comparing the absolute scales here versus those in Figure E.3 it becomes apparent that this is indeed a finite-width effect, as the absolute scale of $\|\Delta W x\|_2$ here is on the order 10^{-1} and 10^{-2} for input and hidden layer, respectively, whereas the pure update effects under last-layer zero initialization are of at most order 10^{-4} for both layer types. Clearly for sufficient width, the differing scaling exponents will induce a phase transition toward the predicted scaling exponents. While the input layer learns features width-independently under last-layer zero initialization, as predicted by TP theory, this is not the case at realistic scales under standard initialization. The qualitative statement that standard parameterization with width-independent learning rates is not activation stable in deep networks is still accurate at moderate width.

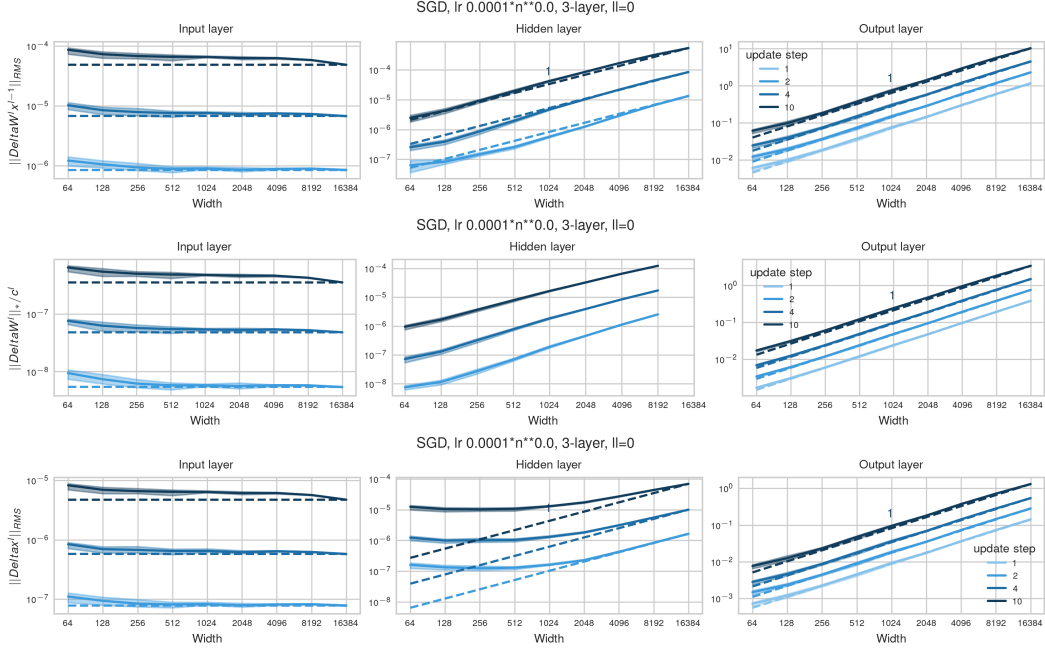


Figure E.3: (Accurate exponent predictions in SP with last-layer zero initialization under large learning rate scaling) Same as Figure E.2 with width-independent $\eta_n = 0.0001$ but initializing the last layer to zero. Here, the TP scaling predictions are accurate. Hidden layer activation updates explode as n^1 , and input layers learn features width-independently. Observe a smaller absolute scale of the pure update effects here versus in Figure E.1 that explains the differing exponents there. The updates in the input and hidden layers vanish in the first step, as the gradient for backprop is $W_0^{L+1} = 0$.

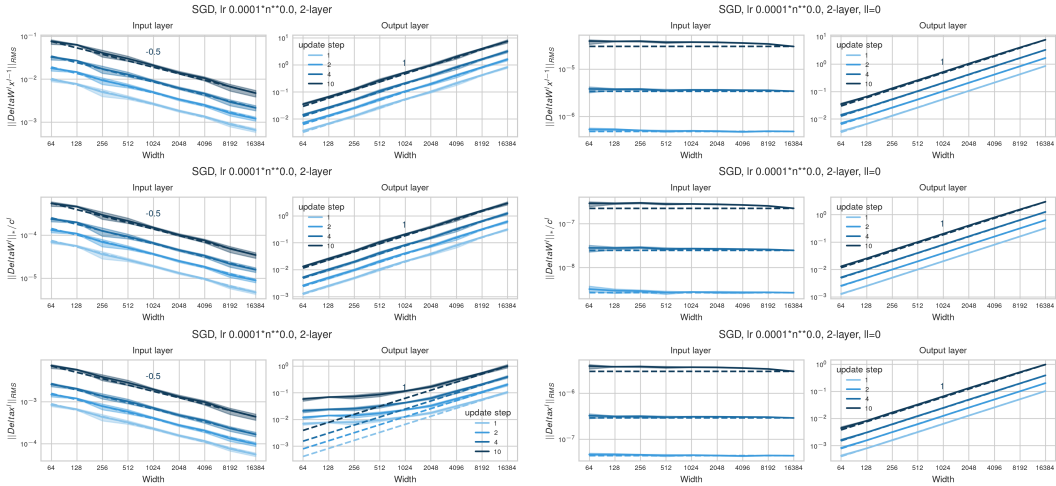


Figure E.4: (Shallow nets learn features width-independently under large learning rate scaling) Same as Figure E.1 but for 2-layer MLPs trained in SP with width-independent $\eta_n = 0.0003$ with standard initialization (left) and last-layer initialized to 0 (right). The input layer and output layer scalings behave as in the 3-layer nets. Since there is no exploding hidden layer, activation stability is preserved in 2-layer nets under $\eta_n = \Theta(1)$.

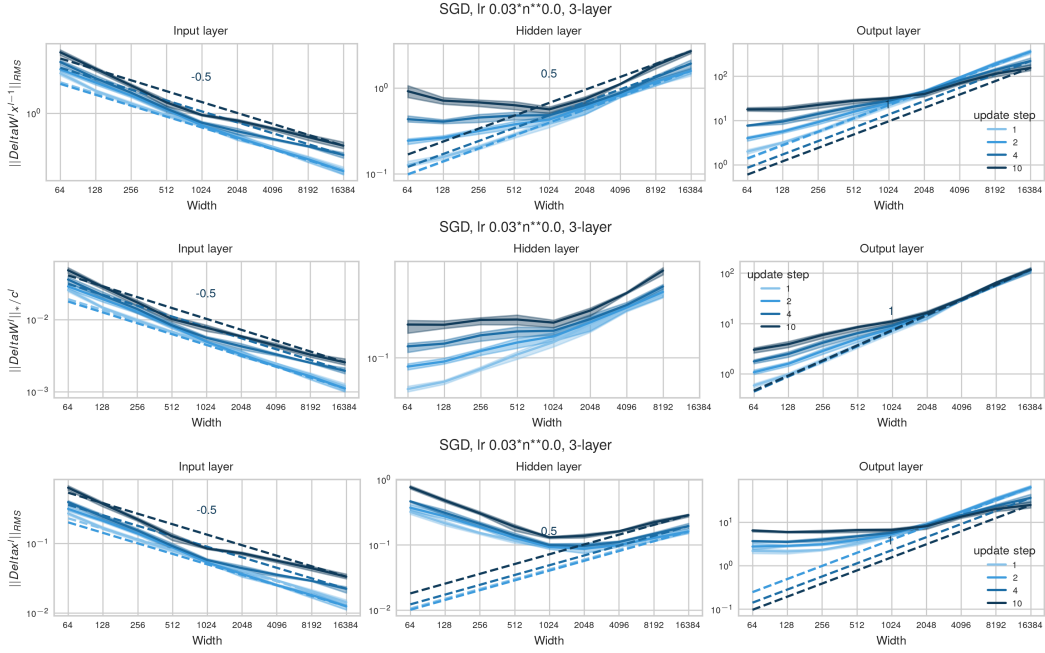


Figure E.5: (Large finite-width effects at optimal learning rate in shallow 3-layer MLPs) At the optimal learning rate $\eta_{256} = 0.03$ with width-independent scaling, non-vanishing input layer feature learning confounds the scalings after few update steps up to moderate widths $n \leq 1024$, similar to Adam (Figure E.9).

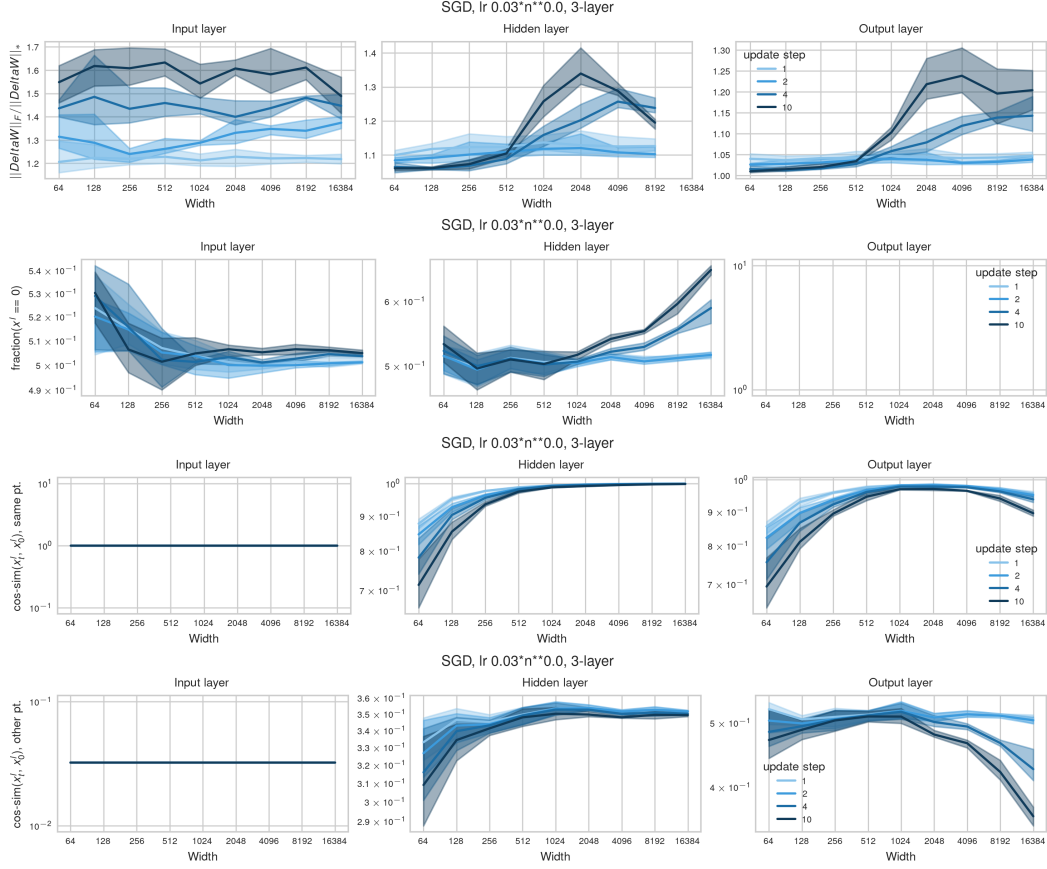


Figure E.6: **(Activation sparsification at the optimal learning rate)** Effective l -th layer update ranks $\|\Delta W_t^l\|_F / \|\Delta W_t^l\|_*$, activation sparsity and cosine similarity between activations to each layer comparing time 0 and time t on the same input training point and on differing training points in the same batch of 3-layer MLPs trained with SGD in SP with width-independent learning rate $\eta_n = 0.03$ as in Figure E.5. As opposed to the gradient flow regime, at the optimal learning rate, there are significant self-stabilization effects at large width already after 10 steps through activation sparsification but less through activation rotation.

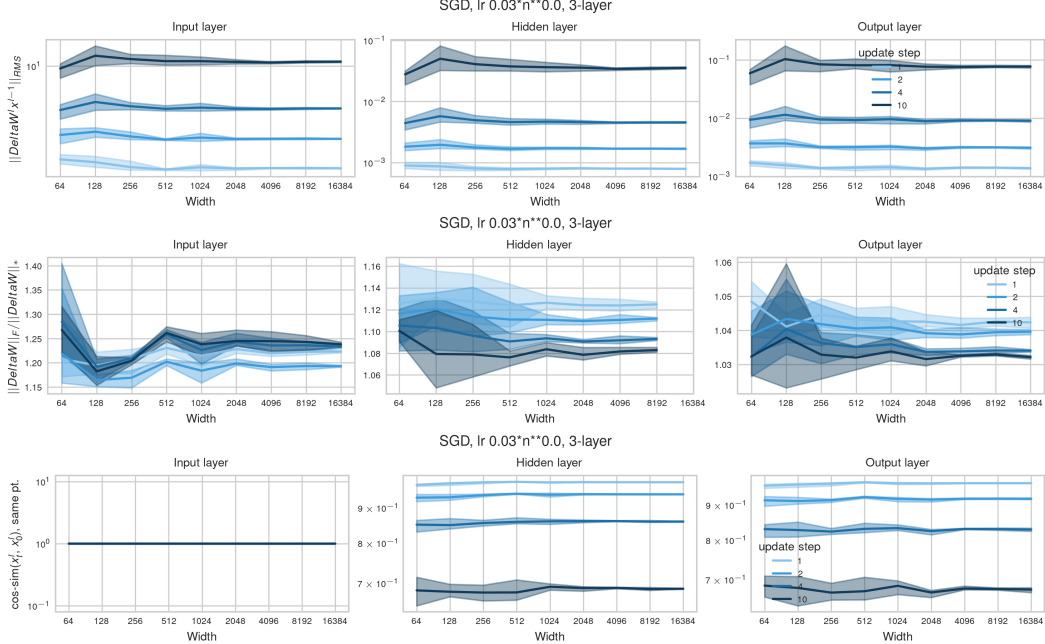


Figure E.7: **(Full width-independence in $\mu\mathbf{P}$)** Effective l -th layer updates (top), effective update ranks $\|\Delta W_t^l\|_F / \|\Delta W_t^l\|_*$ (second row) and cosine similarity between activations to each layer comparing time 0 and time t on the same input training point (bottom) of 3-layer MLPs trained with SGD in $\mu\mathbf{P}$ with width-independent learning rate $\eta_n = 0.03$. As expected, all statistics behave width-independently. The effective update rank is remarkably small, as for SP. The activation are rotated quite quickly.

E.2 Adam

With $\eta_n = \Theta(n^{-1/2})$, the optimal learning rate scaling for 3-layer MLPs with Adam on CIFAR-10 is larger than predicted (Figure F.22). Figure E.9 shows that this may be due to large finite-width effects for Adam at optimal learning rate multiplier $\eta_{256} = 0.0003$ and moderate width $n \leq 8192$. While the weight update spectral norm scales as predicted, the input-layer gets large updates at moderate width (Figure E.10) and induces a strong rotation of the activations. As a result, the activation explosion only sets in at large width $n \geq 8192$. This qualitative change toward vanishing input layer feature learning will result in a phase transition toward unstable scaling at large widths which is hard to predict at small scale from measurements alone, except when measuring both $\|\Delta W^l\|_*$ and the alignment $\|\Delta W^l x^{l-1}\|_{RMS}$.

As opposed to SGD, observe large finite-width effects in the activation updates even under small absolute learning rate 10^{-6} at moderate width $n \leq 8192$ (Figure E.8).

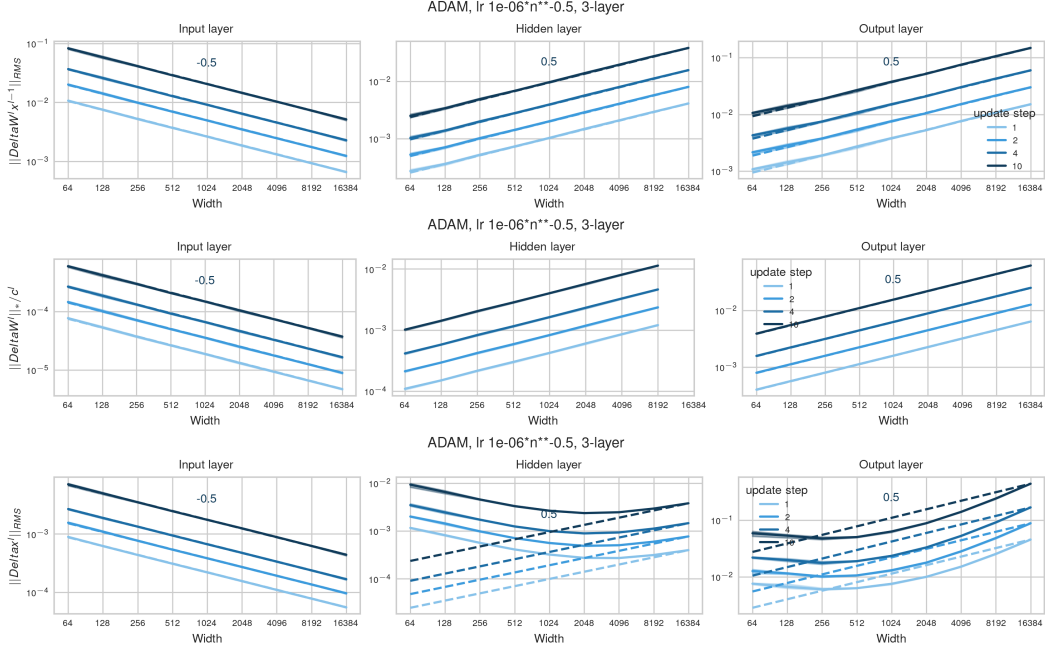


Figure E.8: **(Large finite-width effects from input-layer updates in Adam)** Effective l -th layer update scalings $\|\Delta W_t^l x_t^{l-1}\|_{RMS}$ (top), weight update spectral norm $\|\Delta W_t^l\|_*$ (2nd row) and activation update norm $\|\Delta x^l\|_{RMS}$ (bottom) of 3-layer MLPs trained with Adam in SP with $\eta_n = 10^{-6} \cdot n^{-1/2}$. Observe the theoretically predicted exponents in $\|\Delta W^l\|_*$ do not transfer to the activation updates at moderate width $n < 8192$ due to large non-vanishing input layer updates at moderate width. Even the effective updates $\|\Delta W_t^l x_t^{l-1}\|_{RMS}$ do not perfectly align with the scaling law at infinite width, indicating that the alignment between ΔW_t^l and x_t^{l-1} evolves non-trivially across width and that the spectral norm $\|\Delta W^l\|_*$ and pure infinite-width predictions are less useful for explaining the behaviour of Adam at moderate width.

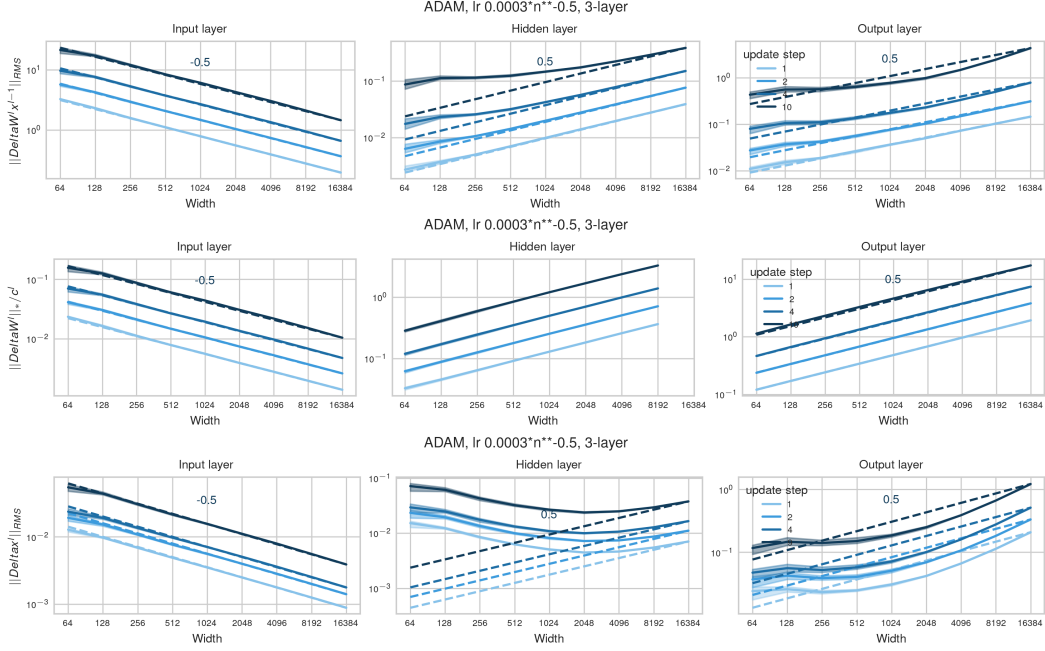


Figure E.9: **(Large finite-width effects from input-layer updates in Adam)** Effective l -th layer update scalings $\|\Delta W_t^l x_t^{l-1}\|_{RMS}$ (top), weight update spectral norm $\|\Delta W_t^l\|_*$ (2nd row) and activation update norm $\|\delta x^l\|_{RMS}$ (bottom) of 3-layer MLPs trained with Adam in SP with large $\eta_n = 0.0003 \cdot n^{-1/2}$. Observe the theoretically predicted exponents in $\|\Delta W_t^l\|_*$ do not transfer to the activation updates at moderate width $n < 8192$ due to large non-vanishing input layer updates at moderate width. Even the effective updates $\|\Delta W_t^l x_t^{l-1}\|_{RMS}$ do not perfectly align with the scaling law at infinite width, indicating that the alignment between ΔW_t^l and x_t^{l-1} evolves non-trivially across width and that the spectral norm $\|\Delta W_t^l\|_*$ and pure infinite-width predictions are less useful for explaining the behaviour of Adam at moderate width.

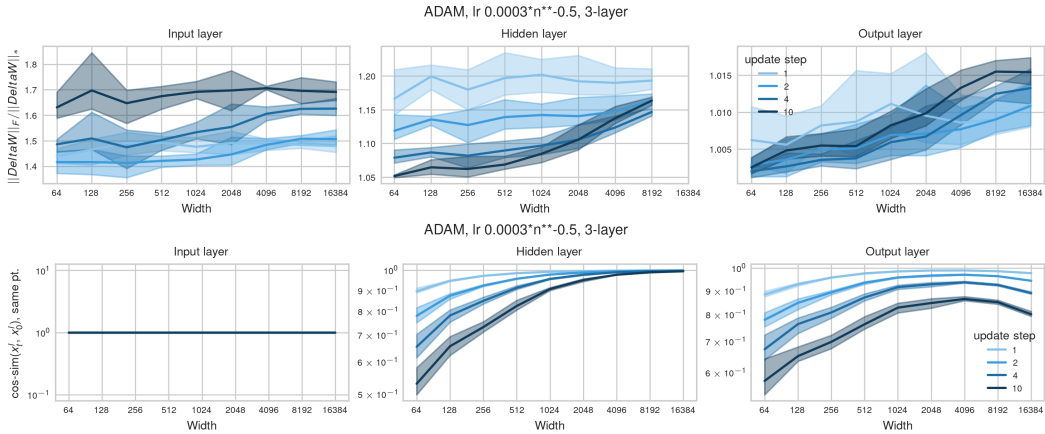


Figure E.10: **(Strong activation rotation under Adam at moderate width)** Effective l -th layer update ranks $\|\Delta W_t^l\|_F / \|\Delta W_t^l\|_*$ (top) and cosine similarity between activations to each layer comparing time 0 and time t on the same input training point (bottom) of 3-layer MLPs trained with ADAM in SP with large $\eta_n = 0.0003 \cdot n^{-1/2}$. The effective update rank is mostly growing in time in the input layer. Already after a few steps, the first-layer activation coordinates are drastically rotated at moderate widths. This induces a u-curve in the hidden-layer activations that inherit large rotation from the input layer at moderate width and update too much at large width under $\eta_n = \Theta(n^{-1/2})$.

E.3 Normalization layers and Adam provide robustness to miss-initialization

For MLPs trained with SGD, initialization greatly impacts the training dynamics as both the forward and the backward pass are affected (Figure E.11). Large input layer initialization induces update instability at large width, which is stabilized by extreme activation sparsification (Figure E.13).

By adding normalization layers, the forward pass can be enforced to scale width-independently. This may affect the gradients. But the gradient norms become irrelevant under Adam with sufficiently small ϵ . Adding both normalization layers and Adam to MLPs, observe that initialization is barely relevant for update scalings (Figure E.12), and other downstream statistics such as activation sparsity (Figure E.14). Here we use RMSNorm to fairly compare activation sparsity, but we expect LayerNorm to induce the same scaling behaviour.

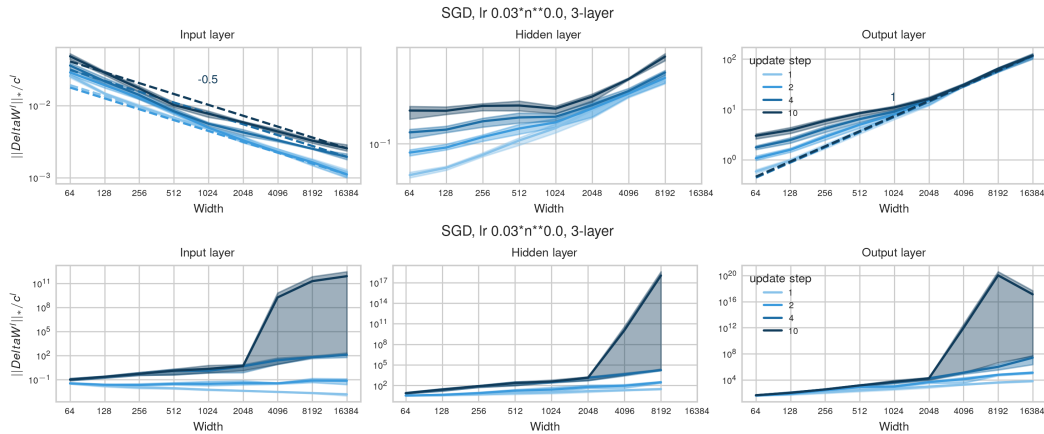


Figure E.11: **(Initialization matters in MLPs with SGD)** SP (top), SP with large input layer variance 2 (bottom). The initializations induce significant differences in the training dynamics. Large input layer normalization becomes unstable at large width.

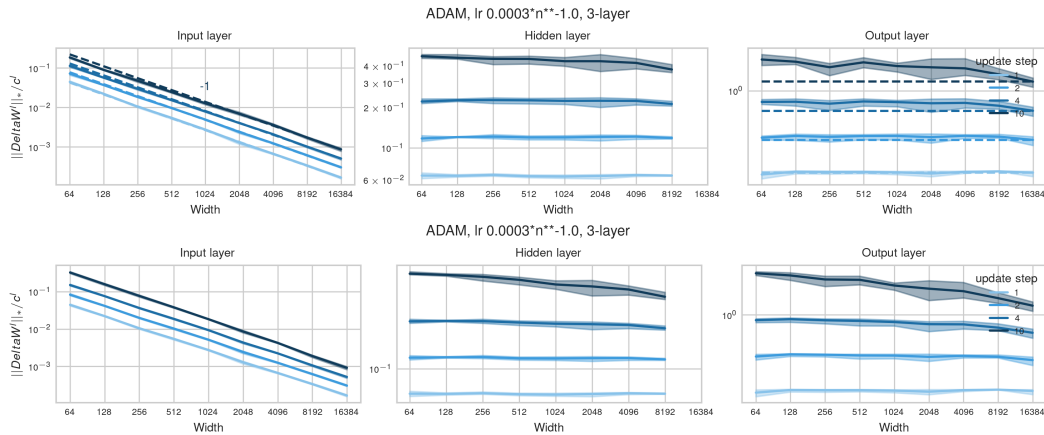


Figure E.12: **(Differing initialization barely matters with normalization layers and Adam)** Update spectral norms of MLPs with the most basic normalization layer RMSNorm after every layer trained with Adam and initialized with SP (top) versus SP with large input layer variance 2 (bottom). Here, initialization barely impacts the update scaling.

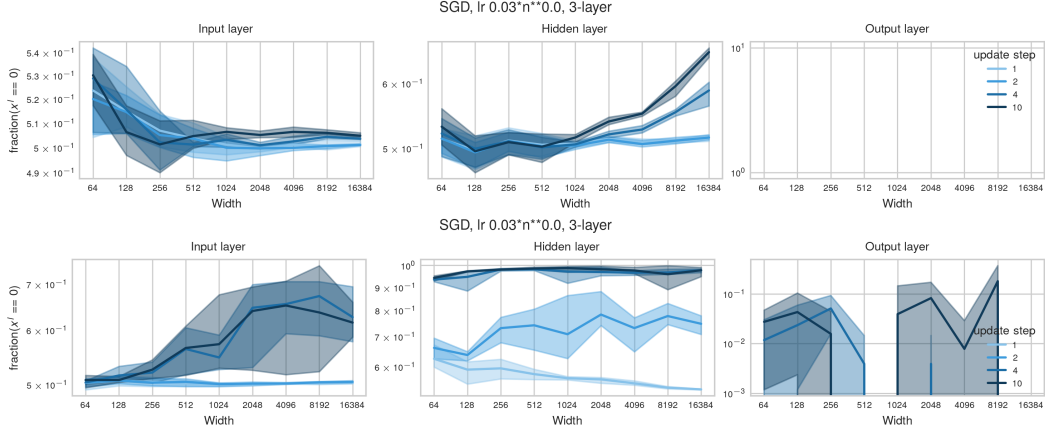


Figure E.13: **(Big difference in activation sparsity under SGD)** SP (top), SP with large input layer variance 2 (bottom). Large input variance has to be stabilized by increased activation sparsity.

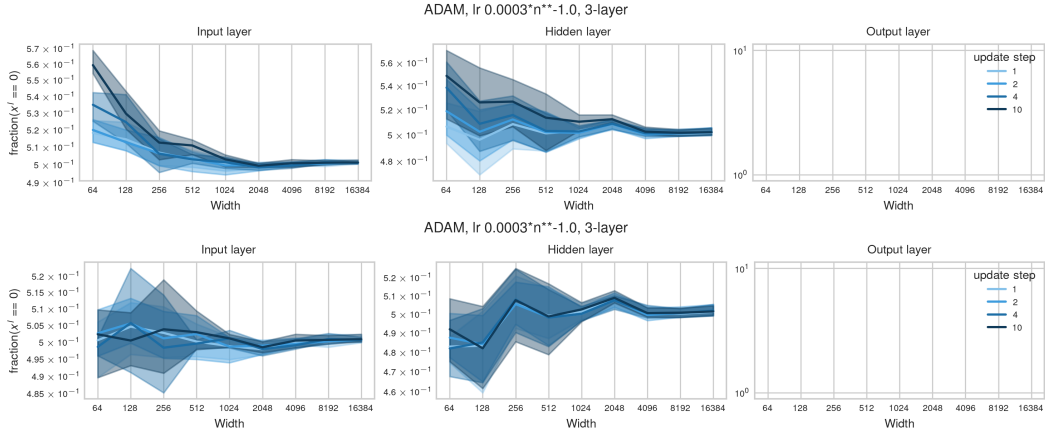


Figure E.14: **(Activation sparsity barely affected under normalization)** Same as Figure E.12 but showing the fraction of activation entries that equal 0. Both initializations do not significantly sparsify activations beyond 50%.

E.4 Alignment and update scaling in Transformers

Since we measure width-independent alignment $\alpha_{W_0^{L+1} \Delta x_t^L} = \Theta(1)$ (Figures 2 and E.15), under large output dimension $d_{\text{out}} \gg n$ (as is typical in language settings), $\|W_0\|_{op}$ approximately scales $\Theta(1)$ (Vershynin, 2010), as opposed to $\Theta(n^{1/2})$ at sufficient width $n \gg d_{\text{out}}$. The term $W_0^{L+1} \Delta x_t^L$ therefore induces approximately width-independent logit updates even under standard last-layer initialization, in the regime $d_{\text{out}} \gg n$ (cf. Figure E.17), but it induces logit divergence at sufficient width $d_{\text{out}} \ll n$.

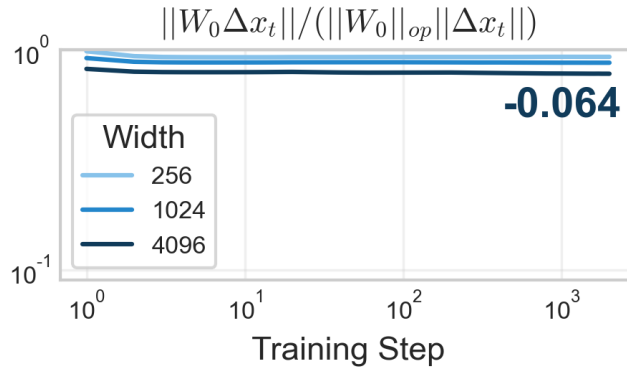


Figure E.15: **(Updates propagate maximally in the readout layer in SP-full-align)** The operator norm ratio for propagating activations in the readout layer for training GPT with AdamW in SP-full-align with near-optimal learning rate $\eta_n = 0.00316$. The ratio is barely width dependent so that propagated activations can be computed when knowing both $\|W_0\|_{op} = \|W_0\|_{RMS \rightarrow RMS}$ and $\|\Delta x_t\|_{RMS}$.

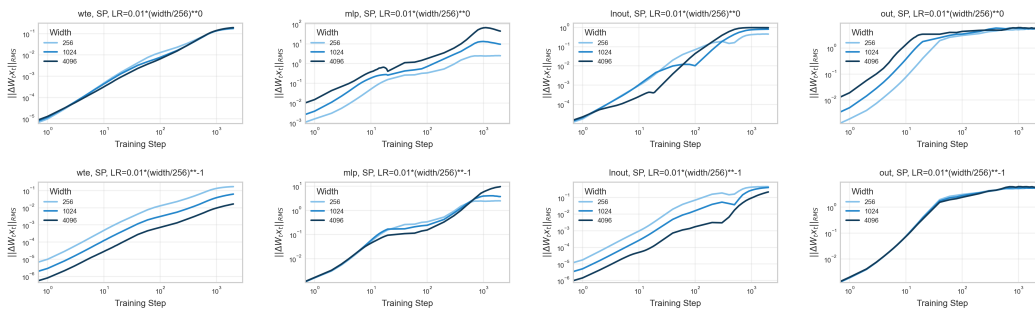


Figure E.16: **(Effective updates follow predictions)** Effective updates $\|\Delta W_t x_t\|$ for constant learning rate scaling $\eta_n = 0.01$ (top) and stable learning rate scaling $\eta_n = 0.01 \cdot (n/256)^{-1}$ (bottom) in GPT models of varying width (the darker, the wider) for the embedding layer, the first MLP layer in the Transformer block 2, the last LayerNorm before the readout layer and the readout layer (from left to right). At constant learning rate, hidden and output layers diverge with width. At optimal learning rate, embedding and normalization layer updates vanish with width.

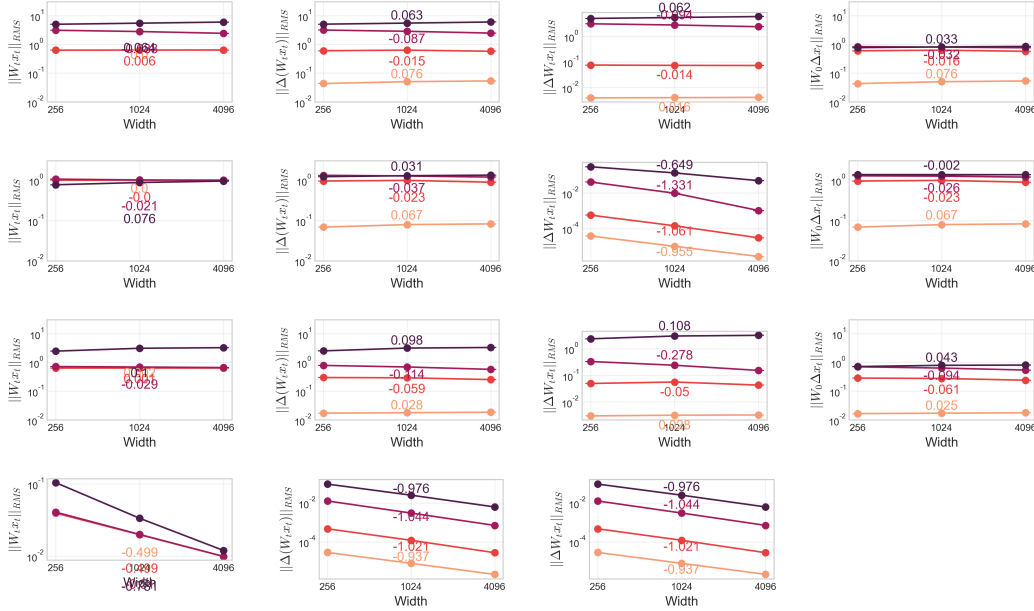


Figure E.17: **(Refined coordinate checks for GPT in SP with Adam and $\eta_n = 0.01 \cdot n^{-1}$)** From left to right: Activation norm, activation updates, effective updates $\|\Delta W_t x_t\|_{RMS}$, propagating updates $\|W_0 \Delta x_t\|_{RMS}$ after 2, 10, 100 and 700 batches of training (the darker, the more batches). Layers from top to bottom: readout, last LayerNorm, first MLP layer in Transformer block 2, embedding layer. Infinite width-scaling predictions are accurate in all effective update terms $\|\Delta W_t x_t\|_{RMS}$: Embedding and LayerNorm layers scale input-like and their updates vanish as $\Theta(n^{-1})$, all hidden and output layers are effectively updated width-independently. Against the infinite-width prediction, logit updates do not explode, not because of miss-alignment but because output dimension is much larger than width $d_{\text{out}} \gg n$, which changes the approximate scaling of $\|W_0^{L+1}\|_{RMS \rightarrow RMS}$ from $\Theta(n^{1/2})$ in the infinite-width limit, to $\Theta(1)$ in the large output dimensional regime.

F Empirical learning rate exponents

F.1 Summary of the MLP experiments in this section

In general, the optimal learning rate exponent appears to be architecture- as well as data-dependent. We conjecture that the optimal learning rate scaling is subject to opposing objectives. Ideally, the effective updates in all layers scale width-independently. Since this cannot be achieved with a single learning rate for input, hidden and output layers, the layer types act on the optimal learning rate scaling as opposing forces.

SGD under MSE loss. For SGD under MSE loss, output blowup results in unstable training dynamics so that the maximal stable and optimal learning rate robustly scales as $\eta_n = \Theta(n^{-1})$ across architectures and datasets. As a consequence of vanishing feature learning, neither training nor test loss monotonically improve with scale under MSE loss.

Random feature models. When only training the last layer, fully width-independent training dynamics are achieved with $\eta_n = \eta \cdot n^{-1}$. Figure F.18 shows that this exponent clearly results in learning rate transfer for 2-layer ReLU random feature networks on CIFAR-10. Also observe that since all learning rate scalings recover activation-stability, larger than optimal learning rates still result in non-trivial classification accuracy.

Deep MLPs. With an increasing amount of hidden layers, their width-independence eventually outweighs input layer feature learning in vision datasets. For at least 6 layers, we see approximate learning rate transfer under $\eta_n = \Theta(n^{-1/2})$ for SGD and $\eta_n = \Theta(n^{-1})$ for Adam as predicted for width-independent hidden layer feature learning for both CIFAR-10 and MNIST.

Shallow ReLU MLPs at moderate width and (deep) linear networks are not useful proxy models for deep nonlinear networks. For shallow MLPs, we often observe stronger finite-width effects than for deeper networks causing larger than predicted optimal learning rate scaling at moderate width, as divergence in fewer hidden layers can be stabilized over the course of training up to larger widths (cf. [Appendix E](#)). In linear networks, on the other hand, feature learning is not essential as the learned function always remains linear. Consequently we often observe that optimal learning rates decay faster than maximal-stable learning rates in (deep) linear networks even under CE loss ([Figures F.12](#) and [F.31](#)). These differences between deep non-linear networks and toy architectures suggest that shallow MLPs and deep linear networks do not serve as useful proxy models for practical non-linear networks in terms of optimal learning rate exponents at moderate width.

Input layer task. Under multi-index data with a sparse signal and high-dimensional isotropic covariates (explained in [Appendix D.2](#)), learning the two signal input dimensions is particularly useful for good generalization. [Appendix F.3](#) shows the predicted exponent $\eta_n = \eta \cdot n^0$ for input layer learning in 2-layer MLPs. Deeper MLPs recover hidden layer stability with optimal learning rate scaling $\eta_n = \Theta(n^{-1/2})$. Observe that generalization suffers when the input layer does not learn to align with the signal dimensions, so that only the 2-layer MLP with CE loss generalizes well at large width.

Standard initialization with μ P learning rates (SP-full-align). While [Everett et al. \(2024\)](#) report good transfer properties of SP-full-align, [Appendix F.8](#) shows that the optimal learning rate clearly shrinks across image datasets and our multi-index data. We also introduce a variant of this parameterization that matches the $n^{1/2}$ logit blowup rate from the term $W_0^{L+1} \Delta x_t$ in the effective last-layer updates by increasing the last-layer learning rate. This variant performs similarly well as SP-full-align. In particular, both variants seem to be less learning rate sensitive than μ P.

Adam learns features with $\eta_n = \eta \cdot n^{-1}$. Adam simplifies the learning rate scaling for weight W to $\eta_W = \eta / \text{fan_in}(W)$, because the gradient is normalized but still correlated with the incoming activations since the sign is preserved in each entry. Thus $\eta_n = \eta/n$ is expected to induce width-independent hidden- and output-layer learning, but vanishing input-layer learning since here `fan_in` is fixed and hence would require constant learning rate scaling. As for SGD, we still observe the optimal learning rate scaling $\eta_n = \eta \cdot n^{-1}$ in deep MLPs on MNIST ([Appendix F.5](#)) and on CIFAR-10 ([Appendix F.7](#)), indicating that width-independence in hidden- and output-layer dominates input layer feature learning.

F.2 Transformer experiments

As we consider single-pass training, training and validation loss approximately coincide, so that statements about the training loss transfer to statements about the validation loss irrespective of the optimizer. All figures in this section show training loss on the left and validation loss on the right.

Stabilizing techniques like gradient clipping can improve the absolute learning rate multiplier in front of the scaling law, but do not seem to change the width-scaling exponent for SGD ([Figure F.4](#) vs [Figure F.5](#)).

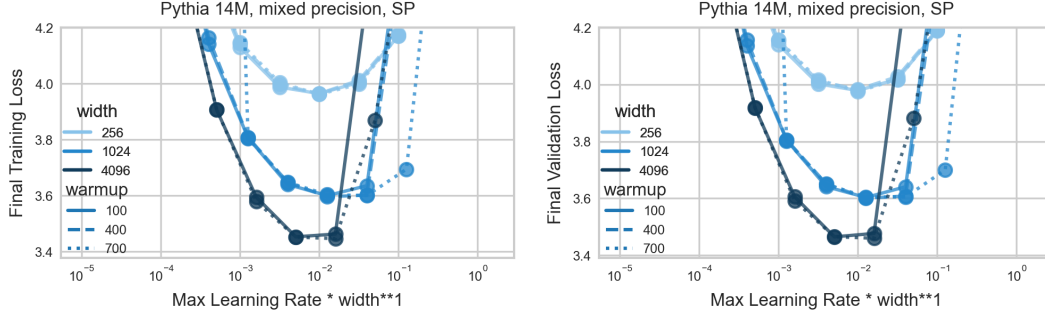


Figure F.1: **(Instability without qk-Layernorm)** Train loss (left) and validation loss (right) of single-pass AdamW training without qk-Layernorm. Training and validation loss approximately coincide. Optimal learning rate scaling is dominated by the maximal stable learning rate scaling that is at most $\Theta(n^{-1})$. But without qk-Layernorm, the stability threshold is decreasing faster than $\Theta(n^{-1})$ even when increasing warmup length, so that it may be that the instability threshold would decay beyond the ideal learning rate and performance suffers. As our computational budget does not allow us to scale further, this setting remains inconclusive.

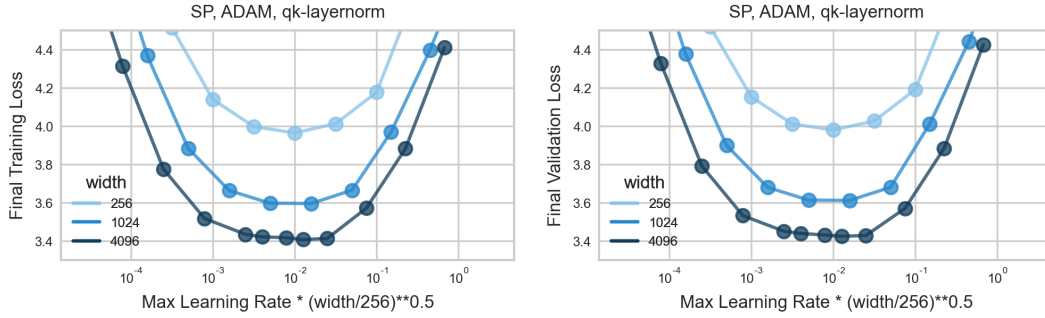


Figure F.2: **Large learning rate stability with qk-Layernorm** Same as Figure F.1 but with qk-Layernorm as recommended by Wortsman et al. (2024). Training and validation loss approximately coincide. The optimal learning rate seems to approximately transfer under $\eta_n = \eta \cdot n^{-1/2}$, so the added Layernorm appears to stabilize learning at larger learning rate scaling, similar to the softmax in CE loss.

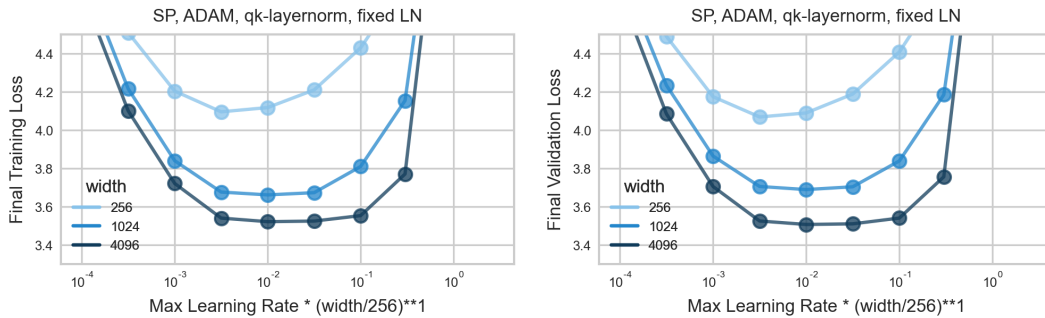


Figure F.3: Same as Figure F.1 with qk-Layernorm as recommended by Wortsman et al. (2024), but all trainable Layernorm parameters are fixed to initialization. Here only the embedding layer behaves input-like, so that all other parameters learn width-independently under learning rate scaling $\Theta(n^{-1})$. While the optimum is drifting toward larger learning rates, an increasingly large plateau of near-optimal learning rates emerges at large width. $\Theta(n^{-1})$ still approximately captures the maximal stable learning rate scaling.

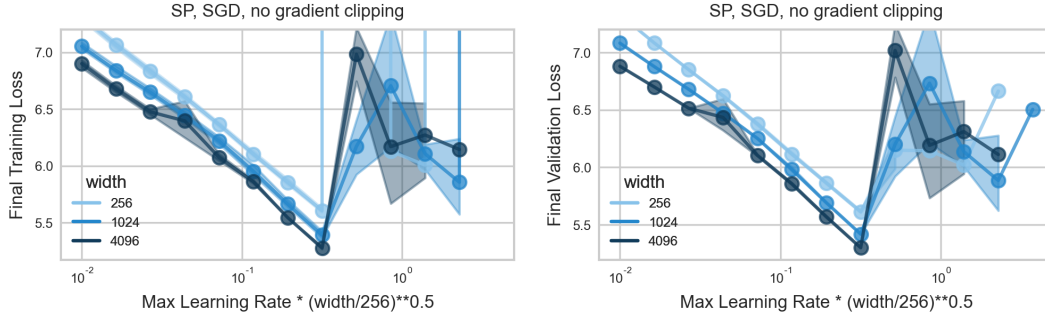


Figure F.4: **(GPT trained with SGD has $\Theta(n^{-1/2})$ -learning rate scaling)** Train loss (left) and validation loss (right) of single-pass SGD training (averaged over 3 random seeds affecting weight initialization and data shuffling). Training and validation loss approximately coincide. Hence also validation-optimal learning rate scaling is dominated by maximal stable learning rate scaling $\Theta(n^{-1/2})$ for hidden-layer stability.

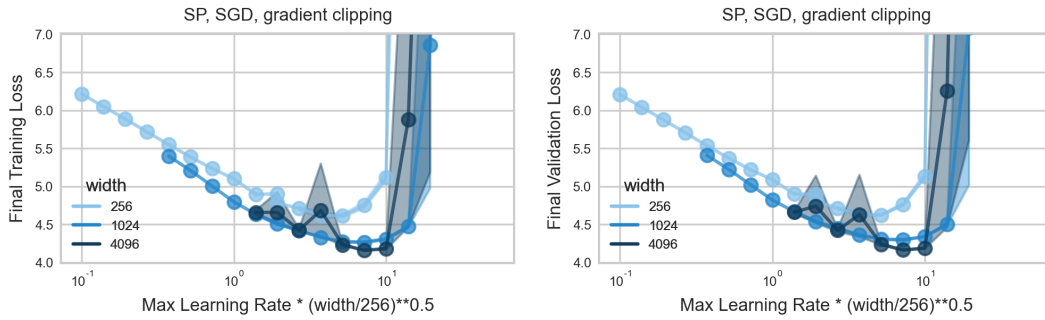


Figure F.5: Same as Figure F.4 but with gradient clipping. Performance is significantly improved as larger learning rate constants are stable (observe similar performance as without gradient clipping at the same learning rate). Optimal learning rate scaling is still dominated by the maximal stable learning rate scaling $\eta_n = \eta \cdot n^{-1/2}$ for hidden-layer stability.

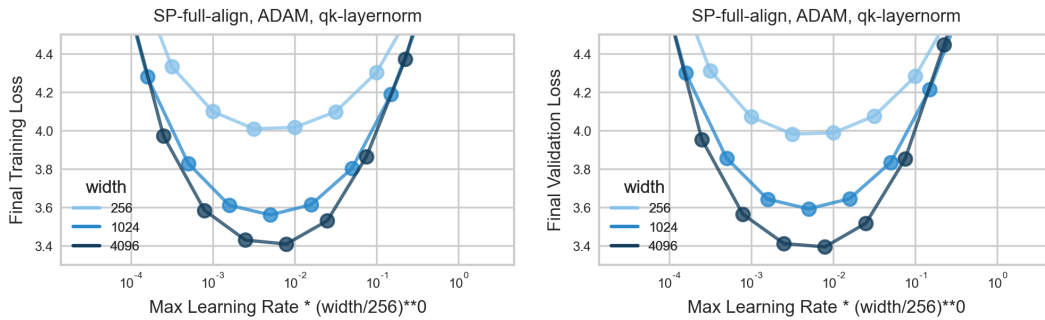


Figure F.6: Same as Figure F.2 but in SP-full-align. AdamW in SP-full-align and SP with a global learning rate seem to have similar performance without multiplier tuning. SP-full-align approximately transfers the learning rate here in the $d_{\text{out}} \gg n$ regime, but not in the $d_{\text{out}} \ll n$ regime in Appendix F.8.

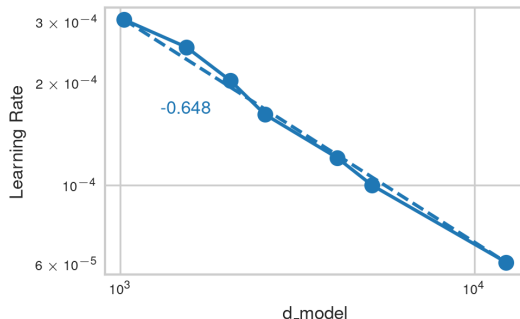


Figure F.7: **Large learning rate exponent in original GPT paper.** Just plotting the reported learning rate and `d_model` values from [Brown et al. \(2020\)](#) results in quite a stable scaling law with exponent -0.648 , which is larger than -1 required for hidden-layer stability but significantly smaller than 0 required for width-independent input layer learning. But note that jointly increasing batch size, `n_layers` and `n_heads` might be confounding factors here.

F.3 Cross-entropy loss enables large-learning rate training

MLPs on multi-index data. Here we train 2-layer and 3-layer ReLU MLPs on generated multi-index teacher data as detailed in [Appendix D](#). These data crucially differ from the other considered datasets in that the target function only depends on the first 2 input dimensions. Due to the isotropic covariate distribution, input layer feature learning is necessary for good generalization. Hence we observe a clear $\eta_n = \Theta(1)$ scaling for 2-layer MLPs with CE loss, necessary for preserving input layer feature learning ([Figure F.8](#)). 3-layer MLPs attain the maximal activation-stable exponent $\eta_n = \Theta(n^{-1/2})$ in CE loss ([Figure F.9](#)). 2-layer MLPs preserve a better validation accuracy compared to their training accuracy than deeper nets, as input layer learning gets increasingly inhibited by $\Theta(1)$ -learning rate instability in the presence of hidden layers. Both for shallow and deeper MLPs with MSE loss, we lose feature learning under the maximal output-stable scaling $\eta_n = \Theta(n^{-1})$, as expected.

In this setting, it becomes particularly apparent that using the MSE loss with a softmax applied to the output of the network is not desirable. Ultimately, the only difference to CE loss is that the loss derivative with respect to the network output $f(\xi) := W^{L+1}x^L(\xi)$ becomes

$$\left(\frac{\partial \mathcal{L}}{\partial f}\right)_j = \sum_{i \in [C]} (\sigma(f)_i - y_i) \sigma(f)_i (\delta_{ij} - \sigma(f)_j),$$

where the inner derivative of the softmax $\sigma_i(\delta_{ij} - \sigma_j)$ vanishes as soon as the outputs diverge $|f_i(\xi) - f_j(\xi)| \rightarrow \infty$ on a training point ξ . Hence, while the softmax still mitigates output blowup in the forward pass, the gradients vanish under output blowup. The CE loss, on the other hand, is exactly the correct choice of loss function to cancel out the inner derivative of the softmax and effectively view $\sigma(f)$ as the output of the network, resulting in $\left(\frac{\partial \mathcal{L}}{\partial f}\right)_j = \sigma(f)_j - y_j$.

Here vanishing gradients under output blowup in the MSE+softmax setting is so severe that output blowup prevents learning under large learning rates and the optimal learning rate scales as $\Theta(n^{-1})$.

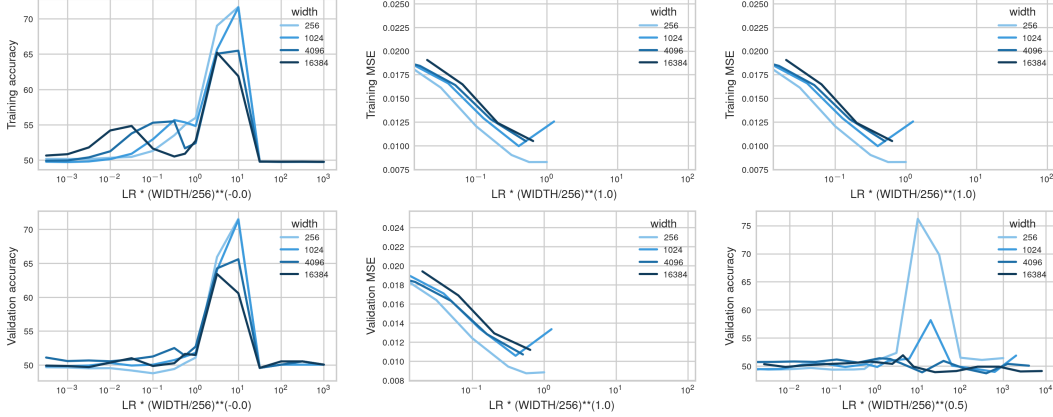


Figure F.8: **(Cross-entropy loss increases maximal stable learning rate scaling to approximately $\Theta(1)$ in 2-layer nets)** Training accuracy (top) and validation accuracy (bottom) for a 2-layer MLP on generated multi-index teacher data (mean over 4 seeds) with CE loss (left), MSE loss (center) and MSE loss with softmax (right). The x-axis scales the learning rate with width-dependent exponents; observe approximate transfer under $\Theta(1)$, $\Theta(n^{-1})$ and $\Theta(n^{-1})$ scaling, respectively. In the MSE plot, ending lines indicate divergence for larger learning rates. MSE loss with softmax on the output does not increase optimal learning rate scaling due to vanishing gradients and gets worse due to a lack of input layer feature learning.

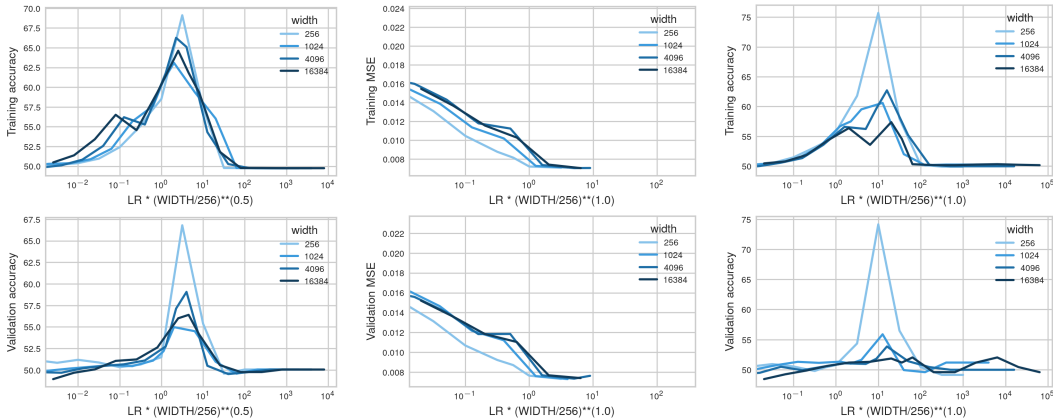


Figure F.9: **(Cross-entropy loss increases maximal stable learning rate scaling to approximately $\Theta(n^{-1/2})$ in 3-layer nets)** Same as Figure F.8 but for a 3-layer MLP. The x-axis scales the learning rate with width-dependent exponents; observe approximate transfer of the maximal stable learning rate under $\Theta(n^{-1/2})$, $\Theta(n^{-1})$ and $\Theta(n^{-1})$ scaling, respectively. In the MSE plot, ending lines indicate divergence for larger learning rates. Observe that wider networks generalize worse with scale as they lose input layer feature learning.

F.4 MLPs with SGD on MNIST

With MSE loss, observe a clear $\mathcal{O}(n^{-1})$ optimal and maximal stable learning rate exponent for all network variants (Figure F.10).

With CE loss, observe that 2-layer MLPs transfer the optimal and maximal stable learning rate n^0 (Figure F.11). 3 and 4 layer MLPs are still able to transfer the maximal stable learning rate, indicating self-stabilization of activation blowup at moderate width. In 6, 8 and 10 layer MLPs the maximal stable learning rate scaling $n^{-1/2}$ becomes increasingly pronounced, as it becomes increasingly difficult to stabilize activation blowup in an increasing amount of hidden layers while an increasing amount of layers is learning under $n^{-1/2}$ learning rate scaling.

3 and 4 layer linear MLPs clearly show how the maximal stable learning rate scales as n^0 whereas the optimal learning rate scales as n^{-1} (Figure F.12). While activations can be shrunk for self-stabilization in linear nets, they lack the ability to learn non-linear features for the improved generalization at large learning rates. Hence losing feature learning but preventing the necessity to shrink activations under small learning rates n^{-1} is optimal. Observe that also deeper linear MLPs are only stable under $n^{-1/2}$ as theoretically predicted.

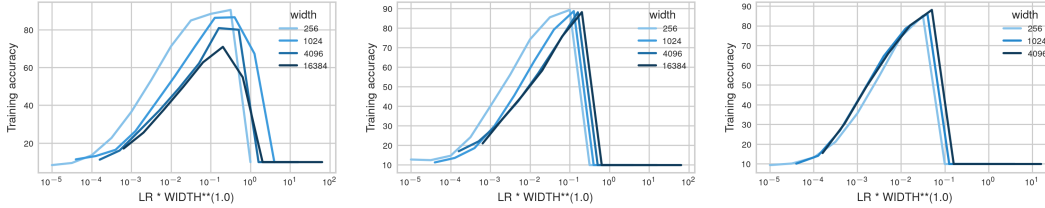


Figure F.10: **(MSE loss on MNIST approximately transfers under $\Theta(n^{-1})$ learning rate scaling)** Both the optimal as well as the maximal stable learning rate approximately transfer under global $\Theta(n^{-1})$ learning rate scaling when training 2, 3 or 10 layer MLPs (from left to right) with MSE loss on MNIST. Loss is not improving as feature learning is lost under $\Theta(n^{-1})$ scaling. Especially in 2 layer nets, the input layer is learning features at small width, but not at large width.

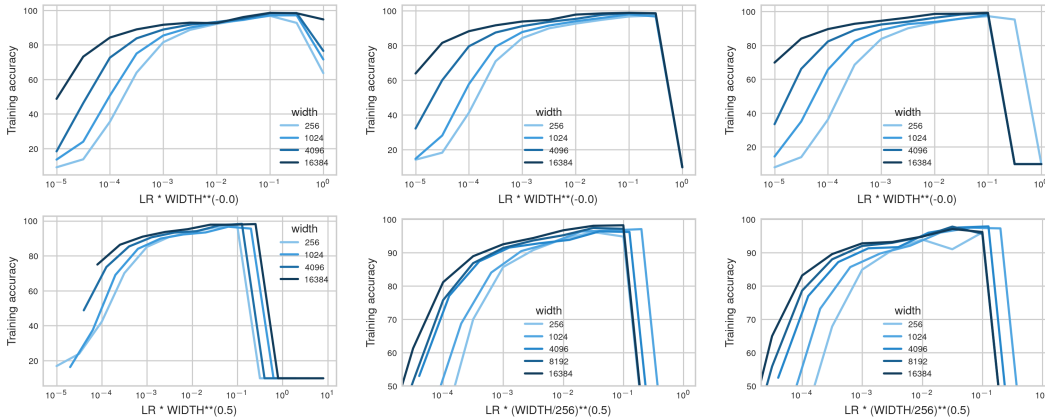


Figure F.11: **(Deeper nets follow infinite width theory increasingly accurately)** Training accuracy after 1 epoch of training MLPs with 2, 3, 4, 6, 8 and 10 layers (from top-left to bottom right) on MNIST. While 2, 3 and 4 layer MLPs self-stabilize under large learning rates $\Theta(n^0)$ and approximately transfer the optimum as well as max-stable learning rate, in 6, 8 and 10 layer MLPs it becomes increasingly apparent that the maximal stable learning rate transitions towards $\Theta(n^{-1/2})$ to prevent hidden layer blowup, which also forces the optimal learning rate to be $\mathcal{O}(n^{1/2})$ for at least feature learning in the hidden layers. Hence the theoretical activation stability predictions hold more accurately in deeper nets, with too many hidden layers to stabilize blowup in all of them.

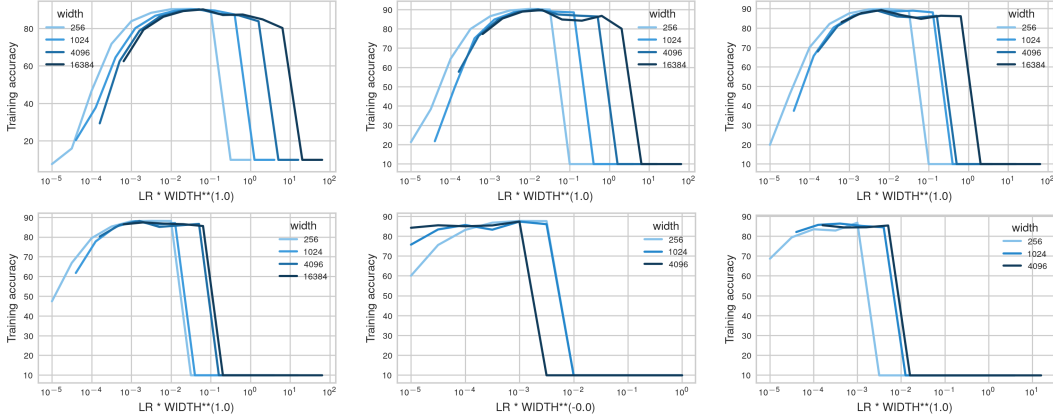


Figure F.12: **(In linear nets on MNIST, the optimal learning rate shrinks faster than the maximal stable learning rate)** Same as Figure F.11 but for linear nets. The maximal stable learning rate scales similarly as for the non-linear nets, but the optimum approximately follows $\Theta(n^{-1})$. Irrespective of the depth, linear MLPs can only learn a linear transformation; hence under sufficient width, feature learning under large learning rates does not provide a benefit over mere last-layer learning.

F.5 MLPs with ADAM on MNIST

Figure F.13 shows that for deep MLPs trained with Adam on MNIST the optimal learning rate scales at most as $\eta_n = \mathcal{O}(n^{-1})$.

MLPs with 2 or 3 layers tend to have larger optimal learning rate scaling exponents around $n^{-1/2}$, but with an increasing amount of layers the conflicting objectives of first layer versus hidden layer width-independent learning are dominated by the increasing number of hidden layers.

For all depths, the instability threshold appears to scale as $\eta_n \approx \Theta(n^{-1/2})$, but since Adam has a wide regime of suboptimal large learning rates where its moments are already harmed (?), the maximal stable learning rate threshold is often less clear cut compared to SGD.

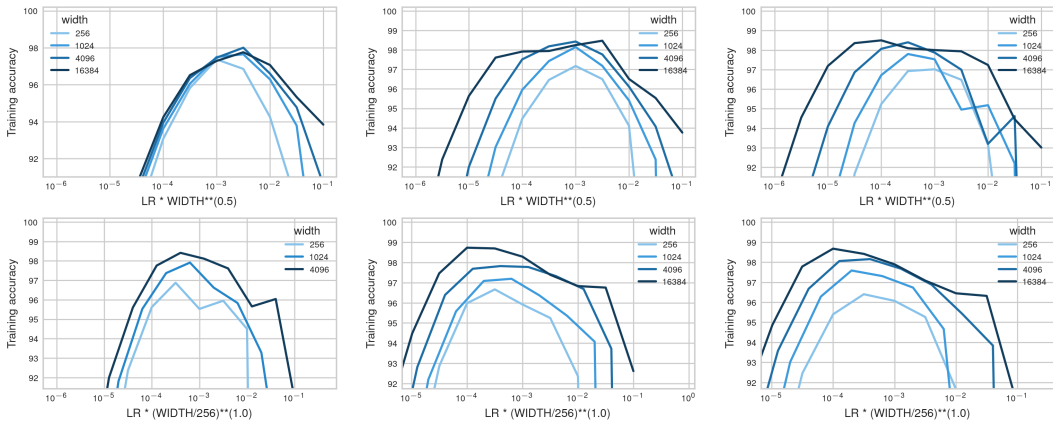


Figure F.13: **(Learning rate transfer in deep MLPs for ADAM on MNIST)** MLPs trained with ADAM on MNIST with 2, 3, 4, 6, 8, 10 layers (from top left to bottom right). In the first row, the x-axis is width-dependently scaled to show approximate transfer under $n^{-1/2}$ learning rate scaling. In the bottom row, the x-axis is width-dependently scaled to show approximate transfer under $\eta_n \approx \Theta(n^{-1})$. Observe the optimal learning rate scaling transitioning from larger than $\Theta(n^{-1/2})$ in 2-layer MLPs toward at most $\Theta(n^{-1})$ with increasing depth.

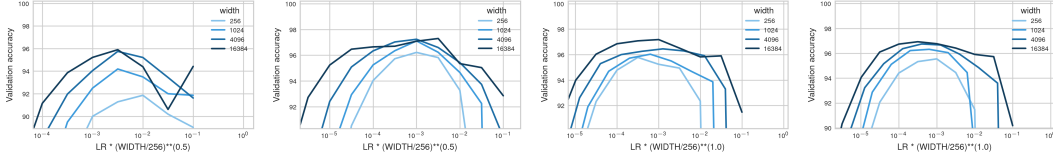


Figure F.14: **(Transfer in validation accuracy in deep MLPs for ADAM on MNIST)** Validation accuracy of MLPs trained with ADAM on MNIST with 2 layer random feature, 3, 8, 10 layers (from left to right). Validation-optimal learning rate in deep MLPs scales as $\eta_n = \mathcal{O}(n^{-1})$. 2 layer RF and 3 layer nets appear to approximately transfer under $\eta_n \approx \Theta(n^{-1/2})$ but lose monotonic improvement and predictability at scale.

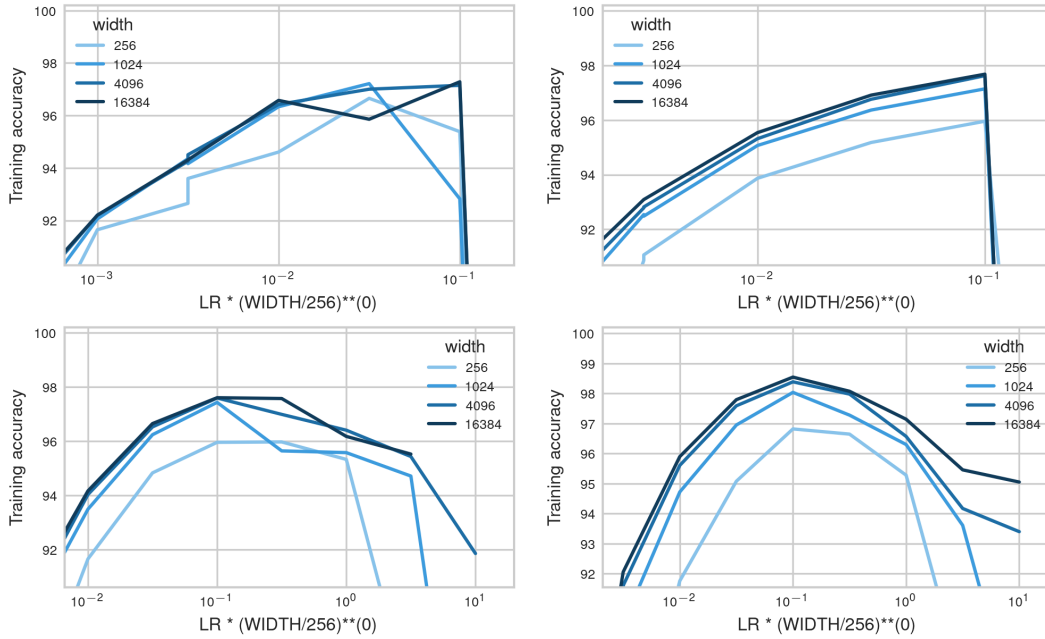


Figure F.15: **($\mu\mathbf{P}$ as a baseline for transfer)** 8-layer MLPs trained on MNIST with SGD (top) and ADAM (bottom) under CE loss (left) and MSE loss (right). No systematic learning rate shifts in $\mu\mathbf{P}$; saturating drifts may occur. Transfer and monotonic improvement looks less noisy under MSE loss.

F.6 MLPs with SGD on CIFAR-10

2-layer random feature ReLU MLPs very clearly transfer under $\eta_n = \eta \cdot n^{-1}$ learning rate scaling under any loss. Under CE loss, also larger learning rates result in non-trivial learning as saturating the softmax does not harm training stability. Under MSE loss on the other hand, training diverges above the edge of stability and results in trivial accuracy of 10%. Under MSE with softmax on the output logits, a exploding logits induce vanishing gradients which also inhibits learning (see Appendix F.3 for more details), and results in worse accuracy than under CE loss.

For 2-layer ReLU MLPs under CE loss, the maximal stable learning rate scales as $\eta_n = \Theta(1)$ as predicted under activation stability. The optimal learning rate however is a trade-off between input layer feature learning and output layer stability. Here an output layer that explodes too sharply appears to perform suboptimally. But under small learning rates $\eta_n = \mathcal{O}(n^{-1/2})$, feature learning is lost and accuracy gets worse with scale.

For 3-layer RELU MLPs with CE loss, the maximal stable learning rate and the optimal learning rate transfer over many widths before beginning to shrink at width 16384. Over 782 updates, an initial catapult can be stabilized at moderate width as long as training does not diverge early such as under MSE loss. Apparently, large hidden layer updates can be stabilized over the course of training. As

an additional inductive bias that self-stabilizes large gradients, activations are sparsified which may enhance generalization under large learning rates.

Figure F.19 shows very slow decay of the optimal learning rate also in 4- and 6-layer MLPs, but deeper MLPs eventually require $\eta_n = \Theta(n^{-1/2})$ for stable hidden layer updates.

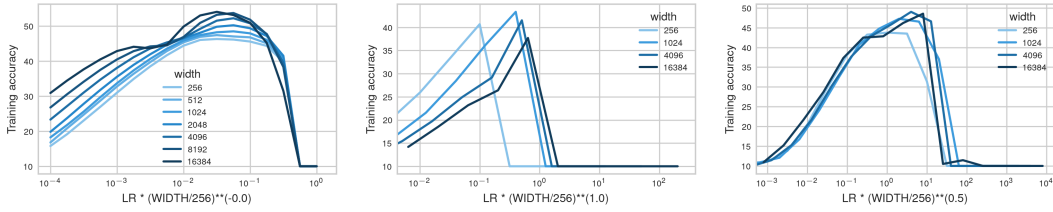


Figure F.16: **(Softmax increases maximal stable learning rate scaling)** Training accuracy after one epoch of training 3-layer MLPs on CIFAR 10 with CE loss (left), MSE loss (center) and MSE loss with softmax (right). The x-axis scales the learning rate with width-dependent exponents to show approximate transfer under $\Theta(1)$, $\Theta(n^{-1})$ and $\Theta(n^{-1/2})$ scaling, respectively.

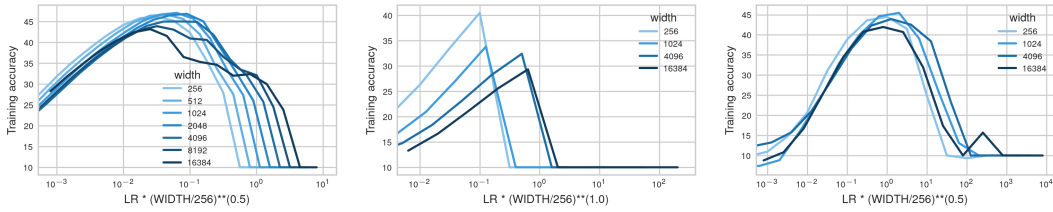


Figure F.17: **(Softmax increases maximal stable learning rate scaling)** Same as Figure F.16 but with 2-layer MLPs and approximate transfer under $\Theta(n^{-0.5})$, $\Theta(n^{-1})$ and $\Theta(n^{-1/2})$. Note how the maximal stable learning rate rather scales as $\Theta(1)$, but the optimal learning rate rather scales as $\Theta(n^{-1/2})$.

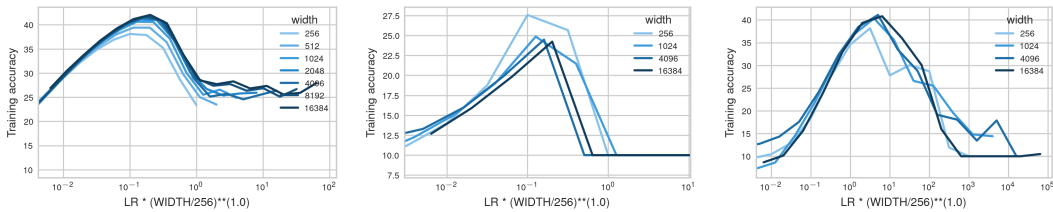


Figure F.18: **(Random feature models approximately transfer under $\eta_n = \Theta(n^{-1})$ for SGD)** Same as Figure F.16 but with 2 layers and only training the last layer results in approximately width-independent dynamics with $\eta_n = \eta \cdot n^{-1}$ independent of the loss function or architecture used. Note that also larger learning rates result in non-trivial generalization because there is no instability caused by activation blowup. The larger learning rates are not optimal, because the usual benefits of larger learning rates like increased feature learning or activation sparsity do not apply to random feature models.

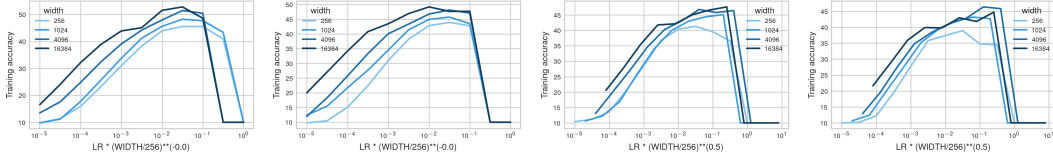


Figure F.19: **(Hidden-layer stability determines learning rate scaling in deep MLPs for SGD on CIFAR-10)** MLPs trained with SGD on CIFAR-10 with 4, 6, 8 and 10 layers (from left to right). First two x-axes are width-independent, last two scaled by $n^{1/2}$. While 4- and 6-layer MLPs self-stabilize sufficiently for approximate transfer under width-independent learning rate scaling, 8- and 10-layer MLPs have a clear max-stable learning rate scaling $n^{-1/2}$.

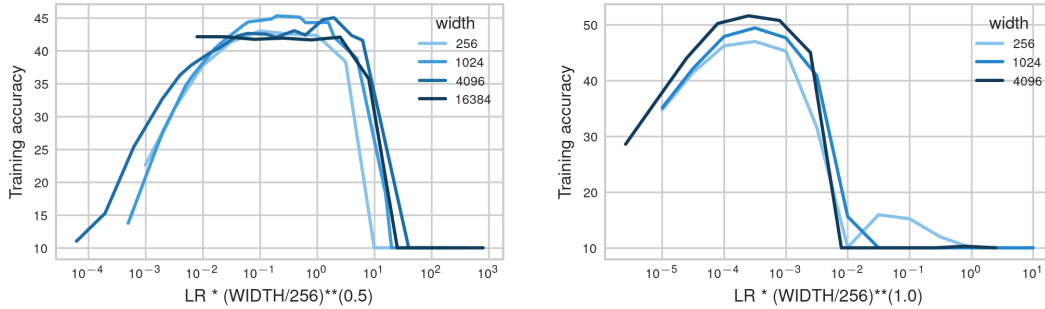


Figure F.20: **(Hidden-layer stability determines learning rate scaling in deep MLPs for SGD on CIFAR-10)** 8-layer MLPs trained with SGD (left) and Adam (right) on CIFAR-10 with MSE loss with LayerNorm applied to the logits. The LayerNorm has a similar stabilizing effect as CE loss and allows learning with logit blowup under $\eta_n = \Theta(n^{-1/2})$. For Adam, hidden and output layers learn width-independently with $\eta_n = \Theta(n^{-1})$.

E.7 MLPs with ADAM on CIFAR-10

All networks in Figure F.21 appear to transfer under large $\eta_n = \Theta(n^{-1/2})$ learning rate scaling. This scaling clearly induces activation blowup in the forward pass. A crucial difference to SGD is that activation blowup does not affect the updates in Adam since the gradient is normalized. For SGD, exploding gradients induce even larger explosion in the next forward pass, which in turn induces even larger explosion in the next backward pass. Hence, without activation stability, even the divergence exponent grows over time in SGD. For Adam, on the other hand, gradients are normalized, so that the forward pass always accumulates the same width-dependent exponent that is stabilized when passed through the softmax. Thus under sufficient numerical precision, from a stability point of view, Adam can even tolerate larger learning rates than the hidden-layer feature learning $\eta_n = \Theta(n^{-1})$, and the optimal learning rate may also be pushed toward input layer feature learning. Indeed, when fixing the first layer (Figure F.22), all MLPs transfer under $\eta_n = \Theta(n^{-1})$, which now achieves full width-independent effective updates. In this variant there are no conflicting objectives trading off hidden-layer and input-layer width-independence.

The fact that Adam with MSE loss (Figure F.23) can have large optimal learning rates $\eta_n = \Theta(n^{-1/2})$ indicates that the crucial effect of CE loss in SGD is stabilizing the gradients. Adam similarly limits the step size as the update scale is independent of χ_t . As for SGD, at large depth hidden-layer width-independence tends to dictate the optimal learning rate.

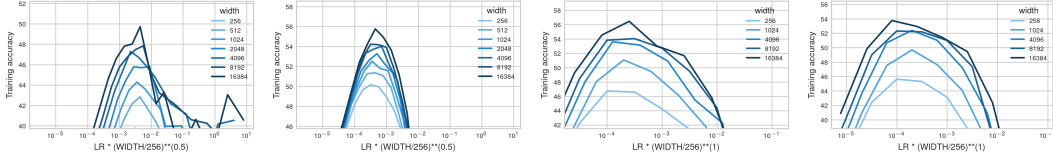


Figure F.21: **(Learning rate exponent $\eta_n = \Theta(n^{-1})$ for ADAM in deep MLPs on CIFAR-10)** MLPs trained with ADAM on CIFAR-10 with 2-layer random features, 2, 8, 10 layers (from left to right). The first 2 x-axes show approximate transfer under $n^{-1/2}$ learning rate scaling, the last 2 under n^{-1} learning rate scaling. As for SGD, in deeper nets hidden-layer width-independence dominates input-layer width-independence and induces optimal learning rate scaling $\eta_n \approx \Theta(n^{-1})$.

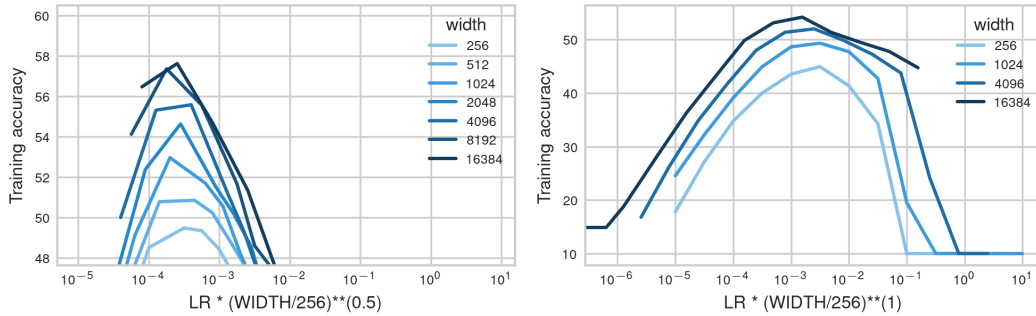


Figure F.22: **(Trade off between input- and hidden-layer width-independence)** 3-layer MLPs trained with ADAM on CIFAR-10 (left) and not training the first layer (right). 3-layer MLPs approximately transfer under $\eta_n = \Theta(n^{-1/2})$, being pushed toward input-layer feature learning. As there are no conflicting goals like preserving input layer feature learning, 3-layer MLPs with fixed input layer follow the width-independent exponent $\eta_n = \Theta(n^{-1})$ that yields hidden- and output-layer width-independent feature learning.

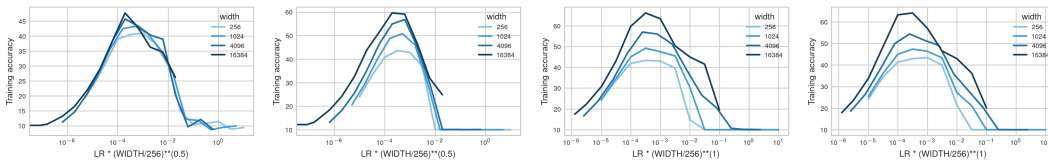


Figure F.23: **(Adam stabilizes the backward pass even under MSE loss)** MLPs trained with ADAM on CIFAR-10 under MSE loss with 2, 3, 6, 8 layers (from left to right). 2 and 3 layers show approximate transfer under $n^{-1/2}$ learning rate scaling, 6 and 8 layers show approximate transfer under n^{-1} .

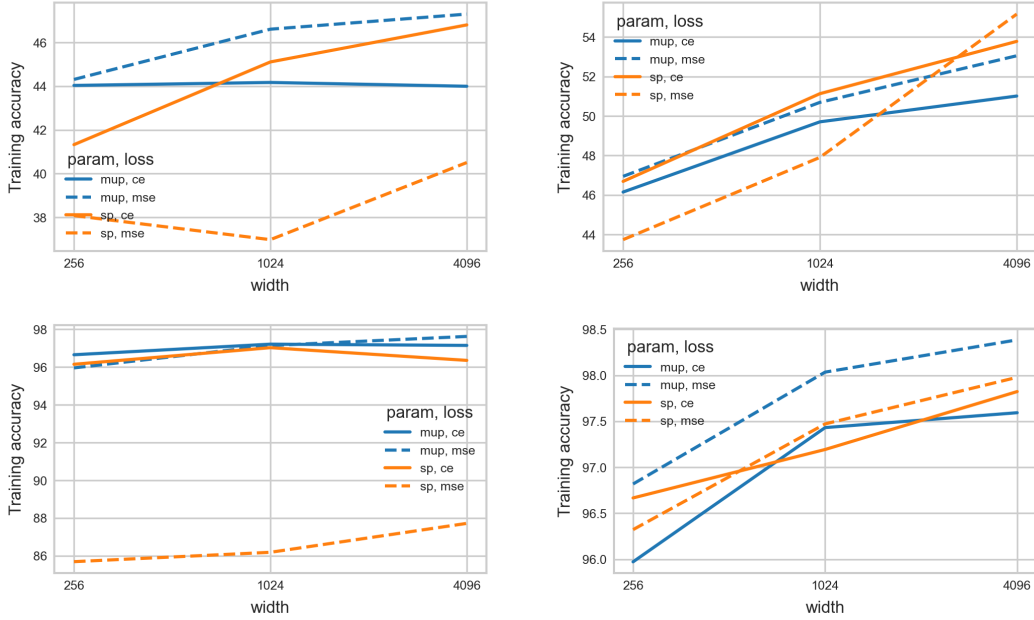


Figure F.24: **(Large performance difference between losses for SGD in SP)** Optimal training accuracy of 8-layer MLPs trained with SGD (left) and Adam (right) on CIFAR-10 (top) and MNIST (bottom) with MSE loss (dashed lines) and CE loss (solid lines) in μ P (blue) and SP (orange). For SGD in SP, CE loss performs much better than MSE loss as large learning rates recover feature learning at large widths. The performance in μ P depends much less on the loss function since features are always learned width-independently. In μ P, MSE loss slightly outperforms CE loss. For ADAM, small learning rates $\eta_n = \Theta(n^{-1})$ in SP recover hidden-layer feature learning so that the difference between losses is much smaller.

F.8 Effective update parameterizations beyond μ P

The logit updates can be decomposed into

$$f_t(\xi) - f_0(\xi) = W_0^{L+1} \Delta x_t^L(\xi) + \Delta W_t^{L+1} x_t^L(\xi),$$

for arbitrary inputs $\xi \in \mathbb{R}^{d_{in}}$ and $\Delta W_t^{L+1} = \sum_{t'=0}^{t-1} \chi_{t'} \cdot x_{t'}^L(\xi_{t'})$.

In this section, we consider vision and generated data sets in the regime $n \gg d_{out}$. First note that under large last-layer initialization $(W_0^{L+1})_{ij} \sim N(0, n^{-1})$ as in SP, fully width-independent training dynamics are impossible, since width-independent feature learning $\Delta x_t^L = \Theta(1)$ implies logit blowup through the term $W_0^{L+1} x_t^L = \Theta(n^{1/2})$ for both SGD and Adam. The fact that logit blowup does not prevent stable training under CE loss explains why we can achieve non-vanishing feature learning under SP last-layer initialization. When dropping the logit stability constraint, we can ask which is the optimal layerwise learning rate scaling under standard last-layer initialization. Following the μ P desiderata, we still want to effectively update all layers, meaning a non-vanishing effect of the weight updates in each layer on the output function. With the correct choice of layerwise learning rates, we can still satisfy these desiderata for all scalings of last-layer initialization variance, which also implies that there is not a unique *abc*-equivalence class to fulfill these effective update desiderata when not requiring logit stability. We will see that SP full-align in [Everett et al. \(2024\)](#), which just uses the μ P layerwise learning rates for SP initialization (which they promote as their overall best-performing parameterization without identifying stability under logit blowup as the key mechanism), fulfills these desiderata, except for vanishing last-layer update effect on the output function. We will introduce another variant with larger last-layer learning rate that recovers effective updates of all layers. For avoiding confusion with SP, meaning using a global learning rate, and with μ P, meaning also achieving width-independence in the logits, we call this last variant *Maximal Update Parameterization under Standard Output-layer Initialization (MUSOLI)*.

For deriving the optimal layerwise learning rate exponents, first consider the scaling of hidden-layer pre-activation updates δh_l , $l \in [2, L]$, and input-layer pre-activation updates δh_1 (Yang and Hu, 2021, p. 51),

$$\begin{aligned}\delta h^l(\xi) &= \Theta\left(W_0^l \delta x_t^{l-1} + \eta_l \chi_{t-1} \frac{\partial f}{\partial h_{t-1}^l} \underbrace{(x_{t-1}^{l-1})^\top x_t^{l-1}(\xi)}_n\right), \\ \delta h^1(\xi) &= \Theta\left(\eta_1 \chi_{t-1} \frac{\partial f}{\partial h_{t-1}^1} \underbrace{(\xi_{t-1})^\top \xi}_1\right),\end{aligned}$$

where it holds that $\partial f / \partial h^l = \Theta(\partial f / \partial x^L) = W_t^{L+1} = \Theta(W_0^{L+1} - \eta_{L+1} \chi_t x^L)$ (at latest in the second step) (Yang and Hu, 2021, p. 52). Hence the correct l -th layer learning rate η_l for achieving a width-independent effect on the next layer’s pre-activations needs to cancel out the backpropagated gradient scaling $\partial f / \partial h^l$ and for hidden layers additionally the LLN-like scaling from the inner product between activations. As we still require activation stability $x_T^L = \Theta(1)$, we have $\partial f / \partial x^L = \Theta(n^{-\min(b_{L+1}, c_{L+1})})$. While under standard μP , it holds that $\partial f / \partial x^L = \Theta(n^{-1})$, the changed gradient scaling must be counteracted by choosing hidden layer learning rate $\eta_l = \Theta(n^{\min(b_{L+1}, c_{L+1}) - 1})$, $l \in [2, L]$, and input layer learning rate $\eta_1 = \Theta(n^{\min(b_{L+1}, c_{L+1})})$. In words, under larger last-layer initialization or learning rate, the hidden and input layer learning rates should be scaled down by the same amount. Finally, SP-full-align achieves a width-independent effect of the last-layer weight updates on the logits. But as the width-independent feature updates $\Delta x^L = \Theta(1)$ induce logit blowup $W_0^{L+1} \Delta x_t^L = \Theta(n^{1/2})$, the effect of the last-layer weight updates on the softmax output is actually vanishing. For last-layer weight updates to affect the softmax output in the same scaling as the updates propagated forward, the last-layer learning rate needs to be $\eta_{L+1} = \Theta(n^{-b_{L+1}})$, hence $c_{L+1} = b_{L+1}$. Hence MUSOLI is defined as SP-full-align but setting $\eta_{L+1} = \Theta(n^{-b_{L+1}})$. This last-layer learning rate is larger than in μP or Everett et al. (2024) under standard last-layer initialization $b_{L+1} = 1/2$, but necessary for fulfilling the desideratum that the weight updates in all layers affect the output function non-vanishingly.

Figure F.34 shows that indeed all weight updates behave width-independently under μP with standard last-layer initialization $(W_0^{L+1})_{ij} \sim N(0, n^{-1})$. But the output logits are dominated by the activations propagated forward as $W_0^{L+1} \delta x_t^L = \Theta(n^{1/2})$, since δx_t^L and W_0^{L+1} are highly correlated. Consequently, the last-layer updates have vanishing effect on the output function, which induces width dependence. By additionally scaling up the last-layer learning rate $\eta_{L+1} = \Theta(n^{-1/2})$, the logit scaling exponent in the term $W_0^{L+1} \delta x_t^L = \Theta(n^{1/2})$ is matched in the last-layer update term $\Delta W_t^{L+1} x_t^L = \Theta(n^{1/2})$ so that $b_{L+1} = 1/2$ and $c_{L+1} = 1/2$ recovers a balanced influence of all layer updates in the softmax output.

Figure F.25 and Figure F.26 show that after single-pass SGD or Adam, for both SP-full-align and MUSOLI the optimal learning rate shrinks with width for both generated 2-class multi-index teacher data as well as MNIST. The optimal learning rate exponent is often closer to -0.5 as we consistently observe under MSE loss, preventing logit blowup. Figure F.27 shows the same for CIFAR-10. This behaviour persisting across 3 data sets suggests that neither SP-full-align nor MUSOLI can be expected to transfer the optimal learning rate in general. An interesting question for future work remains why logit divergence introduces a width-dependence in the optimal learning rate in these parameterizations.

As expected from parameterizations in the controlled divergence regime, Figure F.27 also shows that the maximal stable learning rate scales width-independently, since activation and gradient stability is preserved. Over the course of 20 epochs, the training dynamics under large learning rates in MLPs with at least 3 layers are stabilized and the optimal learning rate indeed scales width-independently under standard last-layer initialization. Hence width-dependence in parameterizations can induce optimal learning rate scaling that varies over the course of long training. But often the optimal learning rate scales like the maximal stable learning rate. In such cases our theory is predictive. Note that SP full-align and MUSOLI are much more robust to poor tuning of the learning rate than μP , both in terms of training and test accuracy (Figures F.28 and F.29). We leave a closer analysis of the multi-epoch setting to future work.

For ADAM, the gradient is normalized in the backward pass, so that input- and hidden-layer learning rates remain the same as in μP under large last-layer initialization. This is again equivalent to the SP full-align parameterization from Everett et al. (2024). The logit update term $W_0^{L+1} \Delta x_t^L = \Theta(n^{1/2})$ should again be balanced with a larger output layer learning rate $\eta_{L+1} = \Theta(n^{-1/2})$ if the weight updates of all layers should have a non-vanishing effect on the softmax output in the infinite-width limit (MUSOLI). Figure F.30 shows that nonlinear networks trained with Adam and large last-layer initialization already tend to transfer better under MUSOLI than under SP full-align after 1 epoch. Linear networks again have smaller optimal learning rate exponent, indicating that avoiding logit blowup improves over feature learning in this case, where feature learning does not even add expressivity. Generalization, learning rate transfer and learning rate sensitivity after 20 epochs tends to be similar in all 3 considered parameterizations in deep ReLU MLPs (Figure F.31), showing again that parameterizations with logit blowup are a viable alternative.

Especially in deep ReLU MLPs, the last-layer learning rate does not seem to have a big impact, and SP full-align and MUSOLI overall behave similarly for both SGD and Adam.

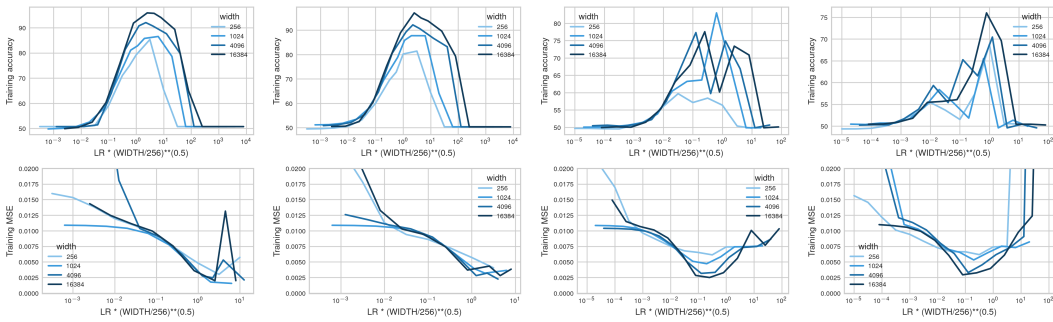


Figure F.25: **(Effective update variants do not transfer optimal learning rates on multi-index data)** Training accuracy of 8-layer MLPs trained for 1 epoch on multi-index teacher data under CE loss (top) and MSE loss (bottom) with SGD in SP-full-align, SGD in MUSOLI, Adam in SP-full-align and Adam in MUSOLI (from left to right). In all cases, logit blowup is avoided by optimal learning rates shrinking as $\eta_n = \Theta(n^{-1/2})$. Under CE loss the maximal stable learning rate remains width-independent, for SGD under MSE loss the maximal stable learning rate decays as $n^{-1/2}$, as necessary for stability.

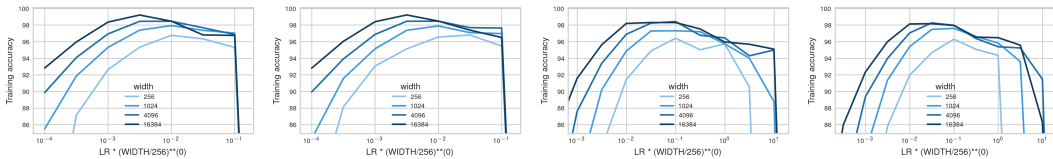


Figure F.26: **(Effective update variants do not transfer optimal learning rates on MNIST)** Training accuracy of 8-layer MLPs trained for 1 epoch on MNIST under CE loss with SGD in SP-full-align, SGD in MUSOLI, Adam in SP-full-align and Adam in MUSOLI (from left to right). In all cases, the optimal learning rate decays with width, while the maximal stable learning rate stays constant.

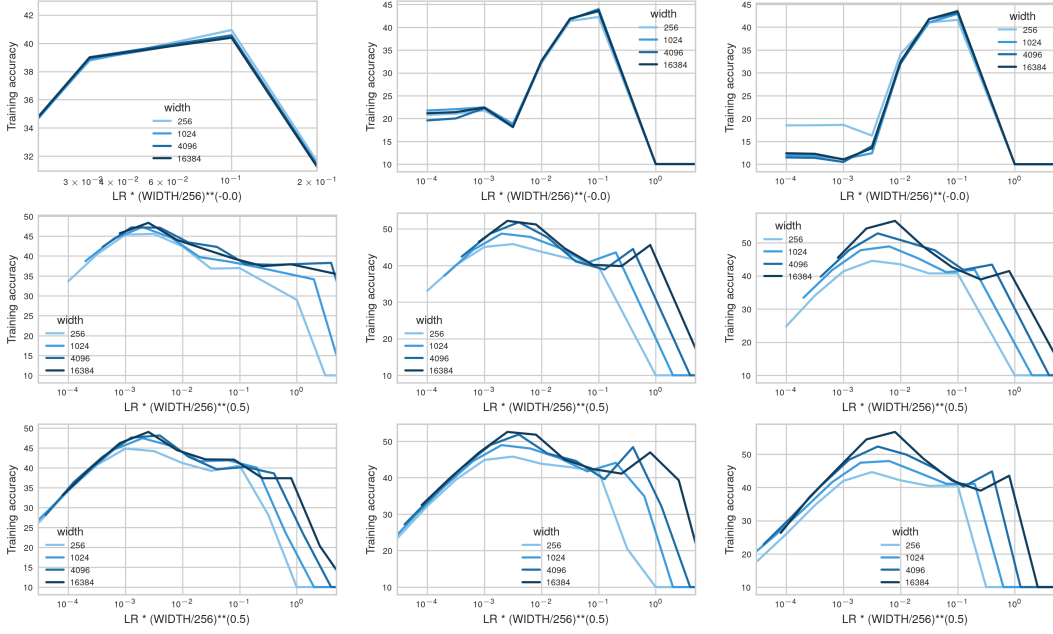


Figure F.27: **(Effective update variants for SGD on CIFAR-10)** MLPs with 2, 3 and 6 layers (from left to right) trained with SGD on CIFAR-10 in μP (top) versus SP full-align from [Everett et al. \(2024\)](#) (2nd row) versus SP full-align with larger last-layer learning rate (MUSOLI) (bottom row). While μP transfers with low variance as expected (left), μP with large standard last-layer initialization $b_{L+1} = 1/2$ and large last-layer learning rate $c_{L+1} = 1/2$ (right) have a non-trivial optimal learning rate scaling between $\Theta(n^{-1/2})$ and $\Theta(1)$, while the maximal stable learning rate scales width-independently.

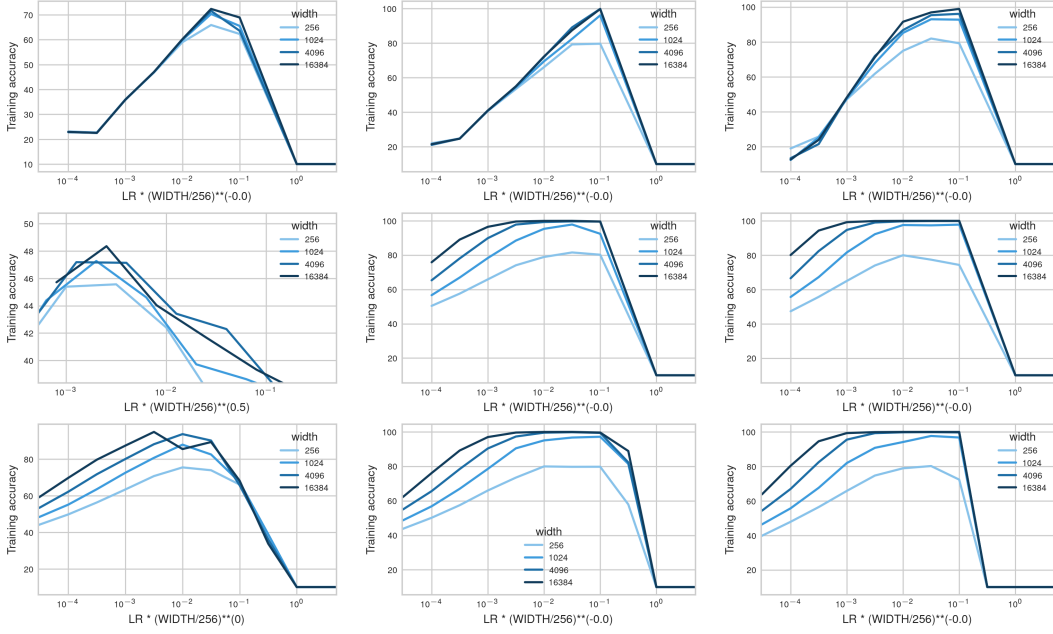


Figure F.28: **(Effective update variants for SGD on CIFAR-10 after convergence)** MLPs with 2, 3 and 6 layers (from left to right) trained with SGD in μP (top) versus SP full-align from [Everett et al. \(2024\)](#) (2nd row) versus SP full-align with larger last-layer learning rate (MUSOLI) (bottom row) as in [Figure F.27](#) but trained for 20 epochs. After sufficiently long training the large learning rate dynamics stabilize in MUSOLI so that the optimum indeed scales width-independently. MUSOLI strictly dominates original μP in training accuracy, and robustness to badly tuned learning rate is strongly improved under SP last-layer initialization compared to original μP . In sufficiently deep MLPs, the larger last-layer learning rate barely matters, but in 2-layer nets SP-full align avoids output blowup and feature learning by transferring under $\eta_n = \Theta(n^{-1/2})$.

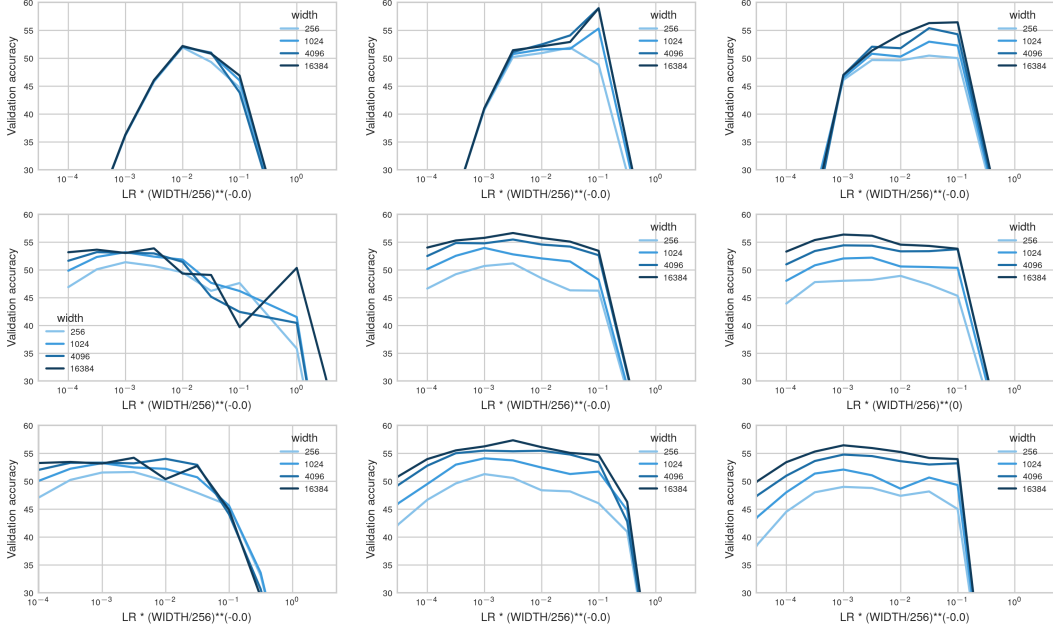


Figure F.29: (Test accuracy of effective update variants for SGD on CIFAR-10 after convergence) Test accuracy of 2-layer, 3-layer and 6-layer (from left to right) MLPs trained with SGD for 20 epochs on CIFAR-10 in μP (top) versus SP full-align from Everett et al. (2024) (2nd row) versus SP full-align with larger last-layer learning rate (MUSOLI) (bottom row). The validation-optimal learning rate scales width-independently in all cases. Observe that, while all variants generalize similarly well, the susceptibility to poorly tuned learning rates is much larger in μP than under parameterizations with large last-layer initialization.

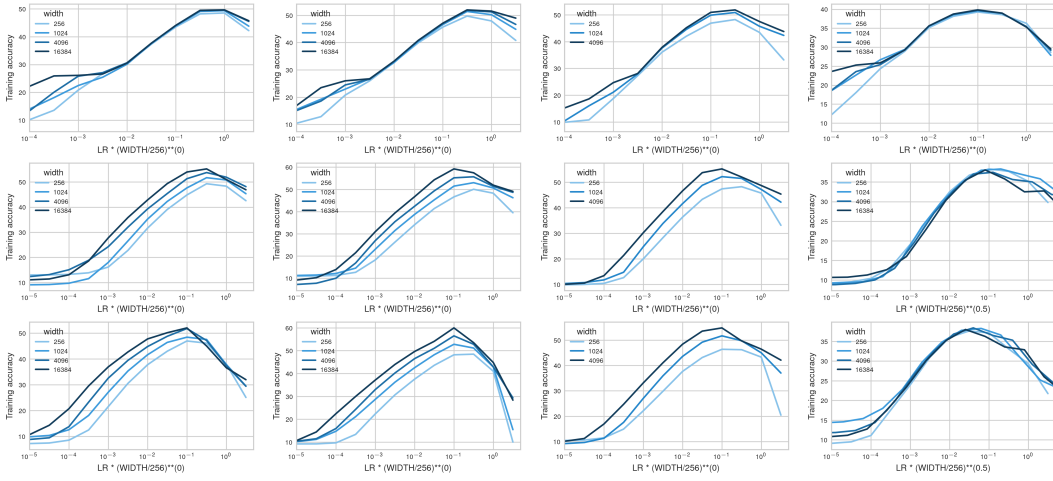


Figure F.30: (Train accuracy of effective update variants for ADAM on CIFAR-10) Train accuracy of 2-layer, 3-layer, 6-layer and 3-layer-linear MLPs (from left to right) trained with ADAM for 1 epochs on CIFAR-10 in μP (top row) versus SP full-align from Everett et al. (2024) (2nd row) versus MUSOLI (bottom row). The learning rate transfers irrespective of the architecture in μP . Large last-layer learning rate improves transfer in MUSOLI over SP full-align. The optimal learning rate scales as $\eta_n = \Theta(n^{-1/2})$ in both parameterizations with large last-layer initialization, as feature learning does not improve expressivity.

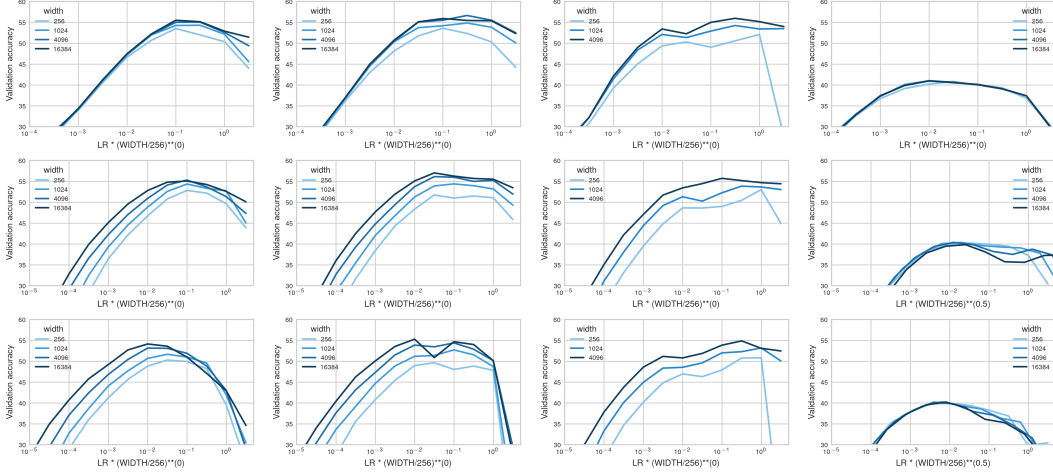


Figure F.31: **(Test accuracy of effective update parameterizations for ADAM on CIFAR-10 after convergence)** Test accuracy of 2-layer, 3-layer, 6-layer and 3-layer-linear MLPs (from left to right) trained with ADAM for 20 epochs on CIFAR-10 in μ P (top row) versus SP full-align from Everett et al. (2024) (2nd row) versus MUSOLI (bottom row). The validation-optimal learning rate scales width-independently in all ReLU MLPs with at least 3 layers. 3-layer linear networks clearly transfer under $\eta_n = \Theta(n^{-1/2})$ in SP full-align and MUSOLI, as for sufficient width learning features does not add expressivity, and instead avoiding logit blowup dominates the learning rate scaling.

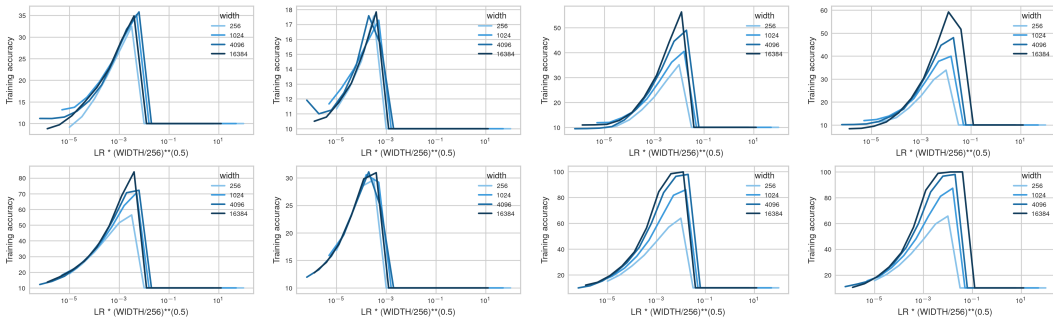


Figure F.32: **(Effective update variants with SGD under MSE loss avoid logit blowup)** Training accuracy of 2-layer, 3-layer linear, 6-layer and 8-layer MLPs (from left to right) trained with SGD for 1 epoch (top) and 20 epochs (bottom) on CIFAR-10 in SP full-align from Everett et al. (2024). Optimal learning rates shrinking as $\eta_n = \Theta(n^{-1/2})$ persists, avoiding logit blowup through $W_0^{L+1} \Delta x_t^L$. Only in 8-layer MLPs is the optimal learning rate saturating at the width-independent stability threshold.

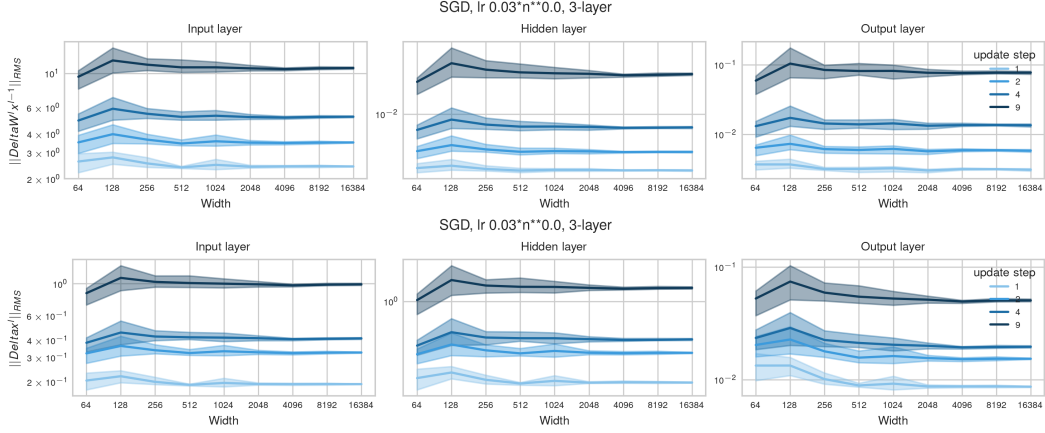


Figure F.33: **(Coordinate check for $\mu\mathbf{P}$ for SGD on CIFAR-10)** $\mu\mathbf{P}$ induces fully width-independent update dynamics.

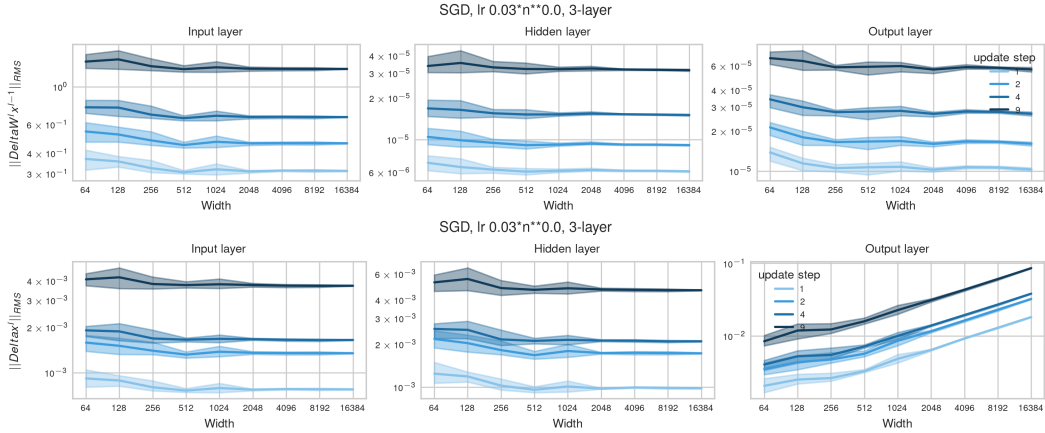


Figure F.34: **(Coordinate check for $\mu\mathbf{P}$ with standard initialization for SGD on CIFAR-10)** Effective updates $\|\Delta W^l x^{l-1}\|_{RMS}$ and activation updates $\|\Delta x^l\|_{RMS}$ as a function of width. The theoretically predicted scaling exponents hold: All layers update width-independently, but due to the large last-layer initialization, the activation updates correlated with W_0^{L+1} propagated forward induce output logits exploding as $W_0^{L+1} \delta x_t^L = \Theta(n^{1/2})$. This motivates increasing the last-layer learning rate to $\eta_{L+1} = \Theta(n^{-1/2})$ so that last-layer updates contribute with the same scaling. Note that in absolute terms, the updates are much smaller than under $\mu\mathbf{P}$ (Figure F.33).